



**Reactivity and Compositional Analysis of the Solid
Electrolyte Interphase and the Cathode Electrolyte
Interphase in Different Electrodes for Li-ion Batteries**

(Untersuchungen der Reaktivität und Zusammensetzung der Solid
Electrolyte Interphase und der Cathode Electrolyte Interphase in
verschiedenen Elektroden für Lithium-Ionen-Batterien)

Von der Fakultät für Mathematik und Naturwissenschaften
der Carl von Ossietzky Universität Oldenburg
zur Erlangung des Grades und Titels eines

Doktors der Naturwissenschaften (Dr. rer. nat.)
angenommene Dissertation

von Herrn Eduardo dos Santos Sardinha, M.Sc.
geboren am 17.09.1991 in São Caetano do Sul

Oldenburg, Juli 2019

This PhD thesis was prepared between July 2015 and May 2019 at the University of Oldenburg in the Faculty of Mathematics and Science at the Institute of Chemistry under the supervision of Prof. Dr. Gunther Wittstock. It was funded by the Conselho Nacional de Desenvolvimento Científico e Tecnológico (Brazil) with a “Ciência sem Fronteiras” scholarship (233204/2014-8).

The silicon electrodes were provided by Dr. Michael Sternad and Prof. Dr. Martin Wilkening from the Technical University of Graz. The lithium electrodes were provided by Dr. Markus Ding from the Helmholtz Institute in Ulm and the Institute of Technology in Karlsruhe. The cathode materials were provided by MSc. Alexander Gräfenstein from the Fraunhofer Institute for Manufacturing Technology and Advanced Materials IFAM in Oldenburg. All external contributions to this dissertation are described in the individual chapters.

Gutachter: Prof. Dr. Gunther Wittstock

Zweitgutachter: Prof. Dr. Rüdiger Beckhaus

Drittgutachter: Prof. Dr. Michael Wark

Tag der Disputation: 18.06.2019

Zusammenfassung

Lithium-Ionen-Batterien (LIB) sind eine der interessantesten Technologien für die Stromversorgung von tragbaren Geräten und elektrische Autos. Ein wichtiger Faktor für ihre Sicherheit und Leistung ist die Festelektrolyt-Interphase (SEI) an der Anode und die Kathodenelektrolyt-Interphase (CEI) an der Kathode. In dieser Arbeit wurde der elektrochemischen Rastermikroskopie (SECM) in situ und unter Argonatmosphäre eingesetzt, um Silizium- und metallische Lithiumelektroden (Anodenmaterialien) unter Verwendung von 2,5-Di-tert-butyl-1,4-dimethoxybenzol als Redox-Mediator in einem Batterieelektrolyt und in einer ionischen Flüssigkeit zu untersuchen.

Zuerst wurden Siliziumelektroden untersucht. Durch die Verwendung der Mikroelektrode zur Schädigung der SiO_2 -Schicht konnte die Wirkung dieser Schicht auf den Elektronentransfer mit einer mit Flusssäure geätzten und einer ursprünglichen Elektrode verglichen werden. Darüber hinaus wurden HF-geätzte Elektroden zunächst in vollen Zyklen und in kleinen Intervallen aufgeladen, so dass die SEI-Bildung allmählich in einem Keimbildungsprozess beobachtet werden konnte.

Das zweite untersuchte Anodenmaterial waren metallische Lithiumelektroden. Unser Kooperationspartner entwickelte ein Gerät, um frische und glatte Oberflächen zu erhalten. Die Elektroden wurden dann in Pentan und bei zwei unterschiedlichen Konzentrationen von Pentylamin in Pentan (0.1 M und 5 M) geschnitten. In allen Fällen wurden die SECM-Untersuchungen durchgeführt und der Vergleich der Proben direkt nach dem Schnitt und nach 100 Ladezyklen ermöglichte es, die SEI- und Dendritenbildung und den Einfluss der verwendeten Lösung während des Schneidvorgangs zu beobachten.

Bei Verwendung von 2,3-Dichlor-5,6-dicyano-1,4-benzochinon (DDQ) als Mediator wurde SECM verwendet, um die Kathoden LiFePO_4 (LFP) und $\text{LiNi}_x\text{Co}_y\text{Mn}_z\text{O}_2$ (NMC) zu untersuchen. Ein geeigneter Mediator wurde gefunden, um in den verschiedenen möglichen Bereichen zu arbeiten. Nach der Entscheidung für das DDQ wurden LFP und NMC in verschiedenen Ladungszuständen untersucht, um die Auswirkungen der CEI-Bildung auf Elektronentransferreaktionen zu verstehen.

Abstract

Lithium-ion batteries (LIB) appear as one of the most interesting technologies for powering portable devices and electric cars. One key factor for their safety and performance is the solid electrolyte interphase (SEI) formed on the anode and the cathode electrolyte interphase (CEI) on the cathode. In this work, the feedback mode of scanning electrochemical microscopy (SECM) was employed *in situ* and under argon atmosphere to investigate silicon and metallic lithium electrodes (potentially anode materials) using 2,5-di-*tert*-butyl-1,4-dimethoxy-benzene as redox mediator in a battery grade electrolyte and in an ionic liquid.

At first, silicon electrodes were investigated. By using the microelectrode to damage the SiO₂ native layer, the effect of this layer on the electron transfer could be compared to an etched with hydrofluoric acid and a pristine electrode. Furthermore, HF etched pristine electrodes were charged, first in full cycles and in small interval steps, so the SEI formation and lithiation could be observed. Within this interrupted charging experiments, the SEI formation could be observed step-by-step in a nucleation process.

The second anode material investigated was metallic lithium electrodes provided in different states of charge. Our collaborator developed a device which made possible to obtain fresh and smooth Li surfaces. The electrodes were then cut within pentane and in solutions with two different concentration of pentylamine in pentane (0.1 M and 5 M). In all the cases the SECM investigations were performed and the comparison of samples directly after the cut and after 100 charging cycles, made it possible to observe the SEI and dendrite formation and the influence of the solution used during the cutting step.

Moreover, using 2,3-dichloro-5,6-dicyano-1,4-benzoquinone (DDQ) as a mediator, the same technique was used to investigate LiFePO₄ (LFP) and LiNi_xCo_yMn_zO₂ (NMC) electrodes, which are materials suitable as cathodes. A suitable mediator was identified to work in the different potential range. After deciding for the DDQ, commercially available (LFP) and a high voltage (NMC) materials were investigated in different states of charge in order to understand the effects of the CEI formation on electron transfer reactions.

Table of Contents

1	Introduction.....	1
2	Lithium-Ion and Potential Future Batteries	5
2.1	The Negative Electrode	5
2.2	The Positive Electrode	7
2.3	Beyond Li-ion Batteries	7
3	Electrolyte Decomposition Layers – SEI and CEI.....	9
3.1	Interphase Formation	9
3.2	Structure and Properties	14
3.3	Conductivity and Performance	20
4	Scanning Electrochemical Microscopy and the Use of Redox Mediators for Batteries	23
4.1	SECM Operation Modes in Battery Research	23
4.2	Choice of the Redox Mediator	28
5	Experimental Details	32
5.1	Chemicals.....	32
5.2	Electrode Materials	32
5.2.1	Silicon Electrodes	32
5.2.2	Lithium Electrodes.....	33
5.2.3	Cathode Materials	33
5.3	Instrumental Considerations	34
5.3.1	SECM in the Glove Box	34
5.3.2	Complementary Employed Techniques and Sample Preparation.....	37
6	Reactivity at Silicon Electrodes	38
6.1	Influence of the Native SiO ₂ Layer on Uncharged Electrodes	38
6.2	Charging of the Si Electrode.....	43
6.3	The Interrupted Charging Experiment.....	48
7	Reactivity at Lithium Electrodes.....	54

7.1	Electrochemistry in an Ionic Liquid Electrolyte.....	54
7.2	SECM and SEM Investigations	55
8	Investigations at Cathode Materials	63
8.1	Mediator for Cathodes	63
8.2	SECM and SEM Investigations	65
8.2.1	LiFePO ₄ (LFP).....	65
8.2.2	LiNi _x Co _y Mn _z O ₂ (NMC).....	70
9	Summary.....	79
10	Outlook	81
11	References.....	83
12	Appendix.....	109
12.1	List of Symbols and Abbreviations	109
12.2	Curriculum Vitae	112
13	Own Publications and Scientific Presentations.....	114
13.1	Own Publications	114
13.2	Oral Presentations	115
13.3	Poster Presentations	116
14	Acknowledgement.....	117
15	Eidesstattliche Erklärung.....	118

1 Introduction

The transition from the use of fossil fuels to renewable energy sources has been one of the most important challenges in the last decades and will continue to be so for the next generations. Within this subject, rechargeable batteries play a very important role as they have a wide range of applications: they store chemical energy whilst providing an efficient route for the conversion of chemical into electrical energy.^{1,2}

More specifically the lithium-ion battery (LIB), which was introduced in the early 90's^{1,3} and has been in constant development since then.⁴ These batteries enabled the rapid development of power tools, microelectronic devices^{5,6} and the high usage of portable electronic devices.^{7,8}

It is important to highlight the more recent usage of LIB in electric vehicles, whose population have increased considerably in the last years, as can be seen on figure 1.^{9,10} That represents a great challenge when considering difference between the driving range, cost and refueling times of vehicles with internal combustion engine when compared to the electric ones.¹¹ Despite the disadvantages, LIB appears as the most suitable for both stationary application and for modern transportation due to its properties such as energy density and lifespan.⁷ Aurbach et al.¹² describe the important impact of LIB in our society even as the “most impressive success story of modern electrochemistry in the last two decades”.

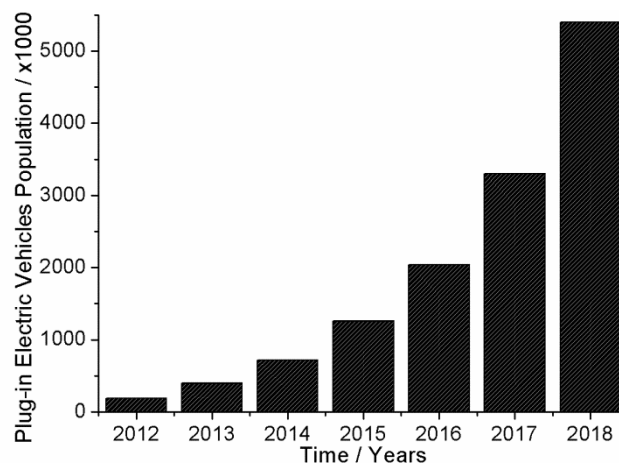


Figure 1: Plug-in electric vehicles population growth (in 1000s) worldwide in the last years (numbers of 2018 are still a forecast; source: ev-volumes.com).

The commercial LIBs are constructed with two different electrodes and a separator to avoid short-circuits.¹³ The positive electrodes are usually made of transition metal oxides such as LiCoO_2 ^{14,15} whilst the negative electrodes are mostly made of graphite nowadays.¹⁶ Figure 2 shows a scheme of a commercial pouch cell battery showing both electrodes attached to current collectors of Cu and Al (used to transfer electrons over an external circuit through them).^{13,17} During the charging process the Li-ions are dislocated from the cathode through an organic electrolyte that contains dissolved Li-ions, as well as through the separator, and intercalate within the graphene layers.^{13,18}

One of the key properties desired for a LIB is a large electrochemical stability window.¹⁸ This is especially required due to the potential of lithiated graphite being close to the standard $\text{Li/Li}^+ = -3.04 \text{ V}$ ¹⁹ potential as well as the relation of the potential of the cathode material, which is 3.9 - 4.2 V vs. Li/Li^+ for LiCoO_2 .²⁰

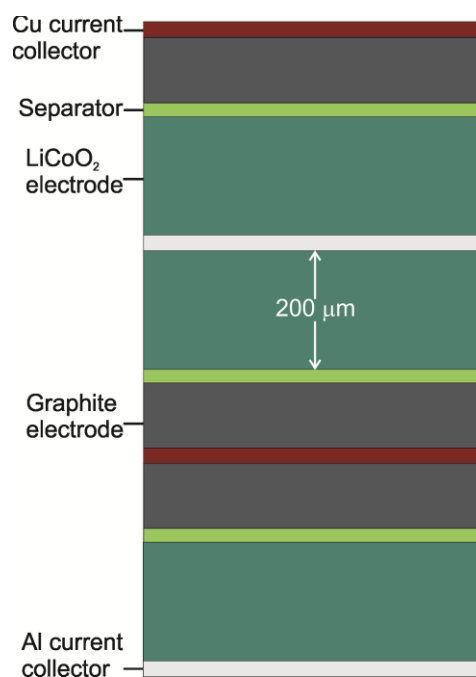


Figure 2: Schematic of a commercial Li-ion pouch cell battery.

When considering the challenges in improving the energy density, environmental impact and safety of batteries in general, there are three main important areas to focus: the electrolyte employed; the cathode and the anode material. With respect to the electrolyte, nowadays the liquid organic ones are the most commonly used but they still present some limitations, especially regarding safety. Therefore, the

general trend points to the usage of non-flammable alternatives and ionic liquids in the near future, while solid electrolytes appear as a solution that requires further research and may become an alternative in the long term.^{11,21}

With respect to the negative electrodes, the current material is graphite. Although considerable research efforts have been devoted to silicon electrodes, their application still face safety, mechanical and rechargeability challenges.^{22,23} Alternative anodes, such as microstructured silicon electrodes²⁴ or composites containing a mixture of graphite and lithium²⁵ are some of the promising alternatives for the near future applications, while lithium electrodes are a step behind of understanding and potential usability.¹¹

One of the biggest concerns when investigating materials to be employed as anodes is the solid electrolyte interphase (SEI). During the first charging cycles of a battery, the potential of the negative electrode decreases causing the electrolyte to be reductively decomposed. The decomposition products form the SEI covering the surface.^{26–28} This interphase is of key importance for the battery safety and performance, which causes that innumerable studies have been conducted in order to understand better its composition and electrochemical behavior.^{26,29–31} The complexity of the SEI associated with its sensitivity makes its proper characterization heavily challenging and both *ex situ* and *in situ* investigations have been performed.^{29,30}

The interphase at positive electrodes has been considerably less investigated, but can also bring improvements for the batteries. Most of the batteries used nowadays contains electrodes made of LiFePO_4 (LFP)¹¹, but some companies are also producing batteries with higher operational voltage cathodes made of $\text{LiNi}_x\text{Co}_y\text{Mn}_z\text{O}_2$ (NMC), in which the ratios between nickel, cobalt and manganese vary.³² These are the most promising materials by employing various composition ratios and crystalline structures. For even further developments, elemental sulfur appears as a potential material for the future.^{11,33}

Analogously to the SEI, the surface of the cathode is covered after the first cycles by the cathode electrolyte interphase (CEI). As proposed by Edström *et al.*,³⁴ it is an unavoidable effect which consists in the decomposition products of the electrolyte but with less pronounced effects on the performance of the battery (in comparison to the SEI).

The interphases formed on both electrodes are known to be complex processes of key importance for the battery performance and stability. Especially for the SEI, the formation happens during charging. Investigating this process and the potentials related to maximum formation²⁴ can lead to better understanding and optimization of this process. Along with investigations on the CEI, it can lead to improvements on the LIB performance.

In this thesis, the feedback mode of scanning electrochemical microscopy (SECM) was used to investigate in situ electron transport of the SEI and the CEI on electrode materials potentially used in LIB.³⁵ Chapter 2 presents some general aspects of the development of LIB and the materials employed as electrodes, while chapter 3 discusses in detail the properties of the SEI and the CEI that are formed. Chapter 4 summarizes methodical aspects of SECM, which is the technique used in most of the experiments in this thesis. Chapter 5 describes the details regarding instrumentation and chemicals used.

Chapter 6 is about the characterization of the silicon electrodes, at first using SECM, atomic force microscopy (AFM) and x-ray photoelectron spectroscopy (XPS) on uncharged electrodes, prior to the SEI formation, just an untreated electrode with SiO₂ layer, one etched with hydrofluoric acid (HF) and one where the microelectrode (ME) was used to abrade a small area.³⁶ Furthermore, experiments that involve the charging of such electrodes were performed both in full cycles and in small potential intervals in order to understand the SEI formation process. Chapter 7 presents the results from the investigations on lithium electrodes, which were prepared using a device that allowed fresh and smooth surfaces to be obtained. The electrodes were then analyzed using SECM with an ionic liquid as electrolyte and compared with another set of electrodes prepared with the same setup but also cycled, in order to investigate dendrite and SEI formation.

In order to successfully apply the FB, redox mediators were added to the electrolyte solution,³⁷⁻⁴⁰ one being the previously investigated 2,5-di-tert-butyl-1,4-dimethoxy benzene (DBDMB)⁴¹ for the anodes, while for the investigations on cathode materials, it was necessary to search for new alternatives suitable for working at the different potential range required for the study of the CEI. The investigations of the CEI on two different electrode materials (LFP and NMC) in different charging states are presented in chapter 8.

2 Lithium-Ion and Potential Future Batteries

The first commercial LIB appeared in the early 1990s and, since then, performance, safety and design of such devices are under constant development in order to reach better energy and power densities, cyclability as well as optimizing costs to make it viable for electromobility, portable devices and stationary applications.^{8,9,42}

Understanding the processes happening at the cell components and interfaces is the key for such improvements,^{43,44} therefore ex situ and in situ techniques were applied with this objective. SECM is one useful in situ approach that was employed recently in a similar way as in this work. Some examples of alternative developed are novel negative and positive electrode materials, enhanced structures or surface modifications.^{32,45-51} Apart from the electrodes, important improvements also happened for the components of the cell such as the electrolyte,⁵²⁻⁵⁴ separator,^{55,56} binder⁵⁷ and current collector.⁵⁸

2.1 The Negative Electrode

Nowadays, the commercially available negative electrode is mainly made of graphite. Research was devoted to the replacement of these electrodes by lithium titanate ($\text{Li}_4\text{Ti}_5\text{O}_{12}$),⁵⁹ a material that has a more positive potential (1.5 V vs. Li/Li^+),⁶⁰ which prevents electrolyte reduction and consequentially SEI formation.^{61,62} These effects improve cyclability and safety among other properties, however it also brings a decrease of the practical specific capacity from $350^{12,62}$ mAh g^{-1} of the LIB with graphite electrodes to approximately 150^{12} mAh g^{-1} .

Another much more interesting approach is to substitute the negative electrode material by silicon, which has a theoretical gravimetric capacity roughly ten times larger than graphite (approximately 3570 mAh g^{-1}).⁶³⁻⁶⁵ That property means both a great advantage and also a challenge for the usage of this electrodes, the volume increases to 270%⁶⁶ during lithiation. Lithitaiton/delithiation cycles cause the Si-Li alloys to crack, which compromises the mechanical stability of the

electrode as well as expose the cracked regions that are non-passivated and are immediately covered by the SEI which causes constant instability in the process.⁶⁷

The Si-Li alloy formation process occurs in a potential window between 0.4 – 0.2 V^{68,69} vs. Li/Li⁺ while the SEI formation starts already at 1.8 V vs. Li/Li⁺.⁶⁸ The Si-Li alloy formed are highly complicated to investigate due to the formation of several different crystalline structure with different elemental ratios. The initial lithiation forms a Li_x-Si amorphous phase, independently whether the initial Si structure is crystalline or amorphous, due to the fact that the small Li atoms during first lithiation do not go inside the Si crystal to react there, the lithiation takes part from the crystal surface layer by layer in a slow kinetic lithiation speed.⁷⁰

After further lithiation, the most commonly observed phase is the Li₂₂Si₅, but studies⁷¹⁻⁷⁴ have also shown that Li₁₂Si₇, Li₇Si₃, Li₁₃Si₄ and Li₁₅Si₄ are formed, usually at high temperatures, whilst at room temperature amorphous structures are more common.⁷⁵ Such amorphous-crystalline phase change brings along phase boundaries and tensions that may lead to cracks inside the material, which stresses the electrode additionally and leads in particular to capacity fading and ageing. Avoiding the potential window below 50 mV would stop the lithiation within the amorphous range, reducing the material ageing.⁷⁶

Simulation studies about the amorphous structures identified that when the Li content is low, the mixing enthalpy is positive when compared to crystalline silicon. This may indicate an initial barrier that prevents Li incorporation into the crystalline Si matrix. The values change to negative at 40% of Li and keeps going down to a plateau between 60% and 80% Li content in the alloy, corresponding to the region of the most stable structures.⁷⁷

A third option could be the use of metallic lithium negative electrodes. This material also has a much higher gravimetric capacity (3860 mAh g⁻¹)⁷⁸ than graphite and a structurally similar SEI is continuously reformed as the battery is cycled.³⁰ The SEI play another important role in the lithium negative electrode because it affects the dendrite formation, which is originally a considerable drawback regarding safety associated with the corrosion and sensitivity of the surface towards the SEI passivation.^{30,79}

2.2 The Positive Electrode

The positive electrodes are generally less studied than the negative, probably due to the relevance and complexity of the SEI and the intense research efforts that are constantly happening. More recently, the CEI formation has also been the aim of some investigations to understand better its properties and impact on the battery performance. The CEI was investigated by Edström et al.³⁴ with different Li_xMO_y (M = Co, Ni or Fe) cathode materials with electrochemical impedance spectroscopy (EIS). It was observed that the impedance increase as the battery was cycled due to a Li_xMO_y film formation on the surface of the positive electrode.⁸⁰⁻⁸²

More recently, studies with high voltage charging of LiCoO_2 cathodes⁸³ in order to try to maximize the Li ions extraction from lattice and increase the specific capacity of such electrodes. This extraction contrarily can lead to the formation of defect structures and faster capacity fading.⁸⁴ The cobalt loss is directly associated with the capacity fading and degradation of LiCoO_2 electrodes due to the degradation of the commonly employed LiPF_6 electrolytes.⁸⁵⁻⁸⁷

It is very important to understand better the electrochemical and structural properties of the CEI as it is known that a stable and dense formation can be helpful in preventing interfacial reactions at the electrode, as well as further oxidation and degradation of the material during cycling,^{87,88} while an unstable and not well structured CEI cannot manage such interfacial reactions leading to a fast decay of the battery performance.⁸³

2.3 Beyond Li-ion Batteries

Among the possibilities of improving electrode materials and other components of LIBs, there is also the alternative of post-lithium-ion batteries, from which lithium-air (Li- O_2) and lithium-sulfur (Li-S) are the two most prominent ones.^{33,89} In both cases, a metallic lithium negative electrode is employed. This electrode material has a lower potential compared to graphite, which causes the surface being always covered with a SEI.⁹⁰ This SEI influences the performance of the battery, as expected, by controlling the dendrite growth and its corrosion.^{30,79}

As positive electrode of these batteries, the transition metal oxides used in LIB are replaced by O₂ or S providing larger specific energies (energy per unit weight),³³ but not so pronounced improvements of the energy density (energy per unit volume).⁹¹ Furthermore, several new challenges are still to be solved regarding such battery systems, which make them likely to be the application in portable devices or electromobility viable only in the long term future.^{33,92,93}

3 Electrolyte Decomposition Layers – SEI and CEI

This chapter presents detailed information regarding the electrolyte decomposition layers formed on the surface of both electrodes of a Li-ion battery, the SEI and the CEI. Both will be addressed regarding thermodynamics of the formation, the structure, properties and composition of such interphases as well as how this affect the performance of the battery. Moreover, some of the methods employed to investigate the formation process, composition and electrochemical behavior are also discussed.

Despite the term “SEI” being proposed by Peled,⁹⁰ the first SEI formation was observed in the early 70’s in a graphite electrode in contact with propylene carbonate (PC) by Dey and Sullivan.⁹⁴ It consists of a passivating film formed on the surface of the anode. It contains mainly solid components originated from electrolyte decomposition. The SEI is still permeable to Li-ions, but it is insulating for electrons. It is too thick⁹⁵ to favor tunneling. Film formation on cathodes, is in general less pronounced, but it was also shown³⁴ and denominated CEI.

3.1 Interphase Formation

The SEI formation mostly happens during the first charging of a Li-ion battery, when the Li-ions lithiate the negative electrode at the moment the potential of the electrode exceeds the stability window of the electrolyte.^{26–29} The electrolyte is usually composed of one or more lithium salt mixed with different solvents.¹⁴ As an example, most of the experiments that will be discussed in this thesis, were performed using a 1 M solution of lithium perchlorate (LiClO_4) in propylene carbonate. What defines the electrochemical stability window of a liquid electrolyte is the energy gap between the highest occupied molecular orbital (HOMO) and lowest unoccupied molecular orbital (LUMO) of its components.⁹⁶ Figure 3 depicts an energy diagram referring to different chemical potentials (μ_i) of various negative (μ_A) and positive (μ_C) electrode materials.⁹⁷

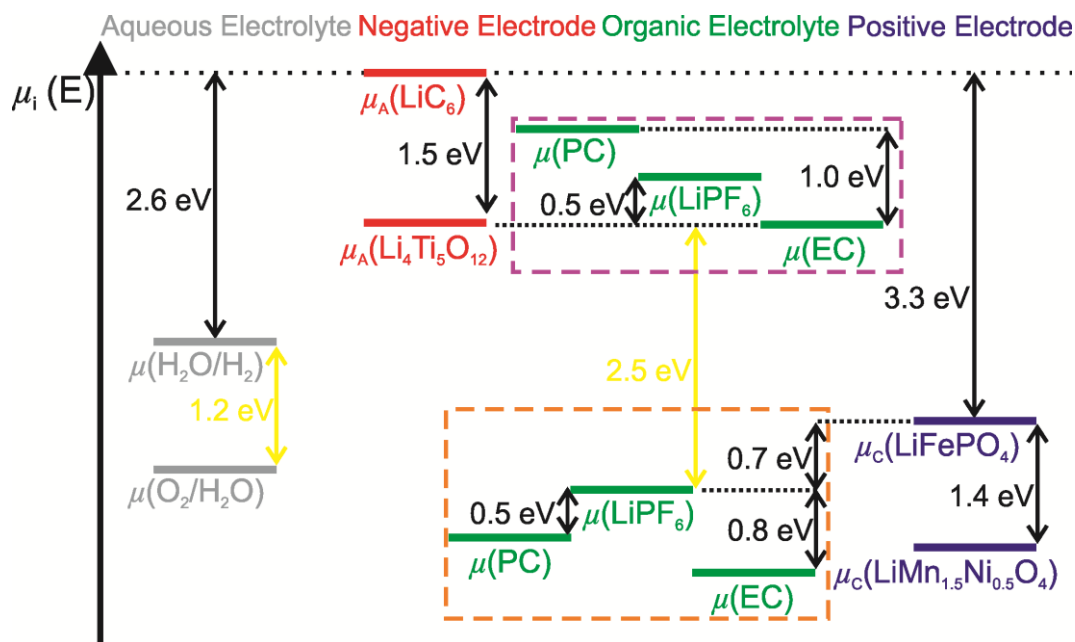


Figure 3: Energy diagram demonstrating examples of electrodes and electrolytes as well as the conditions for the electrolyte deposition. The yellow energy intervals represent the stability window. The purple dashed box indicates the LUMO, whilst the orange indicates the respective HOMO of the referred electrolyte. Adapted from Refs.^{12,98}

As can be seen, the organic electrolyte has a much larger stability window in comparison to the aqueous one. The LUMO energies of the organic electrolyte (LiPF₆ mixture of PC and ethylene carbonate (EC), as example) are ordered as $\mu(\text{PC}) < \mu(\text{LiPF}_6) < \mu(\text{EC})$ ¹² and the EC molecules are the one reduced first. Alternatively, for the HOMO the situation is different, the order is $\mu(\text{LiPF}_6)$ ¹⁰ < $\mu(\text{PC})$ ⁹⁹ < $\mu(\text{EC})$,¹⁰⁰ causing the stability window to be of 2.5 eV (the gap between LUMO of EC and the HOMO of LiPF₆).

The μ_A of the lithiated graphite (LiC₆) considerably exceeds the LUMO of all the electrolyte components, causing them to be reduced and decomposed at the surface under formation of the SEI.^{29,30,38} The electrolyte would be thermodynamically instable when in contact to LiC₆ or a metallic lithium electrode but in a LIB, the SEI separates LiC₆ and the electrolyte thus preventing further electrolyte reduction. Most of the SEI formation occurs during the first charging,²⁹ but it is known that this varies depending on the electrolyte and possible additives.²² The formation time is a more decisive factor to be considered instead of cycle number.¹⁰¹ When looking at the titanate (Li₄Ti₅O₁₂), the situation is completely different as the chemical potential of the titanate is within the stability window, preventing the SEI formation.^{61,102}

For the positive electrodes, the μ_C of $\text{LiMn}_{1.5}\text{Ni}_{0.5}\text{O}_4$ is outside the stability window of both PF and LiPF_6 . In this case the CEI is formed by the oxidation of the electrolyte components.¹⁰³ The CEI is usually thinner than the SEI, because the products of the reduction reaction are more immobilized on the negative electrodes.¹⁰⁴

The data presented on the diagram (fig. 3) show the partial molar Gibbs free energy (μ_i) that consists on the change of the Gibbs free energy G with the number of moles n of the compound i in a mixture as can be seen on Eq. 1.⁹⁷

$$\mu_i = \frac{\partial G}{\partial n_i} \quad (\text{Eq. 1})$$

In the case of electrochemical cells, the cell voltage between two electrodes (U) is proportional to the difference between the potentials of the negative and the positive electrodes ($\mu_A - \mu_C$) (Eq. 2) where F is the Faraday constant and z the number of transferred electrons ($[\Delta G] = [\mu] = \text{kJ mol}^{-1}$).

$$U = \frac{-(\mu_C - \mu_A)}{zF} = \frac{-\Delta G}{zF} \quad (\text{Eq. 2})$$

For the commercially employed graphite electrodes, there are some well known models for the SEI formation considering ternary solvated intercalation compounds and aprotic organic electrolytes.^{30,105–108} As an example a stable SEI that acts as a membrane for lithium ions preventing further intercalation is known to be formed when having EC-based electrolytes.^{30,109} On the other hand, when employing PC-based electrolytes, the effective passivation film may not be formed due to gas evolution.^{41,94,109,110} Other additives such vinylene carbonate (VC) or fluoroethylene carbonate (FEC) can improve the structure and electrochemical properties of the SEI.^{111–113}

The SEI growth is a dynamic process and re-dissolution of the outer layer and further electrolyte deposition are constantly expected.^{12,114} Another point to be considered is, when using LiPF_6 , HF formation can happen as well as metal ions from the positive electrode can be dissolved in the electrolyte.^{115,116} Such reactions are known to accelerate ageing and cause safety issues of the LIB such as Li dendrites growth.^{30,117}

For this thesis, silicon electrodes bring a more interesting discussion due to the experimental part being performed mostly with this material and its promising properties. On the surface of Si electrodes the formation of the SEI occurs at potentials lower than 1.8 V vs. Li/Li⁺ followed by Si-Li alloy formation at even lower potential values under 0.4 V.^{24,68} It has also been discussed that the early stages of the SEI formation mechanism is the decomposition of linear organic carbonates and further lower potentials induce the deposition of cyclic carbonates and the lithium salts.¹¹⁸ The exact mechanism and the steps for the SEI formation are not completely understood³⁰ and will be further discussed, especially in the results of this thesis (Chapter 6.3).

Vogl et al.¹¹⁸ carried out XPS analysis of charged Si electrodes in different electrolyte mixtures that were removed at the potential of 0.5 V, in which no lithiation is expected. As expected, the positive influence of adding VC and FEC on the SEI formation was seen in the spectra, but contrarily to what was first proposed, some peaks relating to Li-Si bonds were also seen. This is due to another factor to be considered in a Si electrode that is the native SiO₂ layer, which can also react with lithium ions and form Li₂O or Li₂Si₂O₅ at this potential.¹¹⁹⁻¹²²

Another interesting study of alternatives to better comprehend the SEI was performed by Lindgren et al.¹²³ using besides the additives, a previously investigated lithium 4,5-dicyano-2-(trifluoromethyl)imidazolide (LiTDI) salt.¹²⁴⁻¹²⁶ In this study, cycling of the battery showed detailed aspects about how the SEI is formed on the first cycles and the impact on the coulombic efficiency in comparison to the usage of LiPF₆.^{111,123,127,128} Regarding the composition, the same study describes a situation that can be seen in figure 4, where polycarbonates forms on the outer layer due to the presence of the additives (VC and FEC) as seen before¹²⁹⁻¹³¹ while lithium alkyl carbonates occur in deeper regions that cover the surface almost homogeneously after the SEI is formed.¹²³

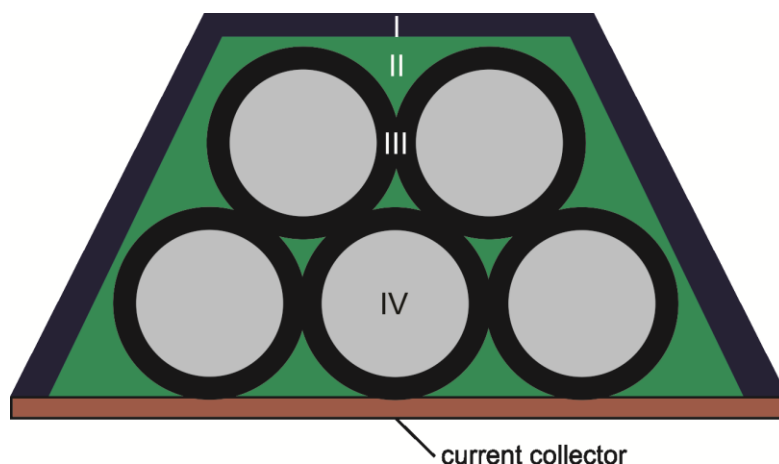


Figure 4: Schematics of the SEI formed on a Si electrode after cycling on an electrolyte with VC and FEC additives and LiTDI salt. (I) The outer layer is rich in polycarbonates, while (II) the inner layer of the SEI is rich in Li-alkyl carbonates. It is also shown a minimum LiTDI deposition that leads to (III) oxide formation directly at (IV) the Si particles. Adapted from Ref.¹²³

The presence of lithium alkyl carbonate deeper in the SEI is probably caused by its higher solubility in the electrolyte in comparison to the larger molecules of the polycarbonates.^{132,133} Something similar was observed by Xu et al.¹³⁴ when comparing the solvation shell of lithium ions in cyclic and linear carbonates. Hence, some of the LiTDI salt was observed to be part of the SEI in this case (fig. 4). Another important influence of the additives employed is that, when comparing to an electrolyte without VC and FEC, lithium silicates were formed much faster, which leads to poor cycling performance and ageing of the battery.¹²³

On positive electrodes, the CEI have been much less investigated, but there are some important aspects of its structure to be discussed. Analogously to what happens on the negative electrode, when surpassing a stability window of potentials, reactions leading to capacity fading happen on the interface between electrode and electrolyte, such as dissolution of cobalt ions (in case this is the material employed) or chemical attack by HF (present if the electrolyte contains LiPF_6).^{85,86} An electrolyte decomposition occur at high voltages (over 4.2 V) preventing further reactions and etching of the cathode material, forming the CEI.^{83,87,88} It is crucial that the CEI formed is stable and dense otherwise it is incapable of limiting the interfacial reactions, causing an increase on the impedance.⁸³

One cathode material that will be further discussed in this thesis (Chapter 8) is LiFePO_4 (LFP) and it has been investigated by Yamada et al.¹³⁵ as one of the alternatives for cathode materials. The iron-based compound has appeared as possible cathode materials due to its abundance and low toxicity, among other advantageous properties. Their disadvantage is insufficient cyclability when using $\text{Fe}^{4+}/\text{Fe}^{3+}$ redox pair.¹³⁵ Contrarily, when moving to $\text{Fe}^{3+}/\text{Fe}^{2+}$ and anions as $(\text{PO}_4)^{3-}$ and $(\text{SO}_4)^{2-}$, it was possible to stabilize the structure.¹³⁶⁻¹⁴⁰

The Li^+ present in this material can be extracted and transferred to the anode during cycling, compensating for the iron oxidation, besides this causes a relatively small shrinkage of the material, which can also compensate for the usual volume increase that occurs on anode materials.¹³⁵ Figure 5 shows an energy diagram of iron materials in comparison to the electrolyte window of interest. The olivine structure of the LFP along with the trivalency of the iron makes it impossible to further oxidize it within the potential window. It is compatible with a 3.4 V vs. Li/Li^+ voltage that make it viable.¹³⁶

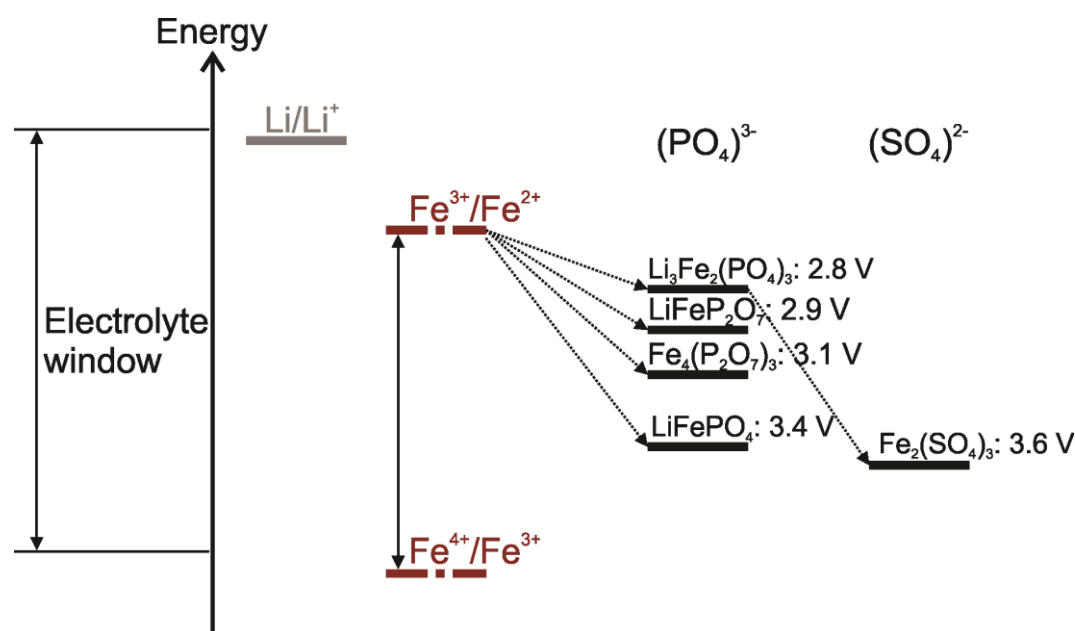


Figure 5: Schematic of the energy levels of $\text{Fe}^{3+}/\text{Fe}^{2+}$ in a structure that belongs to iron-based cathode materials. Adapted from Ref.¹³⁵

3.2 Structure and Properties

Although extensive investigations have been performed for decades, further details and properties of the SEI are still the aim of various research projects and

discussions.^{141,142} Examples of factors known to influence the SEI are the properties of particles that constitute the electrode, the use of pretreatments and the electrolyte composition, all of them can influence the performance of the battery (rechargeability, safety, e.g.) by altering the thickness, morphology and composition, among other properties of the SEI.

Since it was firstly proposed for metallic lithium anodes⁹⁰ and further discussed on the following decades by several different research groups,^{143–146} the SEI is commonly described as a compact multilayer containing an inner part with compounds such as Li_2O and LiF ,^{114,147} that have lower oxidation states and a porous outer region with compounds of higher oxidation states as ROCO_2Li .

The negative electrode material and the electrolyte are the crucially determining factors of the SEI, as it is formed at the interface between the two phases by the decomposition of the electrolyte.^{29,30} Alkyl carbonates are the usual compounds present as a solvent due to their suitable properties, such as stability window, temperature operation range, polarity, low toxicity and safety issues. These compounds can have cyclic structures, as EC that is known to have a positive impact on the SEI on graphite electrodes¹⁴ or PC.

A simplified representation of the SEI can be seen in figure 6, where the different layers can be seen as well as the permeability of Li salt in the electrolyte through it. One important aspect that causes this multilayered structure is the differences in driving force during the formation process. This leads to the first layers being formed under the highest Li-solution potential difference and as this potential difference falls gradually on the films formed, the reduction of solution species therefore becomes more selective.¹⁴⁶

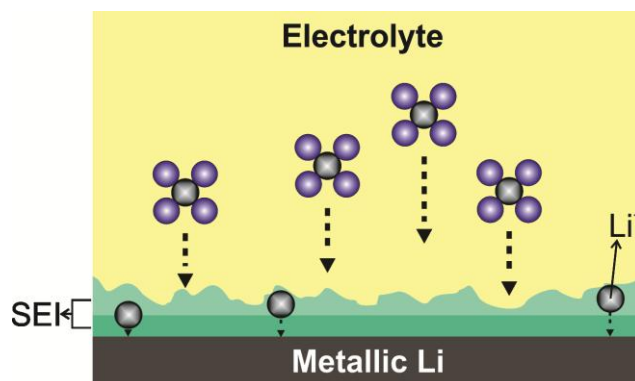


Figure 6: Schematic representation of the multilayered SEI on a metallic Li electrode. Adapted from Ref.¹⁴⁸

Graphite composite electrodes show a similar behavior as lithium.^{114,146,149} Again the multilayer layout for the SEI was proposed, but the formation process on graphite is different and more selective than on lithium.^{114,150} XPS studies performed by Edström et al.^{95,151,152} and Winter et al.¹⁵³ led to a better understanding of the structure of a SEI and the identification of larger LiF crystals and that the outer layer is mostly formed by polymers.

Figure 7 depicts the mosaic model firstly introduced by Peled¹⁵⁴ as a model for both lithium and graphite electrodes. It assumes several compounds that can precipitate at the same time at the surface of the electrode forming microphases within a SEI. They are ordered by the sequence of formation of such compounds.¹⁵

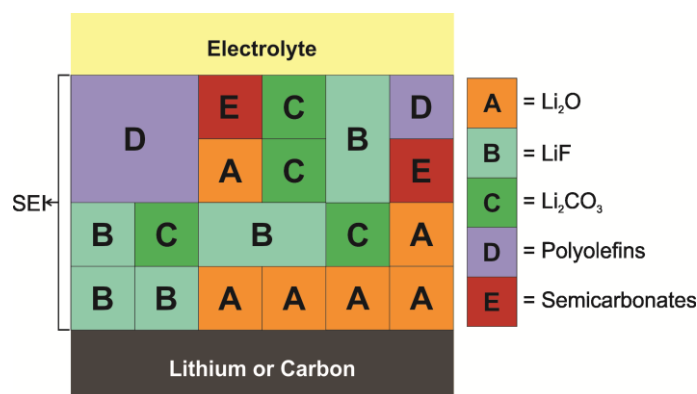
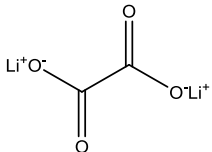
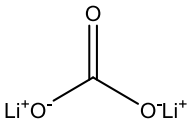
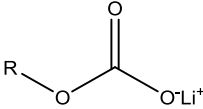


Figure 7: SEI according to the mosaic model. Adapted from Ref.¹⁵⁴

The real composition of the SEI still remains unknown though.²⁹ As discussed before, some lithium carbonates and oxides have been already detected in the SEI in previous studies on lithium and graphite electrodes,^{114,146,149} some of them are presented in table 1. The fact that carbonate based electrolytes are usually employed, make it the most commonly identified component in an SEI. As mentioned before (Chapter 3.1), the use of additives influences the components that will form the SEI. Due to its properties,¹³⁴ it was also seen that cyclic and linear carbonates take part in this process as the initial formation steps involve the reduction of molecules in the solvation shell of lithium ions.¹⁰⁵

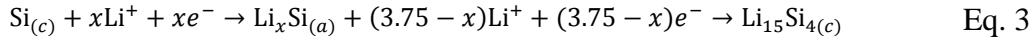
Table 1: Examples of compounds already observed in a SEI on graphite and/or lithium electrodes. Adapted from Ref.⁹⁸

Structure	Name	References
	Dilithium oxalate	Graphite ^{155,156}
	Dilithium carbonate	Graphite ^{145,151–153,157–161} , Li ^{94,162–167}
	Lithium alkyl carbonate	Graphite ^{150,151,156–160,168,169} , Li ^{153,158,162,163,165,170,171}
	LiF	Graphite ^{151–153,160,161,168,172,173} , Li ¹⁷⁰
	LiOH	Graphite ^{156,159–161,170} , Li ¹⁶⁶
	Li ₂ O	Graphite ^{159,161,168,172} , Li ^{166,170}

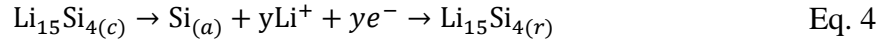
Dilithium oxalate ($C_2Li_2O_4$)²⁷ and dilithium carbonate (Li_2CO_3)¹⁷⁴ are also important constituents of an SEI. The first represents an exception for not being a carbonate, while the second, was reported not to be detected without exposing the cell to air,⁹⁵ which led to the discussion if the Li_2CO_3 is only formed in the aftermath by hydrolysis of some lithium alkyl carbonates.¹⁴³ Other components such as lithium fluoride (LiF),^{29,95,174} lithium hydroxide (LiOH) and lithium oxide (Li_2O) originate from further reactions of the electrolyte salts and, as all of the SEI structure, are still under discussion.^{95,152,159}

More recently, silicon appeared as an electrode material of interest. Its high gravimetric capacity and abundance make silicon one of the most promising materials for negative electrodes for the next generation of batteries^{63,175} and investigations on the SEI influence is of high relevance.

In silicon electrodes, the SEI is expected to be more similar to the one formed on lithium, as recurring lithiation causes material expansion and cracks, that lead to fresh Si surfaces and a continuous reforming of the SEI.^{7,22,23,30} The first charging cycle is known to be of key importance,^{118,176} and based on previous discussions^{63,75,177–182} Ma et al.¹⁸³ presented a mechanism of lithiation and delithiation of a Si electrode.



An intermediate amorphous phase was identified via x-ray diffraction (XRD),^{63,180,181} and a similar process happens as the battery is further cycled.



These reactions take place mostly on the first cycle and the intermediate two-phase region can be controlled by keeping the potential between 0.1 V and 0.07 V, while from the second cycle onwards, only a single-phase intermediate was observed.¹⁸³

The lithiation process directly influences the SEI properties on silicon electrodes. From the first 10 cycles on a flat Si electrode, a capacity decay was reported from 3260 mAh⁻¹ to less than 200 mAh⁻¹. This is due to two main reasons.¹⁸³ The first one is the large volume variations due to the high amount of Li intercalation, which increases the internal resistance and the loss of contact area between the Si and conductive materials (e. g. current collector) and leads to poor transport of electrons.¹⁸⁴ The other reason is that a SEI is formed by the electrolyte reduction at the lithiated and expanded state of the Si electrode and when the particles shrink, the interphase breaks down exposing fresh material.¹⁸⁵ This causes the SEI to continuously grow which increases the electrode impedance/polarization and decreases the electrochemical activity, as can be seen in figure 8.

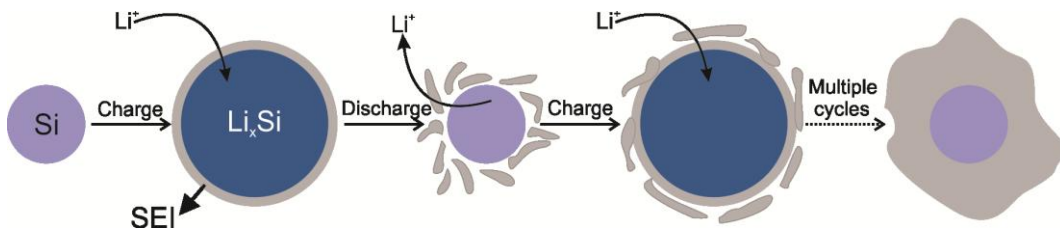


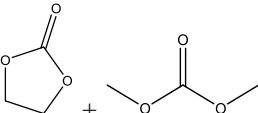
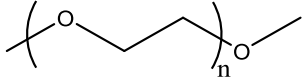
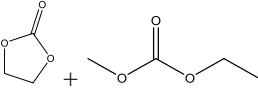
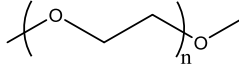
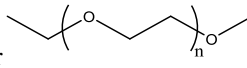
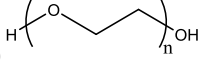
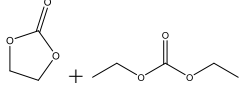
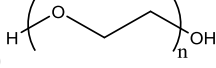
Figure 8: Schematics of the SEI formation and lithiation on a Si particle. Adapted from Ref.¹⁸³

The SEI is a very complex matter as it is formed as a result of several parallel chemical reactions involving sometimes liquid, solid and gaseous components of the system. A further complication is the dissolution of some SEI constituents in the electrolyte during discharging, while others remain insoluble.²⁹

Regarding the positive electrode and the CEI, some techniques already used to investigate the properties of the CEI are atomic force microscopy (AFM),⁸³ transmission electron microscopy (TEM) and electron energy loss spectroscopy (EELS) that could indicate that the overcharging of the battery using a LiCoO₂ cathode, can lead to the reduction of cobalt ions from the surface, thus having different chemical states at the surface than in the bulk of the material. This was shown to impact morphology, composition and stability of the CEI.^{83,186} Raman spectroscopy was used to investigate the thickness of the CEI and identified that if the voltage was increased to 4.5 V when cycling, Li₂O and Co₃O₄ were also formed on the surface.¹⁸⁷

A study performed by Liu et al.¹⁸⁸ using desorption electrospray ionization mass spectrometry (DESI-MS) on the CEI on LiMn₂O₄ cathodes discussed the presence of similar salts that are commonly present in the SEI such as LiF, ROCO₂Li and Li₂CO₃^{189,190} and also some polymeric compounds that varies according to the solvent employed during cycling. Table 2 shows some of the identified compounds.

Table 2: Influence of the electrolyte components on the polymeric compounds present on the CEI. Adapted from Ref.¹⁸⁸

Solvent mixture	Identified Polymers on the CEI
(EC/DMC) 	Poly(ethylene glycol) dimethyl ether 
(EC/EMC) 	 Poly(ethylene glycol) dimethyl ether  Poly(ethylene glycol) ethyl methyl ether  Poly(ethylene glycol)
(EC/DEC) 	 Poly(ethylene glycol)

It is shown that the compounds are directly influenced by the solvent mixture and the reactions with other lithium salts present like alkoxydes and methoxydes.¹⁸⁸ One other possible cathode material that was also investigated in this thesis

(Chapter 8.3) is $\text{LiNi}_x\text{Mn}_y\text{Co}_z\text{O}_2$ (NMC). The metal ions can have different ratios, but Niehoff and Winter¹⁹¹ performed XPS in order to better understand which compounds formed a CEI on such electrodes. Figure 9 shows the schematics proposed for an NMC electrode cycled using LiPF_6 in EC/EMC electrolyte.

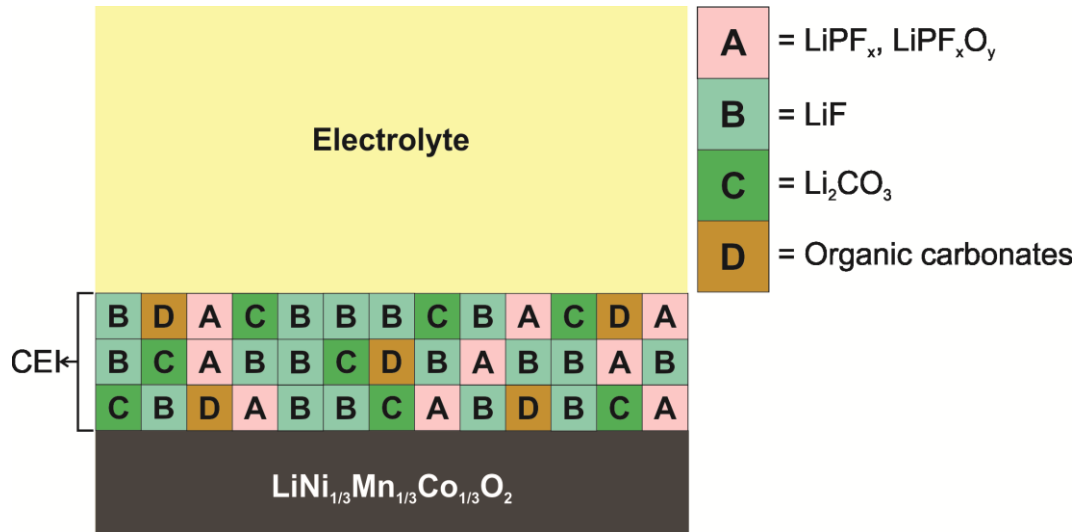


Figure 9: Schematics of a CEI formed on NMC cathode after electrochemical formation. The total thickness of the CEI in this stage is estimated to be 0.8 nm. Adapted from Ref.¹⁹¹

When comparing the schematic representations of the SEI (fig. 7) and the CEI (fig. 9), some similarities can be identified, especially the presence of LiF and Li_2CO_3 , as expected and previously discussed. An interesting point is that some of the compounds that are formed on the positive electrode forming the CEI can be transferred through the electrolyte and integrate into the SEI during cycling.^{83,192} Similar to the situation for the SEI, the electrochemical processes and structural properties of the CEI are still under debate due to the characterization limitations.

3.3 Conductivity and Performance

In principle, the optimal situation for a SEI is to be permeable for Li-ion conduction and impermeable for electron transport,^{29,90} although that is not always the case. Depending on the quality of the SEI, it can affect conductivity and ageing of the battery. In the first model proposed by Peled et al.⁹⁰ the transport of lithium ions occurs through grain boundaries, holes and cracks on the SEI, which was later observed with mathematical model.¹⁹³

Regarding the electron transport, despite being complicated to investigate, it is usually assumed that the SEI is insulating.^{22,29,31,78,149,194,195} Nonetheless, due to two important experimental results, this is still under debate. The first one is that a totally insulating SEI would be contradictory to the operation of overcharge protection agents,^{27,196,197} while Dahn et al.^{101,198–200} presented results showing a continuous growth of the SEI, contradicting the belief that it is only formed during the first cycle. It was already discussed that time can be more relevant to the SEI growth than the number of cycles and this growth is related to the total reduction of compounds to inorganic and organic layers.¹⁹⁵ The inorganic layer, which is closer to the electrode surface, is more dense and seems to be more decisive for the passivation of the electrode than the organic part of the SEI.³⁰

The lithium salt previously discussed in this thesis also has an impact. For instance, the hydrolysis of LiPF_6 generates HF and causes dissolution of SEI components.¹⁹⁵ Some additives that were mentioned in chapter 3.1 can be added in small concentrations to the electrolyte solution as they can be reduced preferentially at the surface of the electrode, changing the SEI composition.²³ Commonly the electrolyte solvents have reduction potentials below 0.8 V^{12} vs. Li/Li^+ while, one of the most employed additives, VC is reduced below 1.3 V^{201} vs. Li/Li^+ . Finally, the SEI properties can also be influenced by impurities, such as water from the atmosphere, that can hydrolyze alkyl carbonates.^{30,202}

When discussing about what is crucial for the performance of a battery, safety is of key importance and this is also directly related to the SEI.²⁹ Forming an unstable and not compact SEI can lead to uncontrolled gas formation or allow metallic lithium deposition on the negative electrode,²⁰³ which can increase cell pressure, cause heating and possibly causing accidents such as burning or explosion.^{22,204} On the other hand, a dense and stable SEI prevents solvent co-intercalation³⁰ and the exfoliation of the electrode material in the case of graphite. In silicon electrodes, the expansion and contraction of the material that happens during lithiation and delithiation respectively, cause an extra stress to the electrode and are associated with difficulties of maintaining a stable SEI.¹⁸³ As the SEI works as a barrier for lithium transport, it is also determining for cycling potential.^{22,30} It is important to mention that a flexible SEI that can accommodate volume changes during cycling can improve the performance of the LIB.¹¹⁴ The

temperature dependence of the SEI components^{22,205,206} has more influence on the performance at lower than at higher temperatures.

The influence of the CEI on the performance are in general similar to that of the SEI as the compounds that occur in both of the interphases are in general similar.¹⁹¹ Furthermore, Krueger et al. demonstrated that the SEI formation is responsible for the initial capacity fade of a battery,^{30,207} but after longer operation periods, the resistance at the cathode is more prominent.^{22,208,209} The study was performed in a LiCoO₂/graphite cell, where the cobalt ions can be dissolved as the cell reaches high voltages (4.2 V vs. Li/Li⁺)⁸⁵ and cause cracks in the electrode. The ions also migrate through the electrolyte and are integrated into the SEI.^{210,211}

As the cell loses lithium ions to both interphases, it tends to overcharging potentials during cycling²⁰⁷ which leads to safety concerns. These problems can be overcome with the addition of additives to the electrolyte. Another factor that was observed by Edström et al.³⁴ is the influence of temperature on the cathode side which is different from the SEI. At the anode, the SEI seem to break down at slightly increased operation temperatures, on the contrary, at the cathode polymeric/polycarbonates structures from the CEI appear to be covering the surface in a stable and efficient way at temperatures around 60 °C,³⁴ leading to a constant increase in thickness with cycling.

4 Scanning Electrochemical Microscopy and the Use of Redox Mediators for Batteries

Scanning electrochemical microscopy (SECM) was developed in the 80s^{212,213} and since then it has attracted interest from several applications such as characterization of electrocatalysts, corrosion and biochemical investigations, among many other local electrochemical studies in solid-liquid and other interfaces.^{35,214}

Here, SECM was employed to investigate the influence of the native SiO₂ on the Si electrode, the SEI layer formation and properties on Si and Li electrodes, dendrite formation on Li electrodes and the CEI on different cathode materials. Previous SECM studies on the SEI in different electrodes^{41,215–220} have shown how useful and how much information can be obtained in such investigations using SECM to better comprehend short and long term behavior of such interphases. Therefore, this chapter provides a discussion about the SECM operation modes and the importance of the mediator for these investigations.

4.1 SECM Operation Modes in Battery Research

SECM studies related to batteries belong to the more recent application of SECM.²²⁰ The technique was mostly employed to investigate either chemical species generated at LIB electrodes before, during and after cycling^{116,221–225} or to analyze the electron transport at the SEI.^{201,215,216,226,227}

There are two most important modes used in the studies of batteries. One is the generation-collection mode, which is useful for detecting chemical species generated during the battery operation. As an example, it was used by Snook et al.¹¹⁶ for the detection of cobalt ions from LiCoO₂ cathodes in ionic liquids. More precisely, in this work the cobalt ions were generated at the sample and collected at the tip of the ME (sample-generation/tip-collection mode), followed by the stripping of the Co²⁺ via oxidation. Figure 10 presents schematically the reactions observed.

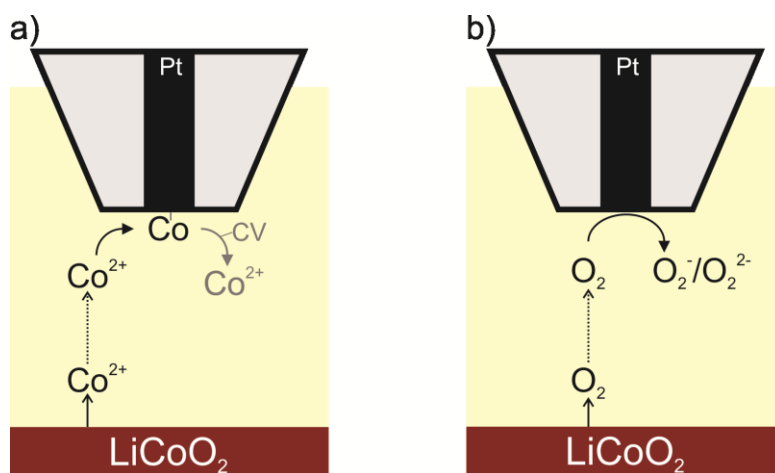


Figure 10: Schematics of the sample-generation/tip-collection mode of SECM employed to detect the (a) Co^{2+} release plus its further stripping using a CV and (b) O_2 formation on a LiCoO_2 cathode.¹¹⁶

Besides, in the same study the electrode was taken to overpotentials and during the discharge process, O_2 was also detected (fig. 10b), which led to different products formation depending on the ionic liquid employed.^{116,228,229}

Another possible way of investigating such reactions is the tip-generation/sample-collection mode, which was used in the study of Li-ion transport.²²³ In this case, contrarily to the most common first example, metallic lithium ME were used to generate the Li^+ ions, promoting local intercalation at a graphite substrate considering that, as previously discussed in this thesis, graphite anodes are suitable for battery applications and the SEI is formed by the electrolyte decomposition and lithium salts.^{90,94,154} This method though was proven later to not describe effectively the SEI properties. The first reason is that the local Li-ion consumption does not depend exclusively on the transport across the SEI, but from many other factors including the intercalation occurring in other areas of the electrode.^{22,30,230} Bülter et al.²¹⁷ also demonstrated that in the long-term, the Li-ion dissolution occur in different rates and that the SEI suffers from stability problems in the presence of metallic Li even at open circuit potential (OCP).

The feedback mode is the other important mode employed in the investigation of batteries and consequently used in this thesis to address the SEI and CEI properties. This mode requires that a mediator compound is added to the electrolyte and it is continuously reduced at the tip of the ME. This oxidized form then diffuses to the substrate surface where it is reduced again, regenerating it to

its original redox state. Depending on the properties of the sample, such as conductivity, the response on the ME may vary and, as an example that will be discussed later in this thesis, a clean Si surface of an electrode reacts differently in comparison to a surface covered with SiO₂³⁶ or a SEI.²³¹

According to the model proposed by Cornut and Lefrou²³² using COMSOL simulations, the current response at the ME depends on the distance between ME and the surface. Therefore, approach curves can be performed while applying a constant potential and recording i_T as a function of distance (d). The results from the simulations are presented in normalized parameters.

$$I = \frac{i_T}{i_{T,\infty}} \quad (\text{Eq. 5})$$

The normalized current (I) is the ratio of the current i_T measured near the surface and $i_{T,\infty}$ measured in the bulk. While the normalized distance (L) is the ratio between the microelectrode-sample distance (d) and the radius (r_T) of the ME.

$$L = \frac{d}{r_T} \quad (\text{Eq. 6})$$

The approach curves can assume different shapes as can be seen from calculated curves in figure 11. When approaching to a conductive surface the current is expected to rise infinitely, as the diffusion of the oxidized species from the ME to the substrate and its regeneration will generate what can be called a positive feedback of current.²¹³ Contrarily, when approaching an insulating surface, the regeneration of the mediator does not occur, leading to a decrease in the current (negative feedback). Naturally, there are many intermediate situations in which the sample kinetics limits the current. This situation also applies to SEI covered electrodes. Eq. 7 allows the determination of an effective first order rate constant k_{eff} [cm s⁻¹] with the normalized first-order rate constant (κ), when provided the microelectrode radius (r_T) and the diffusion coefficient (D) that are known from independent experiments.

$$\kappa = \frac{k_{\text{eff}} r_T}{D} \quad (\text{Eq. 7})$$

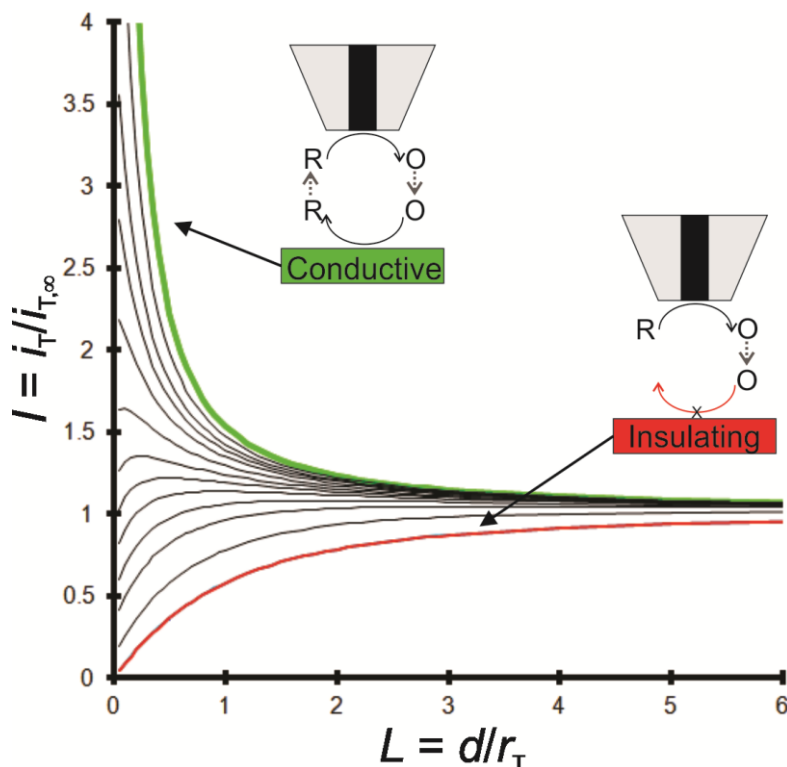


Figure 11: Approach curves according to the model of Cornut and Lefrou.²³² The green line represents the exclusively diffusion-controlled regeneration of R at the sample (positive feedback), while the red line represents an insulating sample (negative feedback). The black lines represent intermediate conditions and κ values.

Performing such approach curves carefully is of high importance to obtain κ from the experimental data.²³² Previous studies have shown the challenges of using the model for rough surfaces like graphite composite electrodes,^{217,218} but for flat surfaces as Si and Li it is expected to be less challenging.

For the feedback mode, it is fundamental to have a suitable redox mediator. It presents a similarity to the operation of redox mediators as overcharge protection agents in LIB, but with the difference that for the feedback mode, the mediator is continuously oxidized at the ME in a confined region, which allows the investigation of local electron transfer properties of the layers. This also represents a difference to other approaches such as rotating disc electrodes (RDE),^{196,233,234} rotating ring-disc electrodes (RRDE)²³⁵ or the four electrode setup^{236,237} when investigating the SEI or the CEI.

Using the feedback mode brings advantages and disadvantages for the studies of the batteries. One of the advantageous points is the distance in which the imaging is carried out, commonly between 5 and 15 μm ,^{36,41,231} avoiding contact with regular samples with relative small to moderate sample roughness,

that could lead to damaging the surface or the SEI/CEI above it. This represents a big advantage in comparison to techniques such as atomic force microscopy (AFM) where the surface can be damaged when investigated using the contact mode.^{238–242} Another point is that, as the mediator diffuses and interacts with the SEI in its oxidized form, the formation of the reduced form by the electron transfer, depends directly on the local properties of the interphase, allowing to identify its shape, boundary and extension. That is not possible when using spectroscopic techniques such as Fourier-transform infrared spectroscopy (FTIR) or XPS.²⁹ XPS can also affect the interphase composition by exposure to high-energy radiation, low energy scattering and Ar⁺-sputtering.^{95,152}

On the other hand, one of the drawbacks of this mode is that redox mediators are not naturally part of the electrolyte of a battery (except when some kind of overcharge protection agent is employed), and these components are known to influence the SEI formation or corrosion²³⁴ depending on the particular compound used (Chapter 4.2).

Apart from the most common modes already described, some research groups went beyond in the search for alternatives. The redox competition mode was proposed by Barton and Rodriguez-Lopez²⁴³ for investigations in LIB using a mercury-capped and a polytetrafluoroethylene-coated (PTFE) Pt ME (fig. 1a). In this study, a higher local activity was observed by the local decrease on the ME reduction current due to increase in Li-ion consumption by the Au-Li-alloy formed, similarly to a tip generation/sample collector mode. The drawback of this method is that is not possible to separate the contribution of varying electrode properties and the influence of the SEI on the current. Even when considering the stability of the Hg-capped ME,²⁴³ the formed Li-amalgam will be covered by a SEI which leads to a variation on Li-ion consumption.

Another approach was the slightly different scanning electrochemical cell microscopy (SECCM). It was for instance used to investigate positive electrodes of LiFePO₄ by employing a single-channel capillary ($r_T = 50$ nm) filled with electrolyte in contact with the electrode via a meniscus at the end of the nanopipette to investigate Li-ion flux.²²⁵ As can be seen on figure 12b, one noticeable difference between SECCM and SECM is that in SECCM only a small

area of the substrate is in contact with the electrolyte, leading to investigations with high resolutions of 100 nm for redox activity.²²⁵

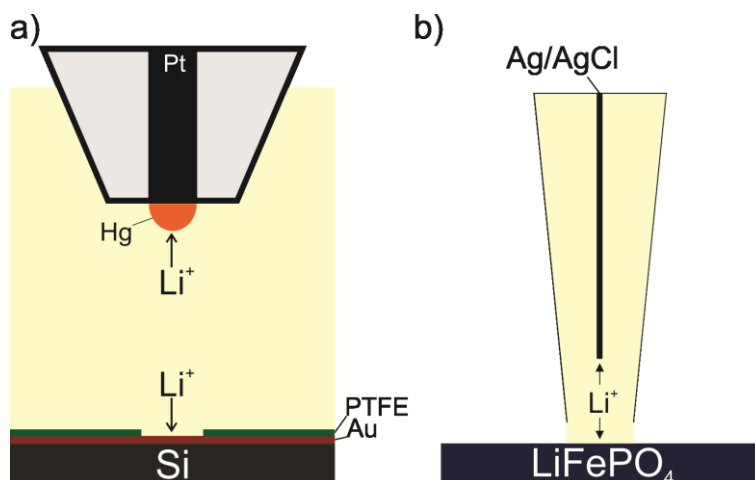


Figure 12: Schematics of different SECM modes applied to batteries (a) redox competition mode using an Hg-capped Pt ME²⁴³ and (b) SECCM for LiFePO₄ investigations.²²⁵

The nanopipette used in SECCM contains in its interior a quasi reference (Ag/AgCl) counter electrode. Similar to the approach with SECCM, scanning electrochemical ion conductance microscopy (SICM) was also used to investigate silicon electrodes by Lipson et al.²⁴⁴ In this study a lithiated tin wire was the source of Li⁺ inside a nanopipette that was approached to two different materials, one composed of silicon nanoparticles mixed with poly(vinylidene fluoride) (PVDF) deposited on copper foil and a tin foil. This made it possible to investigate topographical and electrochemical aspects at a nanoscale, moreover, by correlating both, inhomogeneities on the thickness and local lithiation/SEI formation could be observed locally when inducing the film growth with the Li-ion flux from the lithiated tin inside a nanopipette of approximately 60 nm of internal diameter.²⁴⁴

4.2 Choice of the Redox Mediator

As previously discussed, the redox mediator is of key importance for the use of the feedback mode of SECM as it interacts with the ME and the substrate. Some redox mediators are employed during the operation of batteries as overcharge protection agents which requires that the compound presents stability in both, oxidized and reduced states, large diffusion coefficients and good cyclability.²⁴⁵ In

the case of SECM experiments, mediators provide the possibility of long-term investigations due to the mentioned advantageous properties. Solubility is also a concern when adding a mediator to an electrolyte and is important to mention that, in order to be used as an overcharge protector, the requirements in this regard are much higher in comparison to the mM concentrations needed for an SECM experiment.^{246,247}

Frequently, ferrocene (Fc) was used as a redox mediator for investigations in batteries with the feedback mode.^{201,215,216,226,227} Experiments performed with different anode materials have shown that after SEI formation, the reduction of Fc^+ is suppressed²³⁵ leading to a considerable variation on the SEI formation potential, as it was mostly influenced by the tip-substrate voltammetry.^{201,216,226,227} Some examples were the SEI formation potential of 1.3 V²²⁷ vs. Li/Li^+ for TiO_2 paste electrodes and 0.8 V²¹⁶ vs. Li/Li^+ for glassy carbon electrodes.

Based on previous studies, DBDMB was selected for the investigations of anodes in this thesis. This compound was shown to have high stability as overcharge protector.²⁴⁸ This is corroborated by calculations based on binding energies of the oxidized species compared to the ethyl radical.^{249,250} Even when compared to other mediators, DBDMB has still appeared as the most viable choice.^{248–252} Despite several different redox mediators have been proposed, another important consideration is that the system should present conditions similar to a commercial battery cell, without adding compounds that are not present in commercial systems, for example.

As it is shown in figure 13, DBDMB has similar groups as the typical solvents present in electrolytes, such as EC and DEC, which represents a considerable advantage in comparison to mediators such as Fc.^{201,215,216,226,227,253–255} Furthermore, the DBDMB molecule is larger than typically used electrolyte solvents. This leads to the assumption that when the electron transfer to the DBDMB molecule occurs, the electron transport from the electrode to the electrolyte components is possible. The stability of DBDMB allows the requirements for long-term investigations within an Ar filled glove box and the understanding of the SEI formation process.²¹⁷

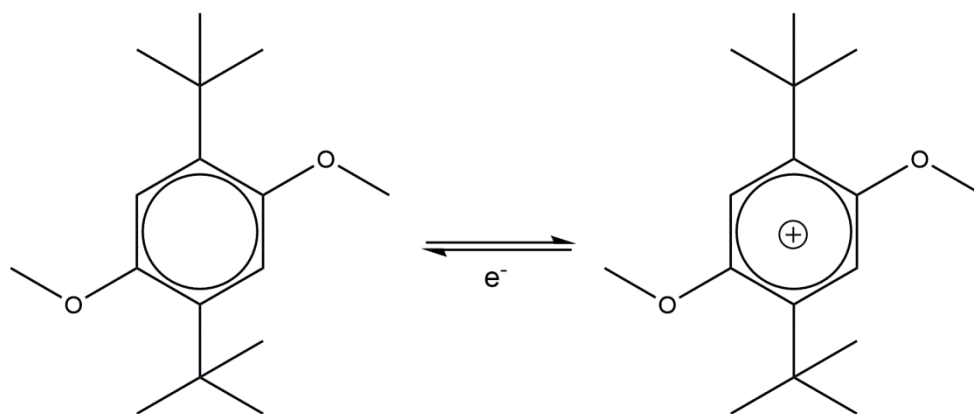


Figure 13: Reduced and oxidized structures of the DMDMB redox mediator.

The usage of DBDMB also prevents that the ME is covered by any passivation film originated from electrolyte deposition due to the fact that the diffusion-controlled oxidation requires $E_T = 4.1 \text{ V}^{41}$ vs. Li/Li^+ while electrolyte reduction would happen in a range of 1.5 V^{12} vs. Li/Li^+ . It is also important to mention that DBDMB investigations for overcharge protection are more recent than the use of Fc and derivatives, which mostly dates back to the early 90s.²⁵³

On the other hand, the fact that the reduction of Fc^+ is suppressed when the electrode is covered by the SEI,²³⁵ can be used for other purposes as quantifying the onset potential of SEI-formation. Another drawback though, is the incompatibility between Fc and metallic Li. The mediator is eventually adsorbed to Li in case this is the electrode investigated or the counter/reference electrodes.²¹⁶

Compatibility with the electrode materials and electrolyte components is a key point when choosing a redox mediator for SECM. It is of equal importance to prevent adsorption or decomposition of compounds at the ME. Previous studies have shown that such negative effects do not occur on Pt ME in presence of a variety of electrolytes, such as LiPF_6 which is very common in commercial batteries and LiClO_4 , that was used in most of the experiments in this thesis.^{201,215,216,226,227} Besides, DBDMB did not show any compatibility issues towards the Pt ME.^{36,41,217–219}

For the investigation of cathodes, Snook and collaborators,¹¹⁶ used the generation/collection mode while Takahashi et al.,²²⁵ used the derived technique

SECCM. The operation potential and the onset of CEI-formation can differ, leading to the need of finding new suitable redox mediators for the SECM investigations in this thesis.

5 Experimental Details

This chapter provides further details about the experiments performed in this thesis. Table 3 presents the chemicals used in this thesis during sample preparation and electrolyte components in the SECM cell, followed by the description of the used techniques, especially about the SECM setup which is the most important for this work.

5.1 Chemicals

Table 3: Chemicals used for sample preparation and in the electrolyte solution.

Name	Formula	Supplier	Grade
BASF G27	LiClO ₄ + PC	BASF	1 M solution
Hydrofluoric Acid	HF	Sigma Aldrich	5%
DBDMB	C ₁₆ H ₂₆ O ₂	Angene	99%
2,3-dichloro-5,6-dicyano-1,4-benzoquinone	C ₆ Cl ₂ (CN) ₂ O ₂	Sigma Aldrich	98%
1-Butyl-1-methylpyrrolidinium bis(trifluoromethanesulfonyl)imide	C ₁₁ H ₂₀ F ₆ N ₂ O ₄ S ₂ (Pyr14TFSI)	Synthesized	
Anthracene	C ₁₄ H ₁₀	Sigma Aldrich	98%
Azobenzene	C ₁₂ H ₁₀ N ₂	Sigma Aldrich	98%
9,10-bis(phenylethynyl) anthracene	C ₃₀ H ₁₈	Sigma Aldrich	97%
Ruthenium-tris(2,2'-bipyridyl) chloride	C ₃₀ H ₂₄ C ₁₂ N ₆ Ru	Sigma Aldrich	99%

5.2 Electrode Materials

5.2.1 Silicon Electrodes

The electrodes investigated in this thesis consisted in 200 μm thick highly boron-doped monocrystalline Si wafer (100 orientation, 8 $\text{m}\Omega\text{ cm}$ specific resistivity, Shin- Etsu, Chiyoda, Japan). To provide a good electric contact, the backside of the silicon wafer was sputter-coated with a 1 μm thick Cu layer. The Cu-covered Si electrodes were then cut into pieces of $4 \times 4\text{ mm}^2$.

One important step required for the test with the Si electrodes was the etching of the native SiO₂ layer with HF.²⁵⁶ A drop of 100 μL of 5 mass-% hydrofluoric acid (HF) solution was put on top of the Si substrates avoiding wetting the Cu current collector on the back side of the substrates. After around one minute the HF was rinsed thoroughly with deionized water and the samples were transferred to the glove box.

5.2.2 Lithium Electrodes

The lithium electrodes were prepared by collaboration partners and the starting material were lithium rods (99.9% trace metal basis, 12.7 mm diameter, Sigma-Aldrich). For the cutting solutions, it was used anhydrous pentane (>99%, Sigma Aldrich) and 1-pentylamine (>98%, Merck). 1-butyl-1-methylpyrrolidinium bis(trifluoromethanesulfonyl)imide (Pyr14TFSI) was synthesized²⁵⁷ and dried at 120 °C for 18 hours to ensure low water content. The ionic liquid was then mixed with Lithium bis(trifluoromethanesulfonyl)imide (LiTFSI) (99.9%, battery grade, 3 M) in the 2:8 molar ratio.

Their developed device included a tungsten wire (99.95%, 0.2 mm diameter, Alfa Aesar) to slice the Li electrodes, as it is a chemically inert material towards lithium, preventing any contamination. The rods were first cut in 1.5 cm length with a scalpel while inside a polypropylene cylinder to preserve the shape of the soft metal. Afterwards, the wires were used inside the same cylinder in a way where it was possible to add the desired solution with the SEI precursor and ensure a reproducible thickness (2.3 mm).²⁵⁸

5.2.3 Cathode Materials

The first cathode material investigated consisted of commercially available carbon-coated LiFePO₄ (LFP Life Power P2, Clariant) as an active material, polyvinyl difluoride (PVDF Kynar ADX 111, Arkema) and carbon black (Super P-Li, Timcal) as conductive additive. The composition (LFP/PVDF/carbon black) is 84:10:6 by weight percent.

The second cathode material consisted of lithium nickel manganese cobalt oxide (NMC 811, POSCO ESM) as the electrochemically active material, the same PVDF as binder and carbon black (ENSACO Super C 65, Imerys) as conductive additive. The composition (NMC/PVDF/carbon black) is 89:5:6 by weight percent. The compounds are mixed under vacuum conditions (R02Vac IntensiveMixer, Eirch). Both materials were coated in an aluminum foil using a roll-to-roll coater (BA-RRC, Mathis).

5.3 Instrumental Considerations

5.3.1 SECM in the Glove Box

The most important investigations in this thesis were performed with SECM. The battery electrolytes and electrode materials are water and air sensitive, therefore the experiments were all inside an Ar-filled glove box (Uni-Lab, M. Braun GmbH, Garching, Germany). The potentiostat (CompactStat, Ivium Technologies, Eindhoven, The Netherlands), was placed outside of the glove box in order to reduce the noise effect. The cell inside contained a 3-axis micropositioning system (MS30 precision actuator and PS30 distance measurement system, CU30 controller, mechOnics AG, Munich, Germany) and it was operated using an in-house developed software (SECMx).²⁵⁹ Additionally, for the interrupted charged experiment (Chapter 6.3) it was also developed an electronic switch that made possible to connect either the ME or the Si electrode as working electrode. SECMx was also used to run batch sequences of SECM experiments, charging steps, CVs, linear sweep voltammetries (LSVs) and also experiments from the native software of the IviumStat potentiostat. The cell and positioning system were covered by a custom Plexiglas cover that can be seen in figure 14, in order to avoid any interference from the Ar circulation and solvent evaporation.

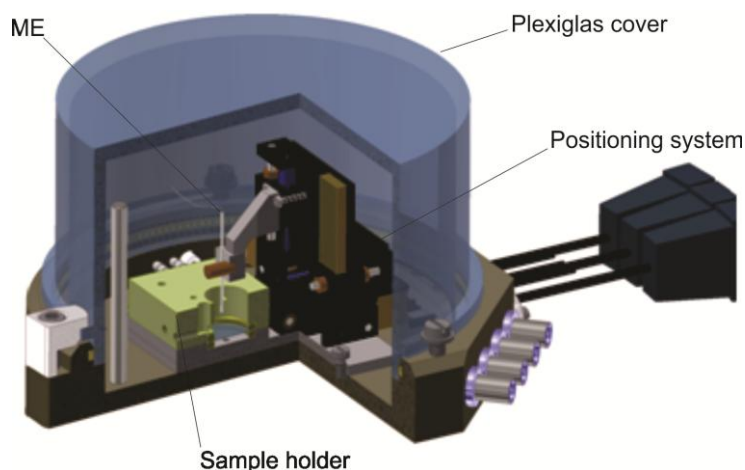


Figure 14: Schematic drawing of the SECM cell with the Plexiglas cover that was placed inside of the glove box.²⁶⁰ Adapted image provided by Folkert Roelfs (University of Oldenburg).

The system described required some subtle adaptations depending on which experiment was performed. For the first investigations on Si electrodes and the investigations with cathode materials, just the wafer was placed inside the sample holder, while for the charging, it was added a copper foil on the back of the wafer that had no contact to the electrolyte solution that made possible to connect the electrode with the potentiostat. Due to the different size of the sample, Li electrodes required a larger sample holder, whilst when trying different mediators a glass plate was the only substrate. Figure 15 shows a schematics of the whole setup.

Besides the already mentioned components, the electrochemical cell also requires a reference electrode (RE) and a counter electrode (CE). Metallic Li stripes were used in all experiments for RE and CE in the experiments with anode materials, while a silver wire was the RE and a platinum wire the CE for the experiments with cathode materials.

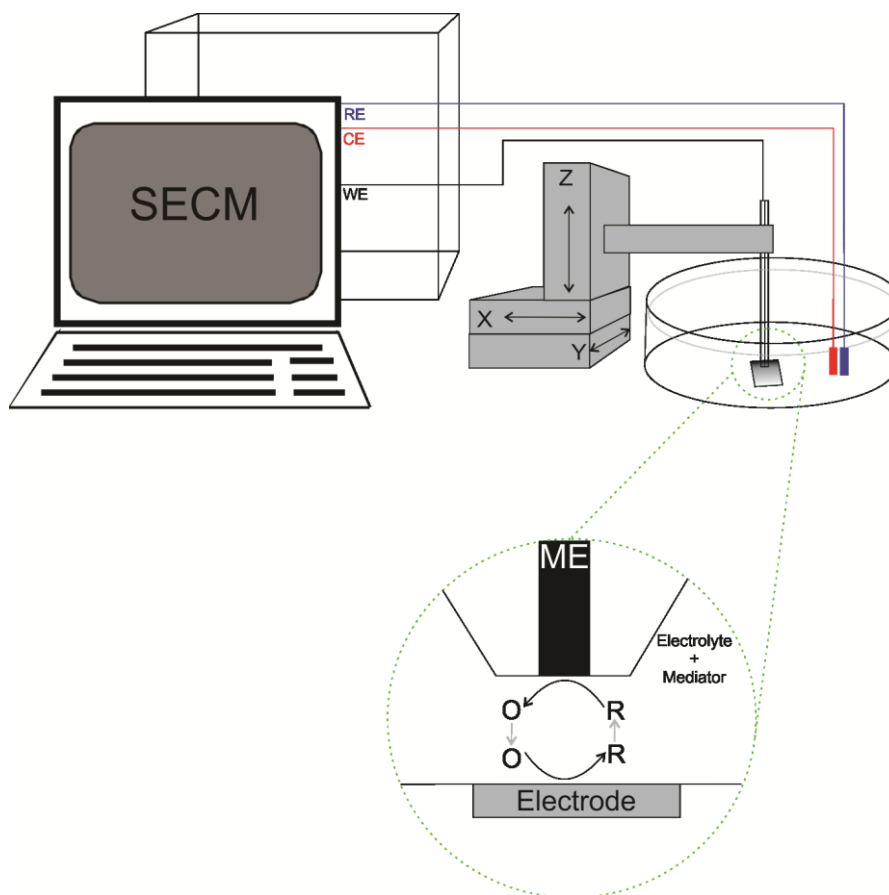


Figure 15: SECM setup used for the experiments.

As discussed, the ME is a key part for the SECM experiments, as it is what makes possible the recording of local electrochemical reactivity.²²⁰ The MEs used in this thesis had a radius $r_T \approx 12.5 \mu\text{m}$ of active surface (Pt wire) sealed in a insulating glass sheath.³⁵ Due to its size, the diffusion does not occur in a planar way as in macroscopic electrodes, instead diffusion is hemispherical,²⁶¹ causing the rapid establishment of a hemispherical diffusion field and a diffusion-limited steady-state current $i_{T, \infty}$ (Eq. 8) where n is the number of electrons transferred per molecule, F is the Faraday constant, D is the diffusion coefficient and c the bulk concentration of the species.^{262,263}

$$i_{T, \infty} = 4nFDcr_T \quad (\text{Eq. 8})$$

5.3.2 Complementary Employed Techniques and Sample Preparation

Apart from SECM, some other techniques were also used to study composition and topographic features and better understand the results. The Si electrodes that will be discussed were investigated also using XPS and AFM. XPS was performed with an ESCALAB 250 Xi (Thermo Fisher Scientific, East Grinstead, UK). Excitation was made with monochromatized Al K α line (1486.6 eV). Apart from survey, high resolution spectra of Si, O, and C were performed. Furthermore, imaging and angle-resolved XPS (ARXPS) was also performed in order to investigate the depth of the SiO₂ layer (Chapter 6.1).

The AFM experiments were performed in contact mode under ambient conditions with a Nanoscope IIIA controller and a Dimension 3100 stage (Veeco Instruments Inc., Santa Barbara, USA). Topographical images were recorded with 256 \times 256 pixel resolution and area of 95 μm \times 95 μm using a triangular Au-coated Si₃N₄-cantilever (MSCT tip, Bruker, Karlsruhe, Germany) with a spring constant of 0.6 N m⁻¹.

The cathode materials were investigated using scanning electron microscopy (SEM). They were performed using a Helios Nanolab 600i system (FEI Company, Eindhoven, The Netherlands) with a detector for energy dispersive analysis of x-rays from 30-10 kV accelerating voltage depending on the sample and in different states of charge (Chapter 8).

6 Reactivity at Silicon Electrodes

This chapter presents results and discussion regarding experiments that were performed using silicon electrodes. As discussed previously, this is a very promising material to be employed as anode material, therefore better understanding electrochemical properties of the material can lead to improvements on the battery performance.

At first, electrodes without charging were investigated, as well as the influence of the native SiO_2 layer that is formed in contact with air. The experiments in this chapter belong to a published paper³⁶ which includes further investigations on the impact of the native SiO_2 layer on Si electrodes, though the results presented in this thesis were the exclusively performed by me. Following this, there were experiments involving the full charge and discharge of an electrode, addressing its limitations and, afterwards, an interrupted partial charging (where only the SEI formation potential ranged was reached) in slow steps will be discussed.

6.1 Influence of the Native SiO_2 Layer on Uncharged Electrodes

In the first steps of this thesis, uncharged Si electrodes were investigated with the feedback mode of SECM to observe the differences between a sample containing the native SiO_2 layer, one sample etched with HF and one sample that was abraded during SECM operation with the glass sheath of the ME. The goal was to understand better the electron transport before the SEI formation as it is of key importance for the performance of Si electrodes.^{67,264}

The native SiO_2 layer formed when in contact with air is known to be 1 – 3 nm thick and can passivate the Si surface.^{265–267} The first part of this published work³⁶ demonstrated that the k_{eff} values of a SiO_2 covered electrode were rather small and not the same but comparable to insulating surfaces, showing almost no reduction of DBDMB^+ . However, some regions presented higher values of k_{eff} , demonstrating a heterogeneous coverage of SiO_2 .

The work proceeded in showing two possible ways of removing the SiO₂ layer. The first one was by physical abrasion, using the Pt ME as a probe to damage the SiO₂ layer mechanically by vertical or horizontal movements as can be seen in figure 16.

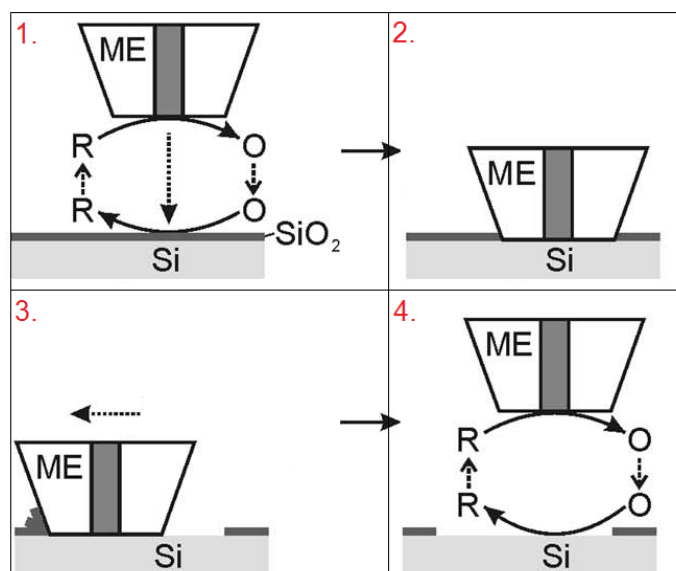


Figure 16: Schematic representation of the SiO₂ layer mechanical abrasion. During the SECM analysis, the microelectrode gently contacts the insulating surface, then moved laterally in a way that can abrade the SiO₂ layer. Adapted from ref.³⁶

This procedure made it possible to observe an increase in the local electrochemical reactivity that could be verified by SECM imaging. Figure 17, presents one image obtained by scanning a region around the abraded area.

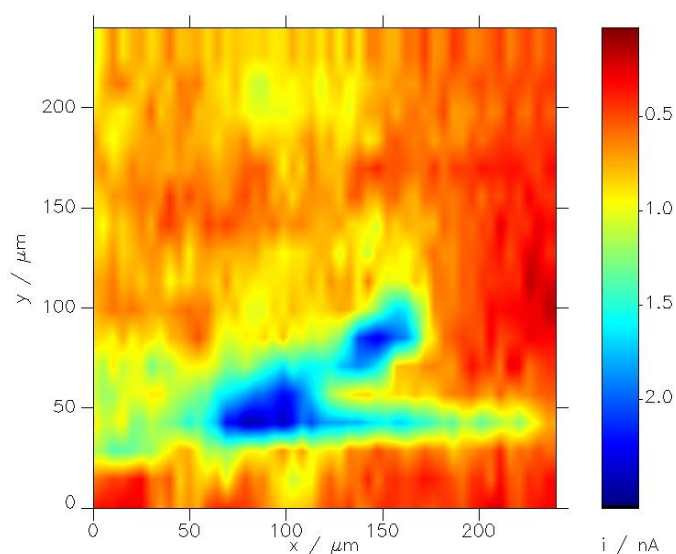


Figure 17: SECM image of the region where the Si electrode was abraded.

It is noticeable the increase in the current originated from the electron transfer and thus regeneration of the DBDMB through what is probably a crack on the SiO₂ insulating layer.

Secondly, the SiO₂ layer was removed from an electrode by HF etching. In this case, the layer is expected to be effectively removed from the Si surface. Therefore, XPS was performed in order to compare the elemental composition of the HF etched electrode, the electrode that was abraded with the ME during the SECM experiment and a pristine electrode without any previous treatment, containing the native SiO₂ layer. Figure 18 shows the sample holder with the three samples. The electrode that was analyzed in SECM prior to the XPS (a) was marked with a glass cutter, so the same region where the abrasion occurred could be investigated.

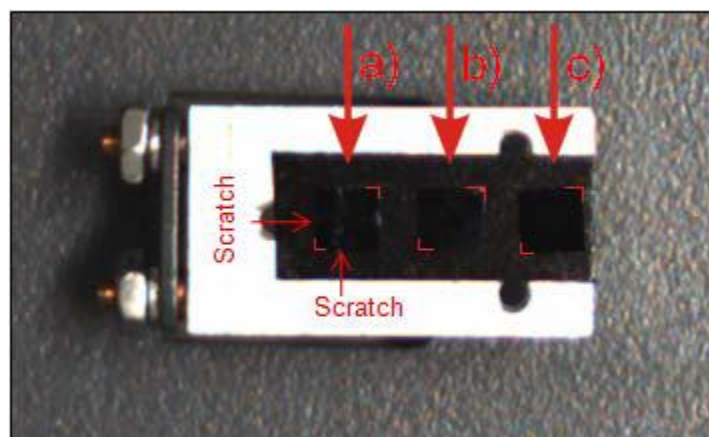


Figure 18: XPS sample holder with (a) the abraded Si electrode (marked with a glass cutter), (b) the HF etched electrode and (c) the pristine Si electrode. Adapted from ref.³⁶

The first experiment performed was survey spectra of each electrode to observe the different compositions, as it is shown in figure 19a. The amount of oxygen observed in the etched electrode is lower in comparison to the other two, as expected by the removal of the SiO₂. What was also observed is the increase in the carbon intensity peak on the etched and on the abraded electrodes, especially in the case of the abraded one. This is possibly due to residuals of the organic solvents used in the SECM experiments.

For further investigations regarding the Si composition, high resolution Si 2p spectra were obtained (Figure 19b). It is already possible to observe in the fitted peak that is associated to SiO₂ (Si⁴⁺) and other oxidation states of the Si with

binding energy around 103.5 eV²⁶⁸ presents a significant reduction in the HF etched sample, but in the case of the abraded electrode, the same behavior is not expected. The ratio is just slightly different than the pristine Si electrode.

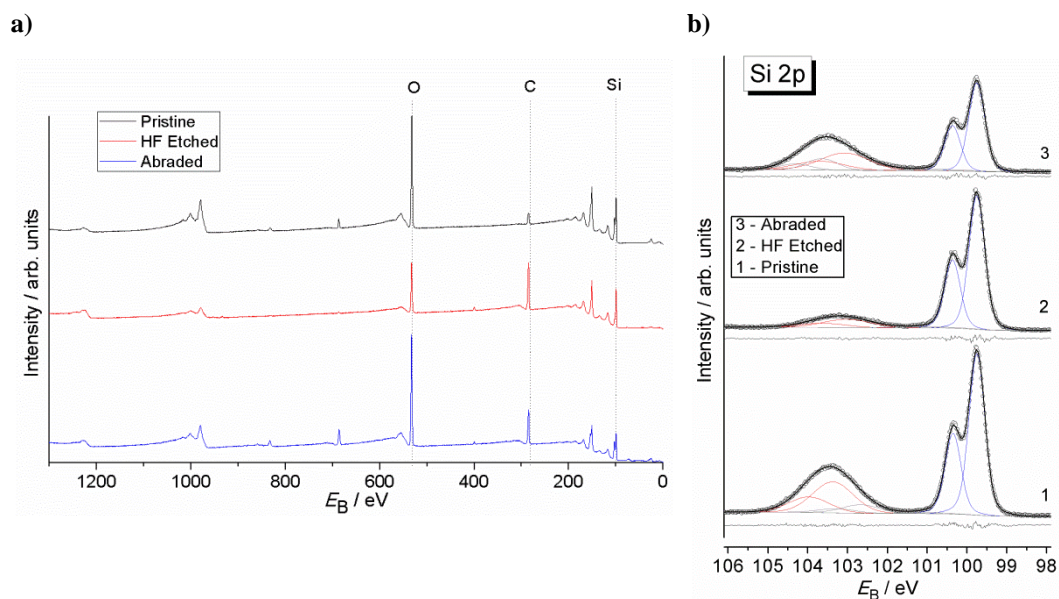
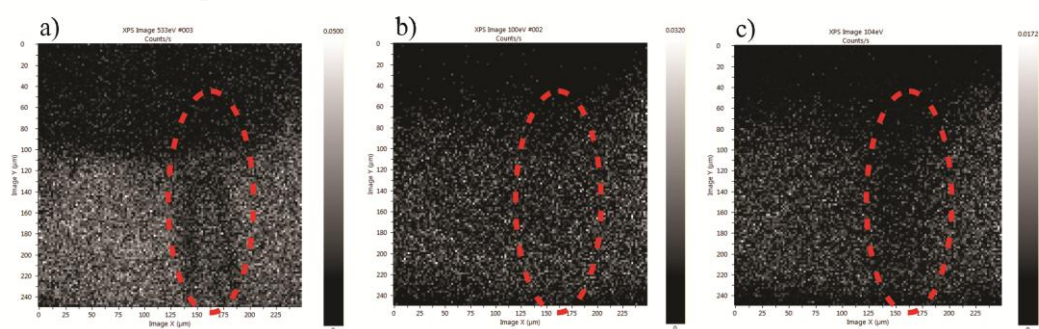


Figure 19: (a) Survey spectra of a pristine, a HF-etched and a mechanically damaged Si electrode. Si 2p, O 1s and C 1s peaks are indicated as they showed the most notable changes; (b) Si 2p Spectra and fits of (1) the pristine, (2) the HF etched and (3) the mechanically abraded Si electrode. Adapted from ref.³⁶

Figure 19b also presents the fits for the peaks associated to the elemental Si, with binding energy at 99.5 eV.²⁶⁸ They present some different ratios, especially in the abraded electrode. This indicates that the mechanical abrasion did not remove a relevant amount of the SiO₂ layer, but has changed the passivating properties by introducing mechanical damage. It is also important to mention that the abrasion is made by the Pt and mostly by the glass sheath, which are softer than the SiO₂ layer.

Further questions kept unresolved, therefore XPS imaging and AFM imaging were employed as an attempt to see if the abrasion could be observed not only by the electrochemical response. Figure 20 shows the XPS imaging, where two regions of the abraded sample were investigated, one where the abrasion occurred and another above the eye visible marks made with the glass cutter. On the region where the electrode was marked using a glass cutter, it can be seen in figures 20a and 20c, which corresponds to the energies of O 1s and Si 2p of SiO₂, the effective damage, whereas in the abraded region, no apparent removal or damage can be observed.

Glass cutted region:



Abraded region

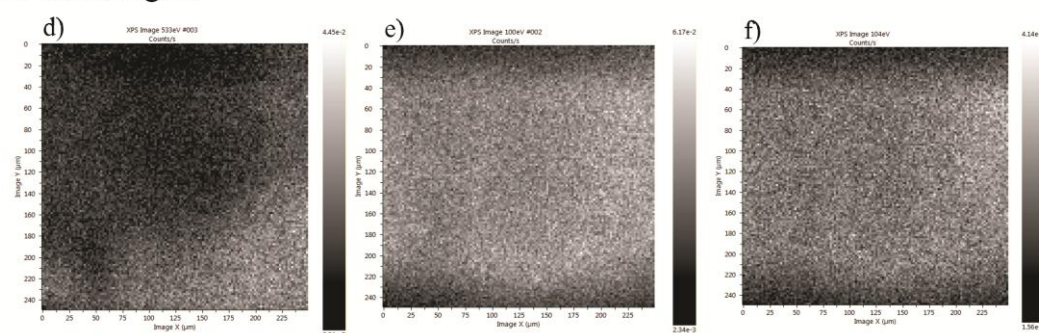


Figure 20: XPS imaging of (a) – (c) the region with mechanical damage by the glass cutter (indicated by the red circles) and (d) – (f) the region abraded by the ME. The images are based on emission of O 1s, $E_B = 533$ eV (a and d), Si 2p (elemental Si), $E_B = 100$ eV (b and e) and Si 2p (SiO_2), $E_B = 104$ eV (c and f). Adapted from ref.³⁶

AFM was also used in order to observe the abrasion, but as previously discussed, the abrasion with the ME does not remove enough SiO_2 to be seen, but only enough to allow the diffusion of electrons through the layer and generate the higher current observed in the SECM image.

Further experiments were carried out to calculate the thickness of the SiO_2 layer before the SEI formation. The idea was to use ARXPS, changing the angle of analysis from 0° to 50° , and calculate considering the different attenuation lengths (λ) that the pristine material and the SiO_2 layer as well as the path the irradiated electrons have to cross when the sample gets tilted inside the equipment. Figure 21 shows a schematic representation of the length of the paths the electrons have to cross at the starting and the final angle of the measurement performed and the corresponding spectra.

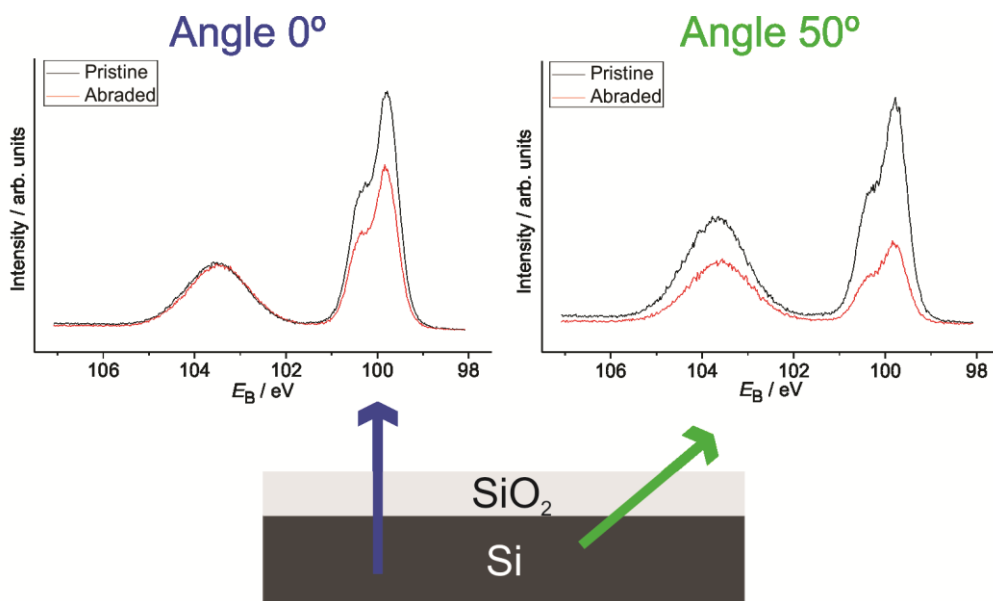


Figure 21: Schematic representation of different analysis angles and the path of the emitted electrons. It causes that the spectra at 0° present more information about the bulk material and at 50° more information about the overlayer.^{36,268}

For the calculations of thickness the Eq. 9 considering the ratios between the photoelectron intensities in Si and in SiO₂ (R), the reference ratio between the photoelectron intensities on such materials in thick (over 100 nm) layers (R^∞), the layer thickness (d) and the attenuation length.²⁶⁹

$$\ln \left[1 + \frac{R}{R^\infty} \right] = d/\lambda \cos\theta \quad (\text{Eq. 9})$$

The values obtained were 2.58 nm for the pristine electrode and 2.30 for the abraded electrode. The difference between both values is within the error margin of the method²⁶⁹ and leads to the conclusion that the SiO₂ layer did not suffer any interference on its thickness neither by the abrasion nor by the contact or deposition of the electrolytes employed in the SECM investigations.

6.2 Charging of the Si Electrode

Towards the investigation of the SEI on Si electrodes, the charging process is known to be of key importance. After a discussing with collaboration partners Dr. Michael Sternad and Prof. Martin Wilkening, an experiment was planned in order

to follow the SEI formation of the anode in situ while imaging with SECM, according to parameters also found in literature.^{24,76}

The first step of the experiment was the etching of the Si electrode using hydrofluoric acid to remove its native SiO₂ layer. By doing so, a crystalline and non-passivated surface was obtained. The electrode was then placed into the SECM setup and contacted through a Cu foil attached to the back of the electrode that had no contact to the electrolyte. Several discharging/charging cycles were applied. The cycles consisted in a CV with slow scan rates ($\mu\text{V s}^{-1}$ range) starting from 1.2 V vs. Li/Li⁺, where no SEI formation or lithiation are expected down to 0 V. Then the potential was swept back to 1.2 V vs. Li/Li⁺. In between each cycle, the same region of the electrode was imaged via SECM. Figure 22 shows the cyclic voltammograms recorded during these charging experiments of the Si electrodes.

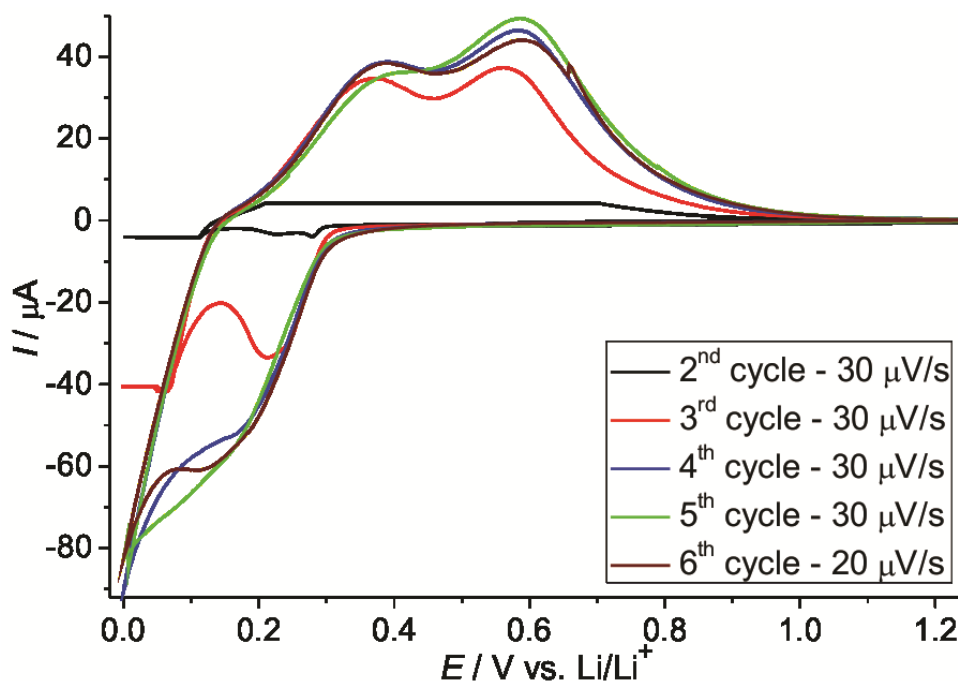


Figure 22: Sequential charging/discharging cycles applied to the Si electrode and its scanning rates. The experiment was performed in 5 mM DBDMB mediator and 1 M LiClO₄ in propylene carbonate.

The first cycle does not appear because it had a current range that was much lower than the following. In these cycles, it cannot be seen any peak within the expected range of the SEI formation ($0.5 \text{ V} < E < 1.2 \text{ V}$),^{24,68,76} as the lithiation peaks have much higher current values and can be seen starting from around 0.3 V for the

charging process. During the discharging, two peaks that can be related to the Li ions leaving the Si electrode can be observed. It is also important to mention that no signal from DBDMB was visible, which is a requirement to make intermittent SECM imaging using this mediator.

Figure 23 shows the SECM images recorded with the ME prior to the cycling and between each of the charge/discharge cycles. All of them were recorded at the same region of the electrode. The trend of a current decay could be observed after consecutive cycles. Also, some features started to appear during the experiment.

As discussed with collaborators, the first time potential is applied to a Si electrode, its behavior is not reproducible. In this case, not much could be seen and this will be further discussed in chapter 6.3 where the charging will be discussed more in detail.

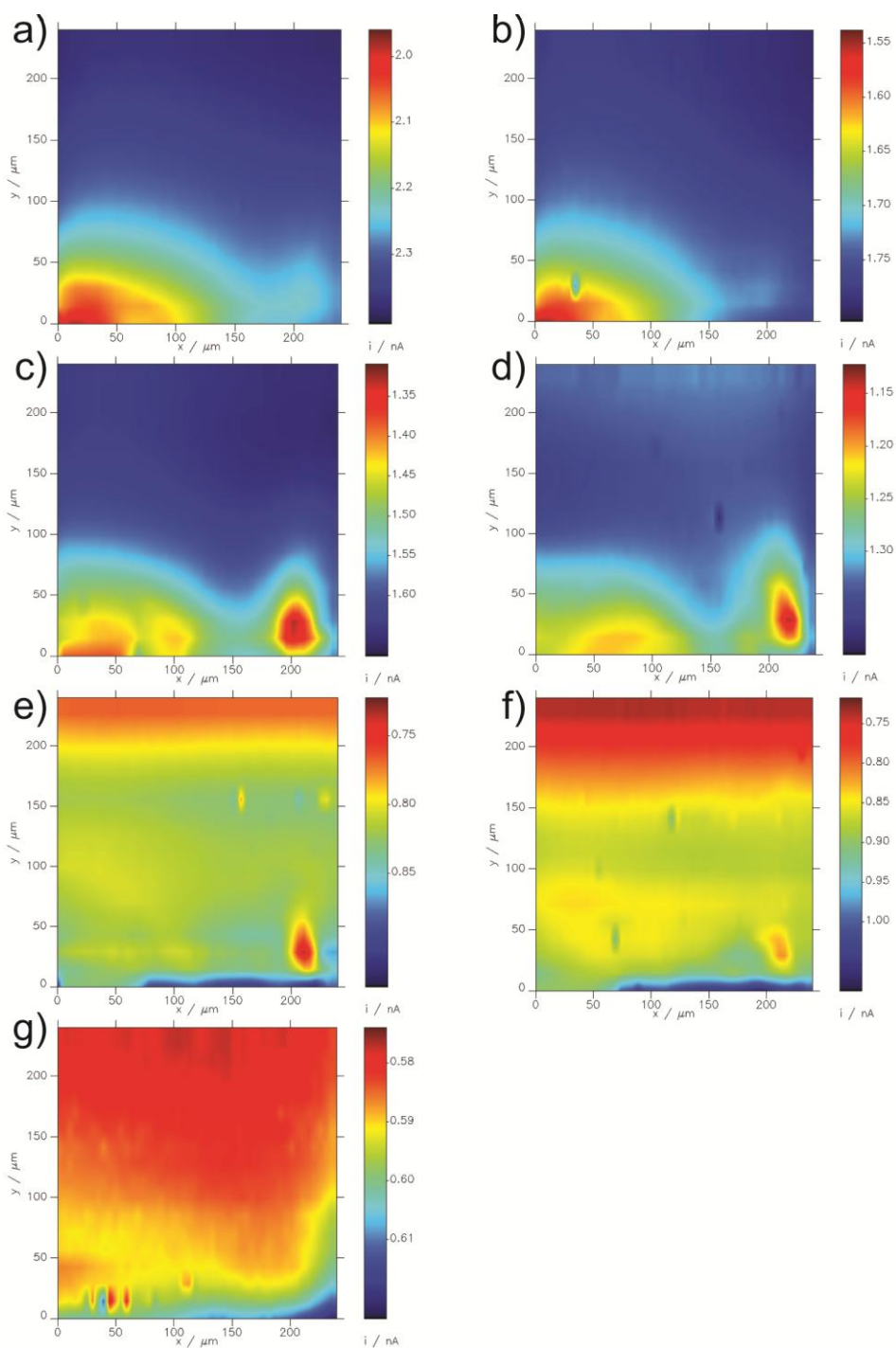


Figure 23: SECM images recorded in 5 mM DBDMB mediator and 1 M LiClO_4 in propylene carbonate (a) before any cycling; (b) after the first; (c) after the second; (d) after the third; (e) after the fourth; (f) after the fifth and (g) after the sixth charge/discharge cycle.

The current decay after the second cycle (fig. 23c) is accompanied with the appearance of some features in the lower area of the image ($y < 50 \mu\text{m}$). Such features appear on all the following images up to the last one (fig. 23g). Both the decay and the low current features can be associated to SEI formation and lithiation of the electrode. Figure 24 shows the data of the current decay along the

experiment. The data points are the arithmetic mean of the i_T current and the $i_{T,\infty}$ after each charging cycle from figure 23. It shows that the decay seem especially in the last images of figure 23 are related to the passivation of the Si electrode, not to the degradation of the ME.

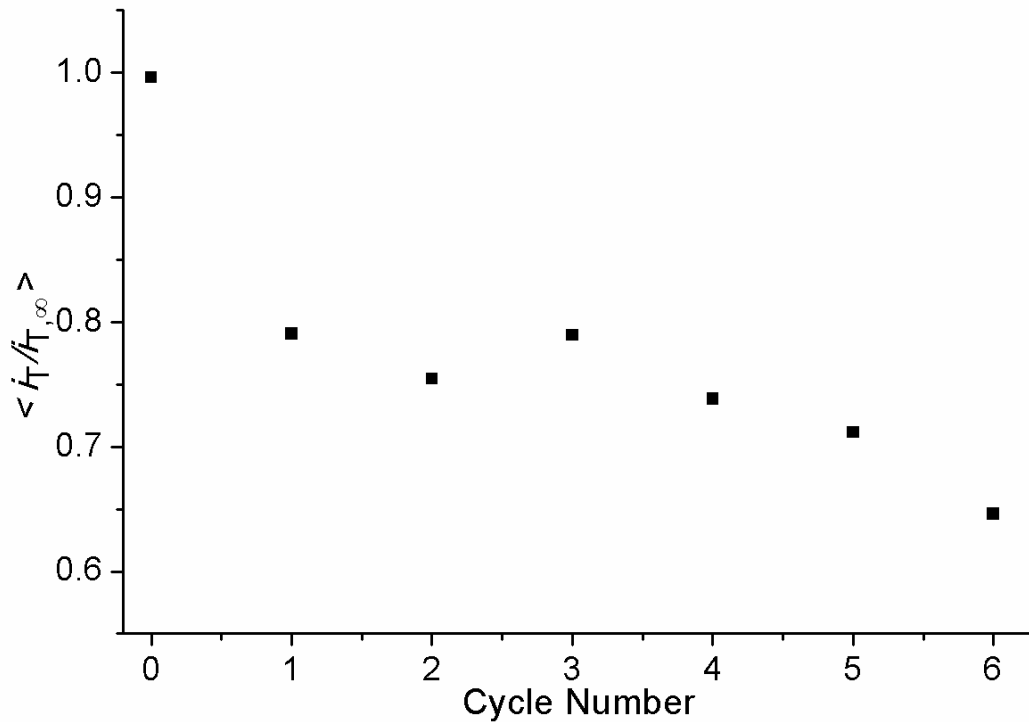


Figure 24: Current decay along the experiment expressed by $\langle i_T/i_{T,\infty} \rangle$.

The charging of a pristine Si electrode is known to have high charge capacity but face several structural problems with the Li insertion.^{68,69} From the fourth cycle on, the images (fig. 23e-g) had a change on the overall aspect (major current decay) in comparison to the previous ones, containing more spikes and an overall only a negative feedback response. These results led to the suspicion of loss of mechanical stability of the electrode. Therefore, the experiment was ended and after disassembling the electrode was broken, as can be seen in figure 25.



Figure 25: Broken Si electrode after the experiment.

6.3 The Interrupted Charging Experiment

The loss of mechanical stability of the Si electrodes was clear with the full charge/discharge cycles, when the potential was swept to the lithiation range. When considering literature values^{68,69} and further discussions, an alternative approach was developed: to prevent the lithiation by charging the electrode just up to the potential range of the SEI formation.

When looking at figure 22, it can be said that the lithiation process is expected to occur starting only below 0.5 V^{24,76} and this is the phenomena responsible for the mechanical issues. Therefore, the experiment was planned to avoid this potential range. Furthermore, instead of a single charging cycle, the idea was to perform the charge of the electrode in linear sweep voltammetries (LSVs) of 0.1 V intervals at a very slow scan rate ($20 \mu\text{V s}^{-1}$) while the ME is kept away from the Si electrode (5000 μm). In between each LSV, the ME is approached and the same region of the electrode is imaged. Figure 26 presents a schematic representation of the procedure in its two different steps.

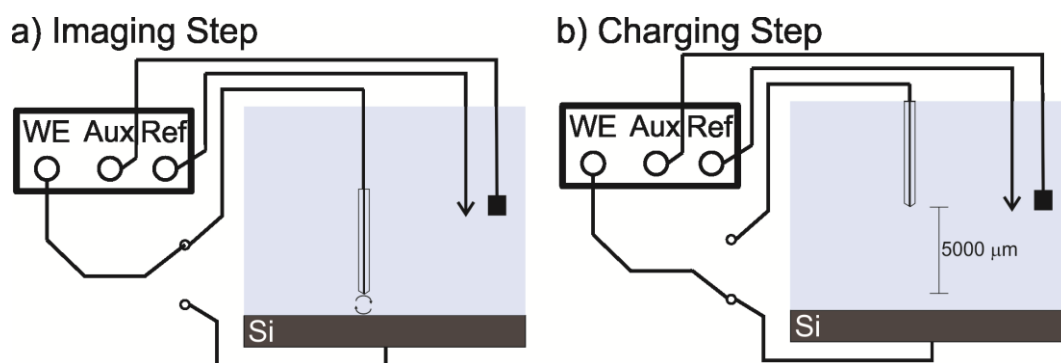


Figure 26: Schematic representation of (a) SECM imaging with a constant potential applied to the ME and (b) charging of the Si electrode by sweeping the potential of the Si electrode while the ME is retracted and at OCP. Adapted from ref.²³¹

At first, the steps were performed without any equilibration time, which led to the profile that can be seen in figure 27. This made possible to investigate this complex process happening step-by-step.

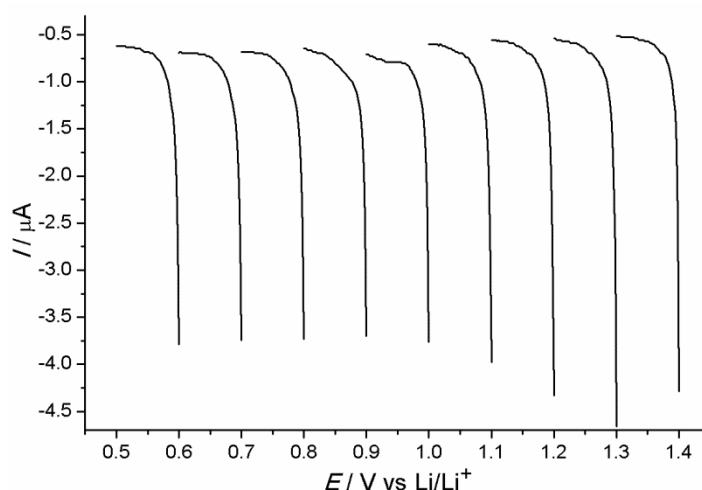


Figure 27: LSVs performed for the potentiodynamic charging of the Si electrode at $20 \mu\text{V s}^{-1}$ in 5 mM DBDMB mediator and 1 M LiClO_4 in propylene carbonate without equilibration time.

After the experiment, it was not possible to observe any relevant changes but some few variations within the most critical potential range $1.0 - 0.7 \text{ V}^{24,76}$ of SEI formation. It was then further discussed and the main reason for that would be that the system would not be in equilibrium when the measurement started. Therefore, a 15 minutes waiting time was added between charging step and SECM characterization. Figure 28 shows the charging profile, presenting much clearer variations of the plateau current at the end of each LSV charging pulse.

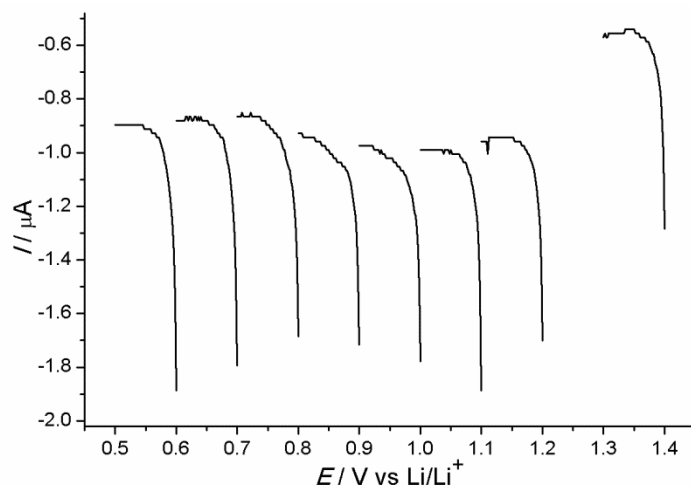


Figure 28: LSVs performed for the potentiodynamic charging of the Si electrode at $20 \mu\text{V s}^{-1}$ in 5 mM DBDMB mediator and 1 M LiClO_4 in propylene carbonate with 15 minutes equilibration time between steps. Adapted from ref.²³¹

In the case of the optimized parameters, a peak-shaped profile with its maximum around 1.0 V can clearly be seen when connecting the plateau values of each LSV. The behavior presented in figure 28 corroborates directly to what was observed during SECM imaging. As mentioned before, the ME is retracted during the charging pulses to avoid any side reactions at the ME.

After each of the LSVs the potential control is applied to the ME and the Si electrode is left at OCP.²³¹ Sequentially, the ME was slowly approached to a position approximately $5 \mu\text{m}$ away from the surface in order to perform the SECM imaging. It is shown in figure 29 the images recorded at the same region of the electrode throughout the whole experiment.

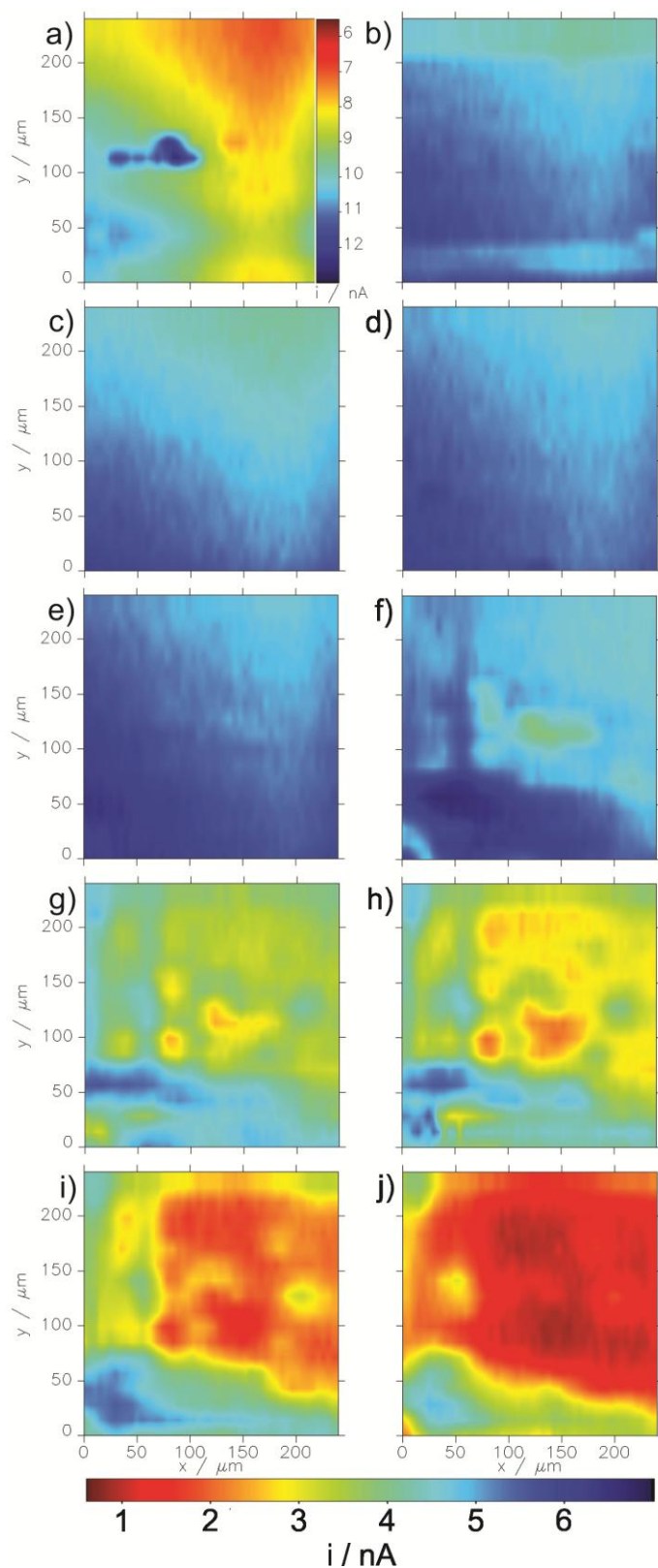


Figure 29: SECM images taken from an identical region of the Si electrode in 5 mM DBDMB mediator and 1 M LiClO₄ in propylene carbonate. **(a)** Before applying external potential control to the Si electrode; **(b)** after sweeping from 2.0 to 1.4 V; **(c)** 1.4 – 1.3 V; **(d)** 1.2 – 1.1 V; **(e)** 1.1 – 1.0 V; **(f)** 1.0 – 0.9 V; **(g)** 0.9 – 0.8 V; **(h)** 0.8 – 0.7 V; **(i)** 0.7 – 0.6 V and **(j)** 0.6 – 0.5 V; $E_T = +4.1$ V, $r_T \approx 12.5$ μm . Adapted from ref.²³¹

The SECM image presented in figure 29a was recorded prior to any LSV and shows a maximum ME currents of approximately 12 nA. Figure 29b shows the image after the application of an external potential where no SEI formation is expected (E_S of 2.0 V swept to 1.4 V). This lead to the little current variation between the figures 29a and 29b apart from noise and sample tilt.

The images in figures 29b-e present only small changes (between E_S of 1.4 V and 1.1 V). The formation of a V-shaped region with lower currents in the upper right part of the imaging frame has an average current of about 5 nA, which is lower than in the rest of the image. However, the uniformity of the V-shaped region changes to a heterogeneous pattern with spots of very low ME currents when the final charging potential approaches the plateau with the largest reduction currents (fig. 29f) where the potential is around 1.0 V vs. Li/Li⁺. The growth patterns are reminiscent to a nucleation process,²⁷⁰ but have also been observed for electropolymerization processes^{271,272} and grafting of organic layers to electrodes. Such reduction-induced polymerization of organic electrolyte components (which in this case is propylene carbonate) results in passivating layers on the Si electrode.

Even on an almost atomically flat Si electrode, the reduction of electrolyte components and the deposition of insoluble reaction products do not occur uniformly but in concentrically spreading spots. While electron transfer reactions occur fast at some parts of the Si electrode, regions of about 50 μm diameter are visible, in which electron transfer reactions are inhibited due to passivation. The growth of the regions with low ME currents after subsequent charging LSV, are indicative for spreading pristine SEI layer, forming until its completion in the lower areas of the image that can be seen in figures 29i-j.

The observation of a local onset of SEI formation on a nearly atomically flat electrode is a novel finding and might be essential for the understanding of film formation on Si. Formation of organic layers has often a local onset, where a critical amount of organic material must be deposited first to form a new phase, that can grow further forming a film. The growth perpendicular to the electrode surface remains small if the organic layer is electronically insulating. In the present case, the lateral dimensions of incipient SEI are clearly detectable for with micrometer resolution.

An alternative way of observing this process and the overall current development along the experiment is with a histogram constructed from the ME currents of the SECM images in figure 29 with a binsize of 3% of the current range of each image. Figure 30 presents that the image before charging has a very high average current and most of the data points above 8 nA. Furthermore, as the potential reach 1.1 V, the current decay is evident. The shape of the histograms is maintained in the next three images.

When the potential of $E_S = 1.0$ V is reached (corroborating the maximum of the reduction currents plateaus in figure 28 and the first indications of SEI nucleation in figure 29f), the overall current decreases to much lower values (0.0 – 4.0 nA) although cyclic voltammograms at the ME far away from the surface prove that this does not correspond to a decay on activity or passivation of the ME probe, which indicates a passivation of most parts of the scanned area. After scanning the Si electrode to $E_S = 0.9$ V, there is a further significant decrease of the ME current that result in an increasing width of the histograms. This trend continues in the images recorded after charging to 0.8 V, 0.7 V, 0.6 V and 0.5 V indicating a nearly complete coverage of the Si electrode by a passivating SEI layer.

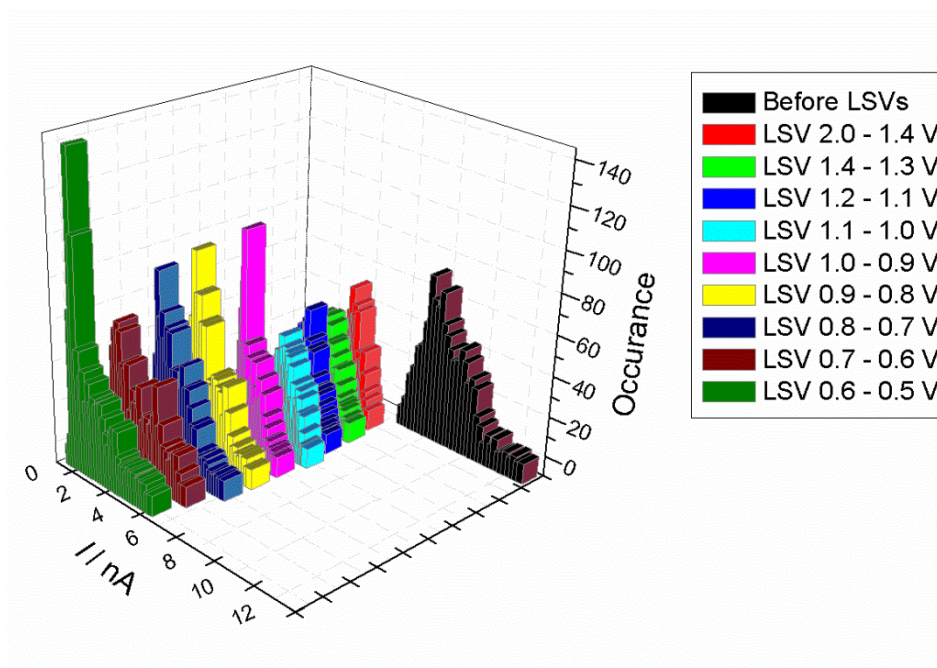


Figure 30: Histograms of ME currents within SECM images. Adapted from ref.²³¹

7 Reactivity at Lithium Electrodes

This chapter presents the experiments performed with metallic lithium anodes that were prepared by using a recently developed device²⁵⁸ which provides a fresh tunable surface containing a SEI precursor. Our collaborators provided samples cut in various solvents, prior and after cycling in a battery cell, in order to observe and understand the phenomena occurring under such conditions.

Also important to mention, is that for this case, the electrolyte in the SECM experiments was an ionic liquid, also synthesized by our collaborators, lithium bis(trifluoromethanesulfonyl)imide : 1-butyl-1-methylpyrrolidinium bis (trifluoromethanesulfonyl)imide (Pyr14TFSI/LiTFSI) which is expected to bring advantages to the operation of batteries (e. g. less safety issues) and influence differently the SEI or dendrite formation in comparison to commonly used electrolytes. The cycling was performed within the ionic liquid for 100 times at 0.1 mA/cm^{-2} .²⁵⁸

7.1 Electrochemistry in an Ionic Liquid Electrolyte

The first challenge during the experiments was the electrochemistry in the ionic liquid itself. Despite the much lower diffusion rates and much higher viscosity in comparison to the common battery electrolytes and the one used for the Si electrodes, consistent results were obtained with the ionic liquid provided by the collaboration partners.

The first point was the solubility of the mediator, but apart from taking a longer time to get dissolved in comparison to the regular electrolyte, this revealed not to be an issue since the first attempts. Figure 31 shows the comparison of CVs between a 5 mM solution of DBDMB in the commercial BASF G27 and in Pyr14TFSI. The CV in figure 31a recorded with 20 mV s^{-1} scan rate in BASF G27 shows a stable sigmoidal response expected for a ME. Contrarily in the Pyr14TFSI (fig. 31b) at the same scan rate, the current is much smaller and the profile is not of a hemispherical diffusion.²⁷³ This is due to slow diffusion rates and the fact that there is no stationary state during the measurement. It was necessary to record the CV with a much lower scan rate of 1 mV s^{-1} , so the

sigmoidal profile could be seen. This also required that equilibration times during SECM experiments to be adapted.

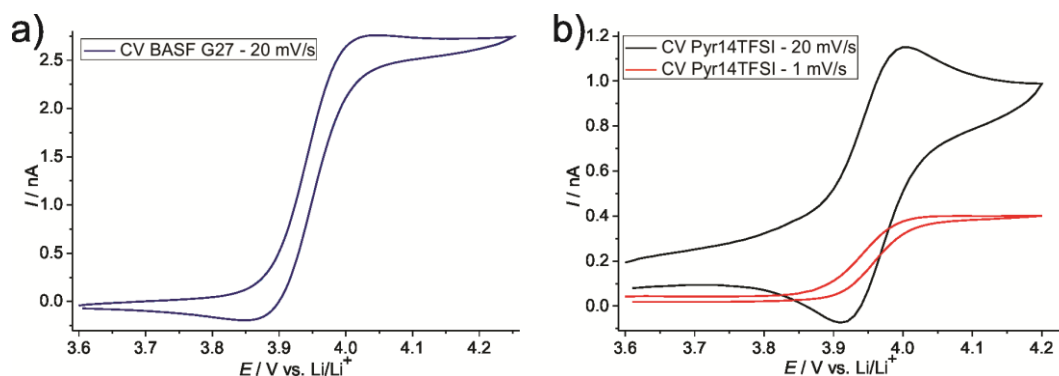


Figure 31: CVs recorded in the bulk of 5 mM solutions of DBDMB in (a) BASF G27 and (b) Pyr14TFSI with different scan rates. $r_T \approx 12.5 \mu\text{m}$.

7.2 SECM and SEM Investigations

Following the preliminary tests and the adaptations of the parameters for working with the ionic liquid, proper experiments with Li electrodes cut with the device developed by the collaborators were carried out. The electrodes were cut in 2.3 mm thick slices from metallic lithium rods inside a glove box with a polypropylene device. The cylindrical chunk was placed in between two jaws inside a beaker and a SEI precursor could be added through small channels. Using a winder and tungsten wires, the Li is cut in a very smooth surface.²⁵⁸

This device made it possible to obtain fresh lithium surfaces with no previous contact with no species but the SEI precursor.²⁵⁸ This can provide tunable surfaces for analysis under inert atmosphere, different electrolytes and even the possibility of varying SEI properties. By this, it is possible to evaluate with higher precision the electrochemical behavior of the material without contact with any undesired solution or gas that could affect the SEI formation or react with the Li surface.

The Li electrodes chosen were cut in three different solutions: neat pentane, 0.1 M pentylamine in pentane and 5 M pentylamine in pentane. The pentylamine added to the solution in different concentrations is expected to influence the SEI formation by the reaction forming Li_3N , which can prevent the side reactions between the lithium and the carbonate-based electrolytes. Besides,

fast Li^+ diffusion from the electrolyte to the Li surface occurs due to fewer reduction species in the electrolyte with Li_3N modification on the Li anode, forming a stable SEI of low resistance.²⁷⁴ Besides, pentane is not expected to react with it and the dissolution helps to control the thickness of the SEI formed. On performance tests, the 0.1 M solution of pentylamine in pentane, the overall interfacial resistance of the electrodes were decreased and performed with much higher stability than with only pentane or with concentrations higher than 1 M pentylamine in pentane.²⁵⁸ The 5 M solution had a negative impact on the SEI due to either dissolution of the primary SEI components or swelling of the organic SEI layer formed.²⁷⁵

After the cutting, the electrodes were sealed and sent from our collaborators. Upon arrival the package was open inside the glove box and the electrode was mounted in the SECM setup for analysis. In order to treat the approach curves according to the model of Cornut and Lefrou²³² it was necessary to obtain a d_0 value that correspond to the closest distance to the substrate. Therefore, approach curves using the mediator solution in the ionic liquid with the same ME used for the other approach curves to the Li electrodes. Figure 32 presents one approach curve to a glass substrate in a function of normalized current (Eq. 5) vs. the normalized distance (Eq. 6).

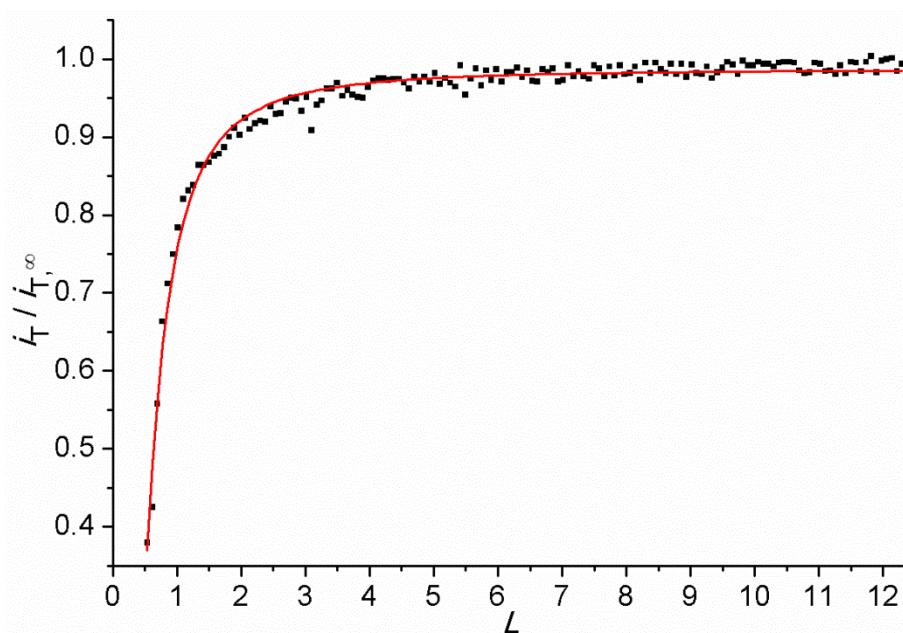


Figure 32: Approach curve using 5mM DBDMB in the ionic liquid. The dots are the data points and the line is the curve fit using the insulator model of Cornut and Lefrou.²³² ($E = +4.1$ V, $r_T = 12.5$ μm , $RG = 5.5$; fitted $r_T = 10.52$, $d_0 = 6.72$).

Figure 33 presents examples of approach curves and SECM images of the electrodes cut in the different solutions. The profile of the approach curves appear to be of finite kinetics, which means that when the ME is approached but is still a few r_T to the Li surface, the regeneration occurring is fast enough to compete with the diffusion happening, leading to the i_T increase as the distance decreases. Further during the approach curve, when the ME gets much closer to the Li, the diffusion of species within the electrolyte between the ME and the substrate becomes faster, leading to the limiting of the feedback and the i_T decreases.

Some heterogeneity can be seen in the ME current in the images which are related mostly to sample tilt or some small variations. Otherwise the current in each image is rather homogenous. It can be seen that the current on the bulk ($i_{T,\infty}$) varied according to the samples, which is related to eventual variations on the batch of ionic liquid received from the collaboration partners.

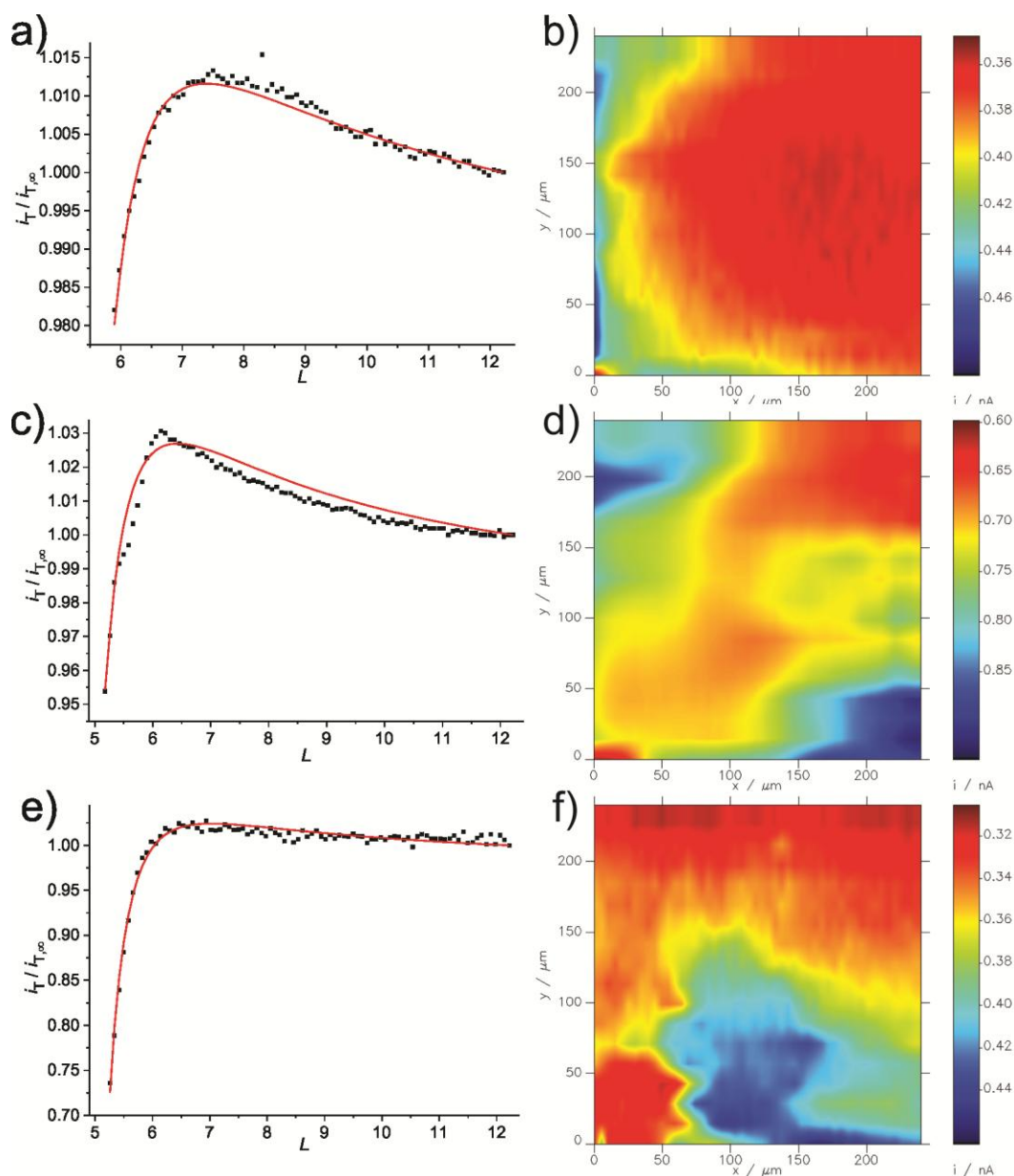


Figure 33: Approach curves and images from the cut electrodes without any previous electrochemical treatment. The electrodes were (a)/(b) cut in pure pentane; (c)/(d) cut in 0.1 M solution of pentylamine in pentane and (e)/(f) cut in 5 M solution of pentylamine in pentane. (Approach curves: 1 μm step size, $E = +4.1$ V, $r_T = 12.5$ μm , $RG = 5.5$, fitted with finite kinetics model).²³²

Another set of electrodes were cycled by the collaboration partners. After the cutting procedure described, the electrodes were put in symmetric cells and cycled galvanostatically at 20 $^{\circ}\text{C}$ with current density of 0.1 mA cm^{-2} . The cut-off potentials were ± 0.5 V vs. Li.²⁵⁸ After cycling for 100 times, the electrodes were again sealed and sent for SECM investigations. Figure 34 presents the approach

curves and images of the electrodes prepared in the same three conditions as the ones presented in figure 33.

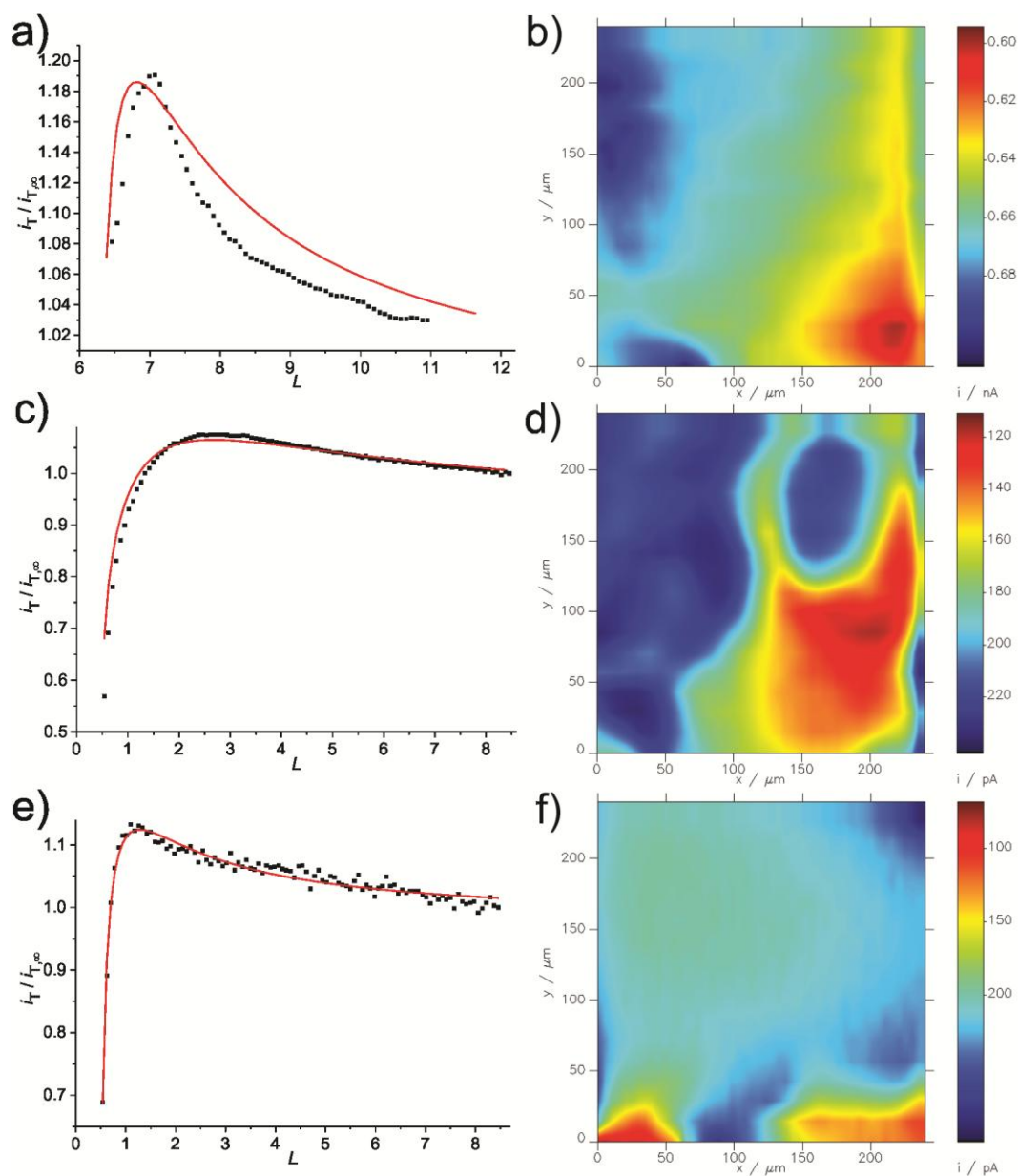


Figure 34: Approach curves and images from the cut electrodes after 100 cycles of galvanostatic charging. The electrodes were (a)/(b) cut in pure pentane; (c)/(d) cut in 0.1 M solution of pentylamine in pentane and (e)/(f) cut in 5 M solution of pentylamine in pentane. (Approach curves: 1 μm step size, $E = +4.1$ V, $r_T = 12.5$ μm , $RG = 5.5$, fitted with finite kinetics model).²³²

By observing the approach curves first, in general they keep the profile of finite kinetics approach just with an overall lower current on the cycled samples. Specifically looking at the electrode cut in pentane, the cycled one (fig. 34a) the current variation was lower than 0.1 nA, which made it hard for mathematical

fitting and reproducibility. That did not seem an issue with any other electrode. Regarding the images, heterogeneities over the scanned area could be seen in most of the cases. As SECM presents convolved information about topography and electrochemical activity, there was still the need to investigate better if the behavior was just due to topographic features or other processes happening on the electrode surface, such as SEI or dendrite formation.

In order to further investigate the electrodes, the region imaged by SECM was marked macroscopically and the electrodes were then stored, sealed inside the glove box and sent back to the collaboration partners for SEM investigations on their equipment that can operate under inert conditions inside a glove box. Figure 35 shows the SEM images recorded of the electrodes in all the investigated conditions.

The first point to consider when looking and comparing the SECM and SEM images is that both techniques scan very small areas with different resolutions that are not visible to the eye. This makes it very different to image the precisely same area even with all the markings on the sample after the SECM and prior to be sent back for the SEM. Another problem can occur during the removal of the electrode from the SECM setup. Despite it was done very carefully, can also happen some bending may happen before the marking, which could lead to a larger difference in the micrometric range.

First, when comparing the images of the electrodes cut in pentane, in uncycled and cycled condition, the current variations in the SECM images are around 0.1 nA (fig. 33b and 34b), while the sample does not have any clear features or any apparent SEI visible in the SEM pictures (fig. 35a-b). This effect is expected, as there is no SEI precursor added in the solution and the current variations are probably just related to sample tilt.

When comparing the electrodes cut in 5 M pentylamine in pentane, the electrode shows a rougher surface without cycling (fig. 35e), while the SEM image show some kind of agglomeration formed probably before the start of the SECM experiment (fig. 33f). In the cycled electrode it looks smoother, only a few topographic variations can be seen (fig. 35f) which correspond to what seems like an inhomogeneous coverage related to the negative effects of such high concentrations of pentylamine in solution, that cannot be conclusively associated to what can be seen in the SECM (fig. 34f).

The electrodes cut in 0.1 M pentylamine in pentane present a general roughness in the SEM (fig. 35c) that can be seen in the SECM image (fig. 33d). For the comparison with the cycled electrode, one feature appears in the SEM (fig. 35d) that can be related to a similar feature in the corresponding SECM image (fig. 34d).

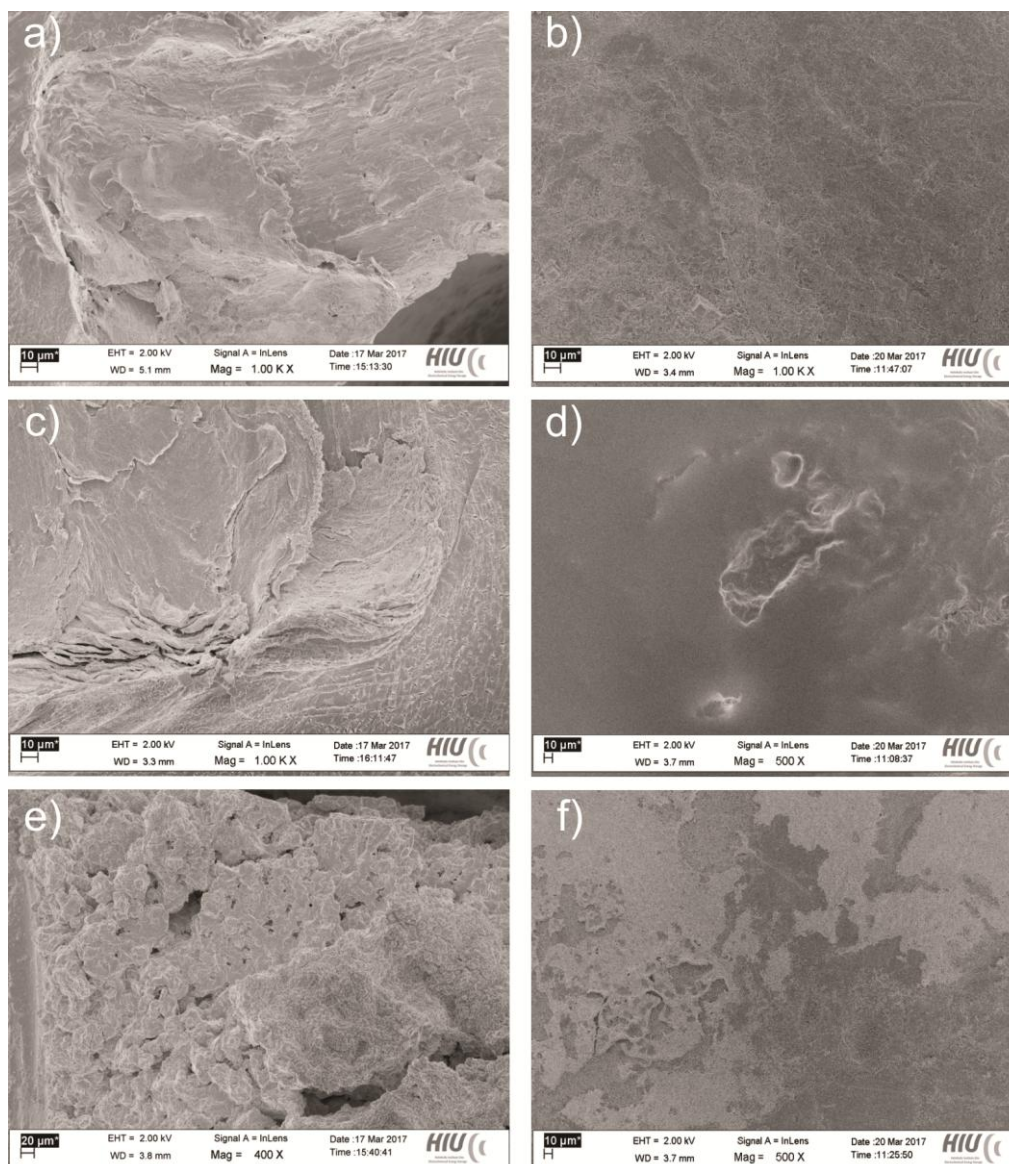


Figure 35: SEM images recorded from the different Li electrodes. (a) cut in pentane, uncycled; (b) cut in pentane, cycled; (c) cut in 0.1 M pentylamine in pentane, uncycled; (d) cut in 0.1 M pentylamine in pentane, cycled; (e) cut in 5 M pentylamine in pentane, uncycled and (f) cut in 5 M pentylamine in pentane, cycled.

The feedback current measured on the ME appear to be higher in the regions with higher topographic features in the images prior to charging, while in this case and for the most it can be compared for the cycled images, this appear to

be the opposite, the current is lower in the regions that appear closer to the ME, indicating the formation of a passivation layer after cycling. In figure 36, the SEM image was cut and rotated so it was easier to compare it with the SECM image. It can be seen on the right region of the SECM image a lower current feature. This feature may be related to a heterogeneously covered region of the electrode and it can also be seen on the SEM image. Such observations corroborates with the performance tests in different concentrations of pentylamine in pentane, as the surface influence of the SEI precursor being the most beneficial effects to the electrode performance in the case of the 0.1 M solution (or the 1 M solution).²⁵⁸ On the top region of both images, it appears a smaller feature that can indicate a growing dendrite.

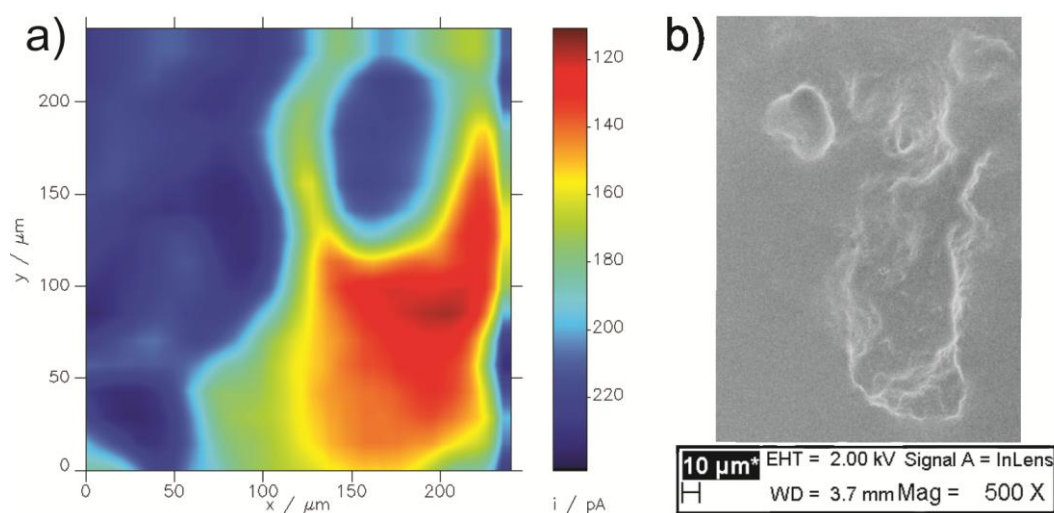


Figure 36: Comparison of the (a) SECM image from figure 34d from the cycled electrode cut in 0.1 M pentylamine in pentane and (b) section of the SEM image in figure 35d of the same electrode area.

8 Investigations at Cathode Materials

This chapter refers to investigations performed with different cathode materials. In this case, most of the work aim was different than in previous chapters. Anode materials are vastly more investigated, therefore the need to find a suitable mediator to work with cathode materials was the first challenge.

Subsequently, a standard cathode (LFP) and a high voltage (NMC) material were investigated using SECM and SEM, comparing what can be observed from topography and electrochemical behavior. Additionally, the samples were investigated in different states of charge in order to observe a potential CEI formation.

8.1 Mediator for Cathodes

The mediator for SECM investigations of cathode electrolyte interphases has similar requirements as the mediator for anodes, such as stable performance with the electrolyte and the electrodes and solubility. On the other hand, the operation potential window is different. The mediator must be first reduced at the ME so that the oxidation proceeds at the cathode material.

After researching literature,²⁷⁶ a number of compounds were selected for testing. For the first tests, the same concentration was used as for the DBDMB (5 mM) in the G27 electrolyte. The compounds selected for a first round of tests were: 2,3-dichloro-5,6-dicyano-1,4-benzoquinone (DDQ), anthracene, azobenzene, 9,10-bis(phenyl-ethynyl) anthracene and ruthenium-tris(2,2'-bipyridyl) chloride. Within those compounds the DDQ was selected due to its multiple substituted structure (fig. 37) and its proven stability,^{277,278} although it has never been used before for any kind of SECM applications in the field of batteries. Anthracene also seemed to present a good stability and solubility in the electrolyte as well as working potential in an appropriate range. The compounds were added to the electrolyte and presented good cyclability, stability towards the ME and the system and are viable in the potential range needed for cathode investigations. All the experiments were performed using a Ag wire as a reference electrode and a Pt wire as a counter electrode.

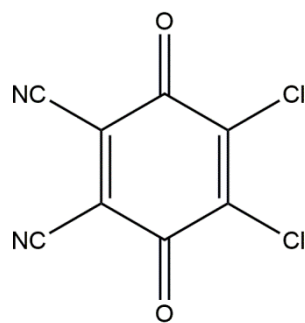


Figure 37: Structure of the DDQ.

In the case of the DDQ, the CV can be seen in figure 38. The molecule has two stable and reversible reduction reactions between -0.6 V and 0.3 V (vs. Ag). On our anode-related experiments the voltage of the ME is 4.1 V vs. Li/Li⁺ during imaging. While using the DDQ as mediator, the voltage applied is within the range between -0.3 V and -0.2 V (vs. Ag), therefore the reduced form can be re-oxidized at the positive electrode material.

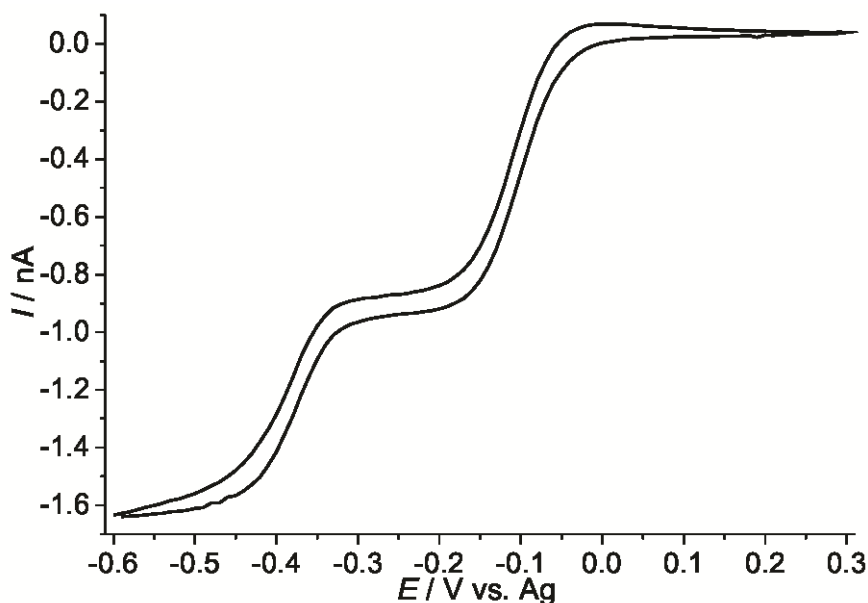


Figure 38: CV of the DDB in a 5 mM solution in G27. Scan rate 20 mV s⁻¹; step size 10 mV.

The anthracene could also be dissolved in the electrolyte and was stable for SECM operation. Figure 39 shows the oxidation of anthracene and the the potential window appears on a higher range but it still can be considered viable. The stable range for applying potential for imaging experiments can be between 0.8 V and 1.0 V. This compound has around 0 V (vs. Ag) in its reduced state, which would cause a different feedback response when approached to an electrode than the DDQ and could work as an irreversible mediator.

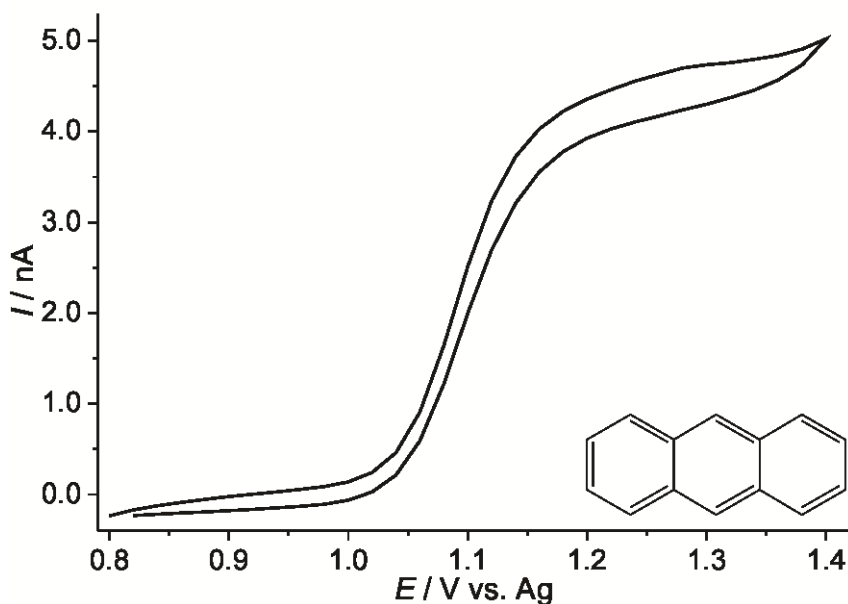


Figure 39: CV of the anthracene in a 5 mM solution in G27. Scan rate 20 mV s^{-1} ; step size 10 mV.

The idea of using anthracene as a second mediator is to have an irreversible redox couple. Working with both mediators would also be an option for further experiments and the DDQ can be used to investigate electrochemical properties and the anthracene to determine exactly the distance between ME and substrate as described in the literature.²⁷⁹ After testing both compounds, the first idea was to perform the investigations using the DDQ, considering its versatility and stability in other systems.^{277,278}

8.2 SECM and SEM Investigations

The following step was to find cathode materials and to verify the performance of the mediator and investigate the materials. Discussions with collaborators from Fraunhofer Institute (IFAM – Oldenburg) led to one standard cathode material (LFP)¹¹ and one high voltage material (NMC).³² Both materials were then investigated using SECM and SEM in order to understand better their performance and the CEI formation process.

8.2.1 LiFePO₄ (LFP)

For the investigations with this material, different samples were prepared from our collaborators with high active content. The first electrode was prior to any cycling, just cut and dried overnight at 80°C and transferred inside the glove box. Afterwards, other electrodes were cycled 100 times and transferred under inert conditions to the glove box at two different states of charge (SOC), 0 which means a fully discharged battery and 100 that is the state in a fully charged battery. This material is not supposed to form a consistent and effective CEI after cycling.

A slight difference can be seen in the CV of the DDQ performed on the three electrodes which is shown in figure 40. All the electrodes maintained the two step redox process already observed, but both cycled electrodes presented a shift in the potential. This is probably caused by the use of a pseudo-reference electrode, which was a Ag wire without Ag⁺ ions in solution.

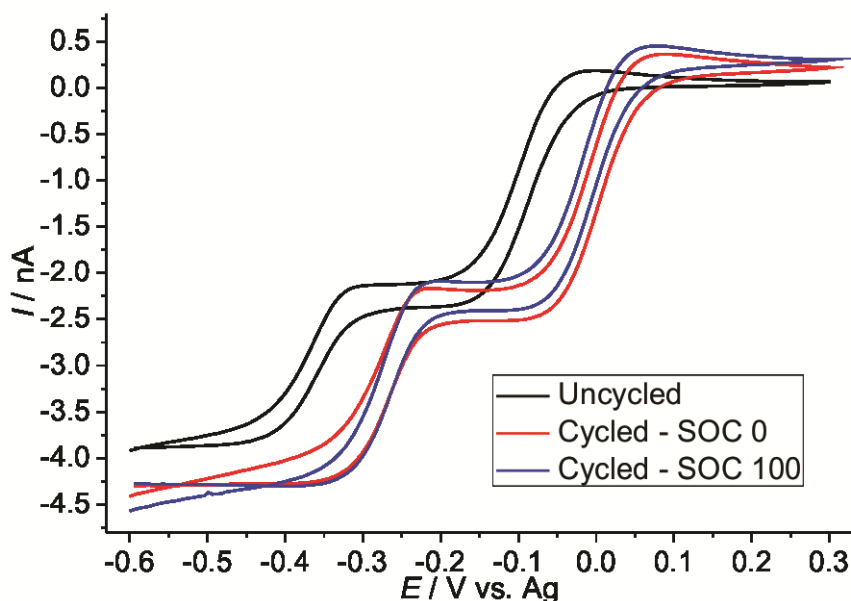


Figure 40: CVs in the bulk of the 5 M solution of DDQ in G27 electrolyte with the different SOC of the LFP electrodes. Scan rate employed in all of the electrodes 20 mV s^{-1} ; step size 10 mV. Reference electrode was a Ag wire and counter electrode a Pt wire.

The next step was to perform approach curves to try to identify if a cycled electrode would have different electrochemical response than the one without any cycling or contact with any other kind of electrolyte. The same way it was done for the DBDMB in ionic liquid. In order to treat the data obtained from approach curves, an approach to a glass substrate was performed. From the fit, the distance of closest approach d_0 was obtained. Figure 41 presents this approach curve, with

the DDQ solution in the G27 electrolyte with the ME used for the experiments with the cathode electrodes.

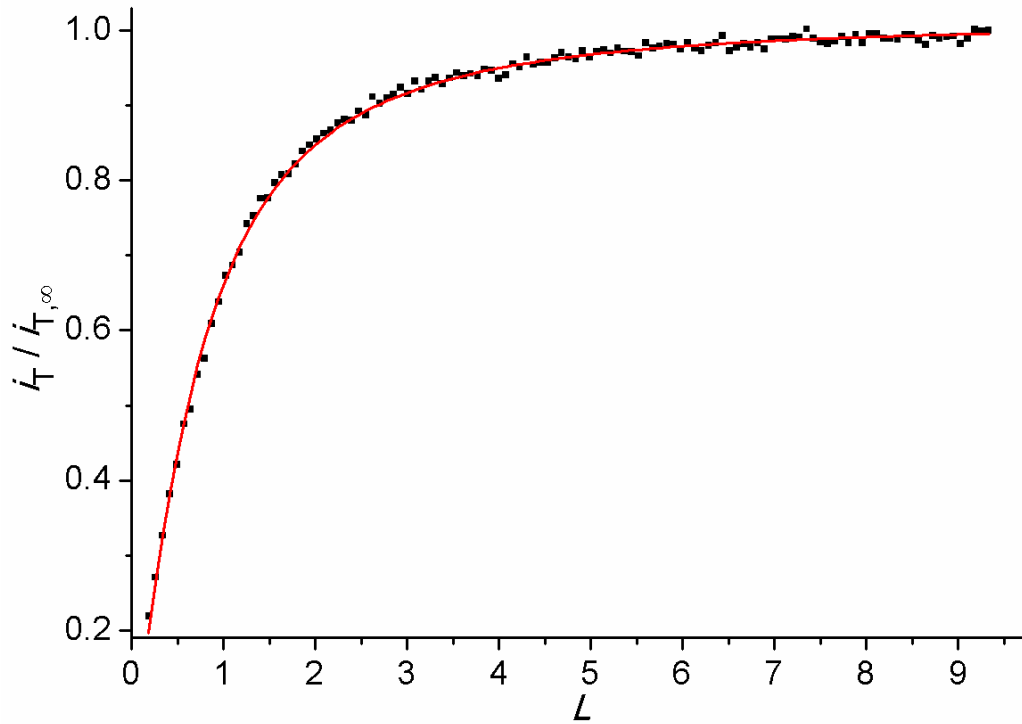


Figure 41: Approach curve using 5mM DDQ in the G27. The dots are the data points and the line is the curve fit using the insulator model of Cornut and Lefrou.²³² ($E = + 4.1$ V, $r_T = 12.5$ μm , $RG = 6.51$; fitted $r_T = 13.12$, $d_0 = 2.44$).

Figure 42 presents the fit of the approach curves performed in the three different electrodes. It can be seen that in all cases the positive feedback indicates that the material is still conductive, reinforcing the fact that the CEI has less pronounceable effects on the passivation of the cathode than the SEI in the anode^{83,186} but still this material was influenced by such interphase after the charging cycles.^{34,135} It can be seen that on the cycled electrodes the current increase prior to the touching point is proportionally smaller in comparison to the uncycled electrode, being the SOC 100 (fig. 42 - curve 3) considerably less conductive, while the SOC 0 (fig. 42 - curve 2) presented an intermediate conductivity.

LFP cathode materials are not expected to form a stable and beneficial CEI for the battery operation. This decay in current observed is possibly related to the deposition of organic and/or inorganic compounds, passivating the surface, which would have a negative impact on the battery performance.

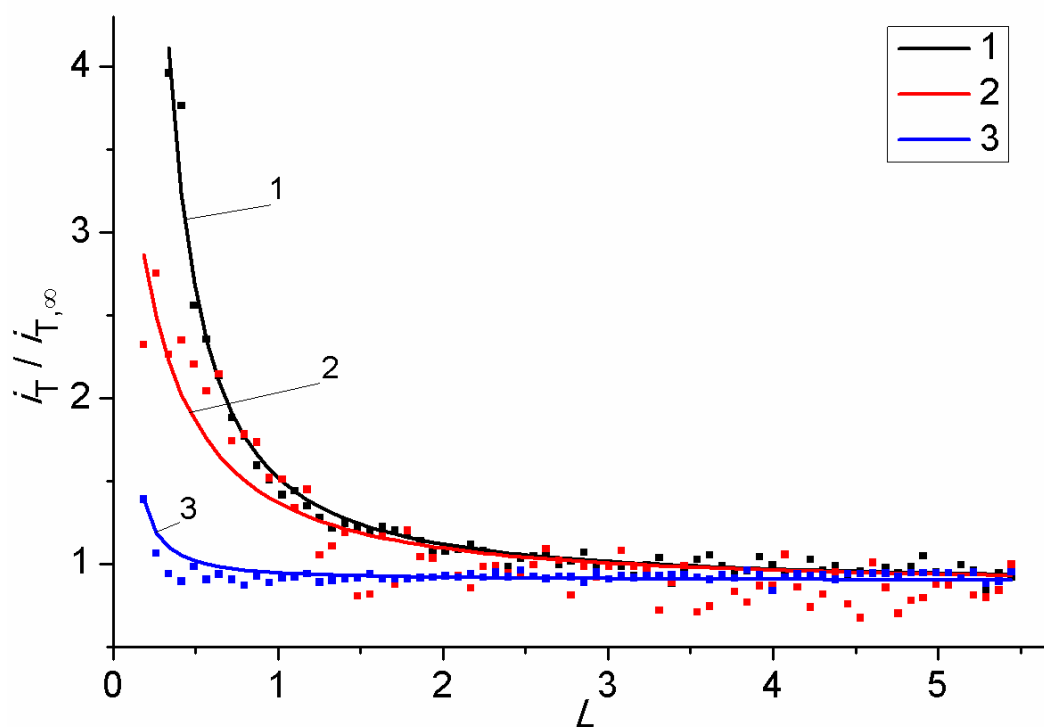


Figure 42: Approach curves and fit from LFP electrodes in 5mM DDQ in the G27 (1) uncycled; (2) cycled, SOC 0 and (3) cycled, SOC 100. (Step size: 1 μm , $E = +4.1$ V, $r_T = 12.5$ μm , $RG = 6.51$, fitted with the conductor model, fitted $r_T = 13.12$, $d_0 = 2.44$).²³²

Additionally, different regions of the electrodes were imaged using SECM. Figure 40 shows the different images obtained where not significant differences could be observed. The ME was approached while observing the increase of the negative current measured at the ME due to the high conductivity of the cathode materials. The experiment was interrupted when the ME reduction current had doubled compared to the current in the bulk solution (distance of about 10 μm to the substrate).

The LFP surface is formed basically by a film made of the particles of the phosphate and some carbon components over a metallic foil. In the image of the uncycled electrodes (fig. 43a) it is possible to see a very homogeneous distribution with very small current variation along the scanned area. More significant differences and even a feature that can be related to a crack in the structure can be seen in the image of the SOC 0 (fig. 43b), which can be derived from the cycling and the potential variation at the electrode. In the image of SOC 100 (fig.43c), no feature can be seen and again, only a small current variation that can be due to the formation of some irregular CEI and a minor sample tilt.

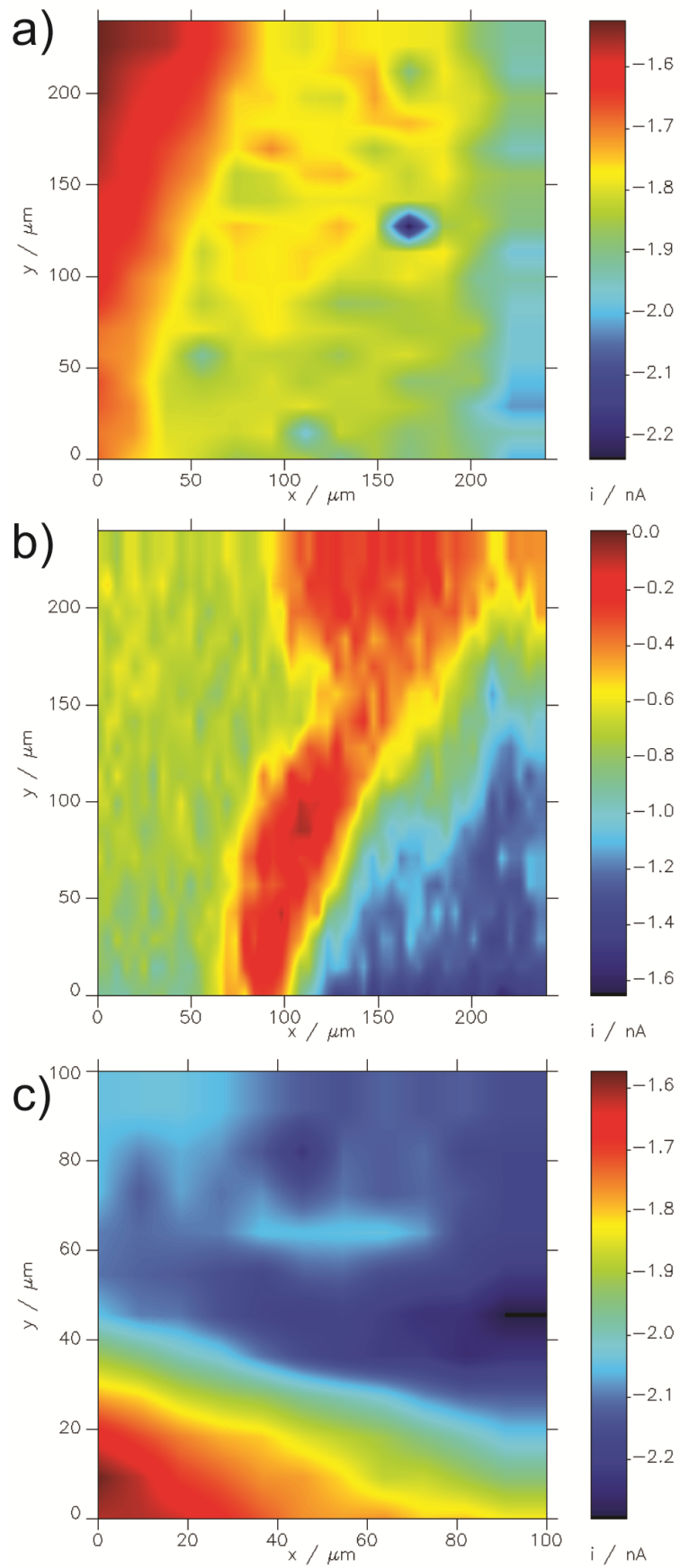


Figure 43: SECM images from the LFP electrodes (a) uncycled; (b) cycled 100 times with SOC 0 and (c) cycled 100 times with SOC 100. ($E_T = -0.2$ V, $r_T \approx 12.5$ μm).

Besides SECM, SEM was also employed in order to investigate the surface of this cathode material. Figure 44 presents the SEM imaging of the uncycled electrode. It can be seen that expected structure of such material, with smaller particles that are carbon rich and the larger ones that correspond to the LiFePO_4 .^{11,135}

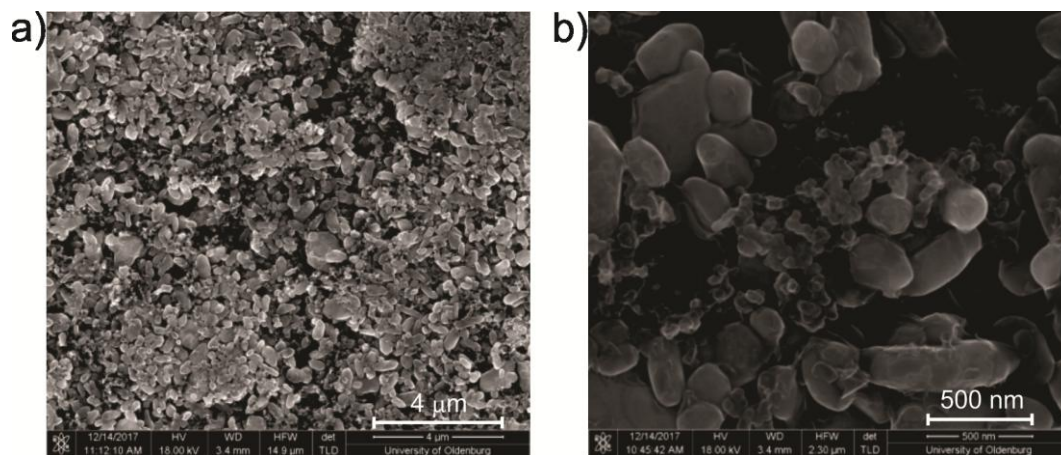


Figure 44: SEM images of the uncycled LFP cathode in different magnifications.

8.2.2 $\text{LiNi}_x\text{Co}_y\text{Mn}_z\text{O}_2$ (NMC)

In order to further understand the effects observed in the LFP, the idea was to compare it with a higher operational voltage material NMC. This kind of electrodes are more prone to the CEI formation and was expected to have more pronounced variations between the uncycled and the cycled electrodes which is of key importance for the performance of a battery.^{83,87,88}

Besides the uncycled electrode that was only cut and dried before analysis in the same procedure used for the LFP, other samples were also cycled 100 times and investigated in three different SOC: 0, 50 and 100. The intermediate SOC was added in an attempt to observe the CEI coverage/formation process undergoing.

The first important difference between the materials can be observed in figure 45, where the CVs for the uncycled and the different SOCs of the NMC presented much faster and different decay ratios. In the uncycled electrode the two step redox processes were not affected, but some current variations were observed, but in the case of the cycled electrodes, in none of the SOCs the mediator lasted stable for the two redox reactions more than 48 hours of experiment. This fact is probably related to electrolyte residuals that further consume irreversibly the DDQ.

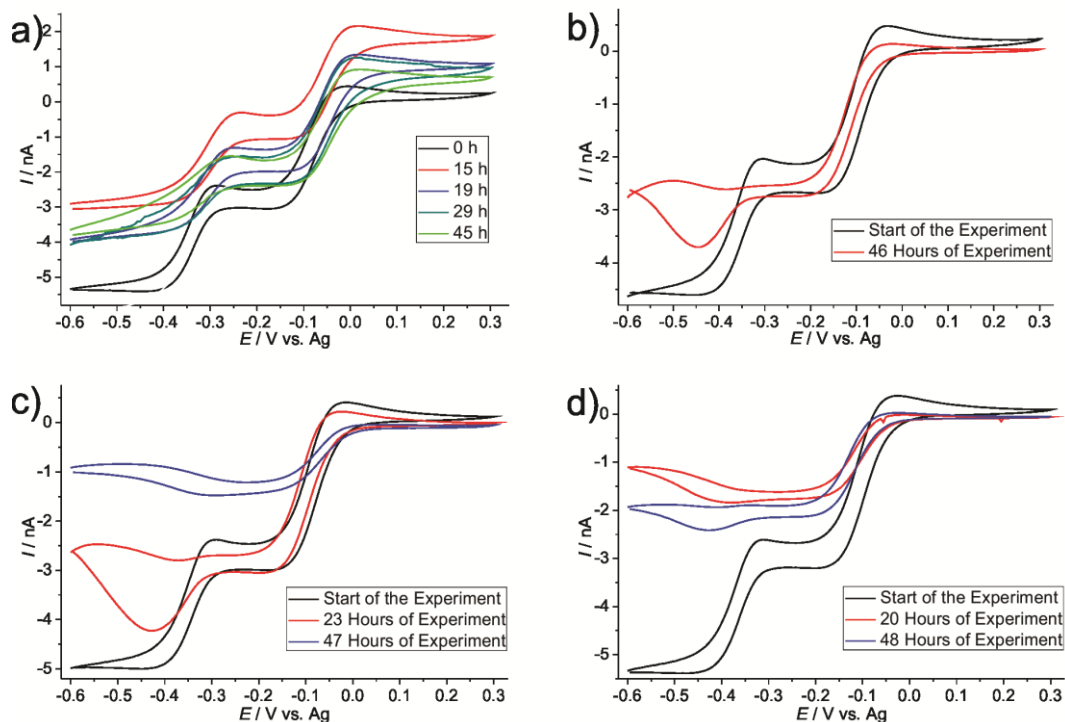


Figure 45: CVs in the bulk of the 5 mM solution of DDQ in G27 electrolyte with the different SOC of the NMC electrodes, being (a) uncycled; (b) SOC 100; (c) SOC 50 and (d) SOC 0. Scan rate employed in CV was 20 mV s^{-1} ; step size 10 mV. Reference electrode was a Ag wire and counter electrode a Pt wire.

In the case of the approach curves performed above the NMC electrodes in the uncycled and in the three different SOC, the differences can be observed on the fits presented in figure 46. Once again the positive feedback is observed for all electrodes, independently of cycling, but in the case of the uncycled sample, the positive feedback is higher. For the cycled samples, a similar current in the ME approach curve and only a small variation between the different SOC can be observed. This is possibly due to the presence of an insulating layer covering the electrode after cycling.

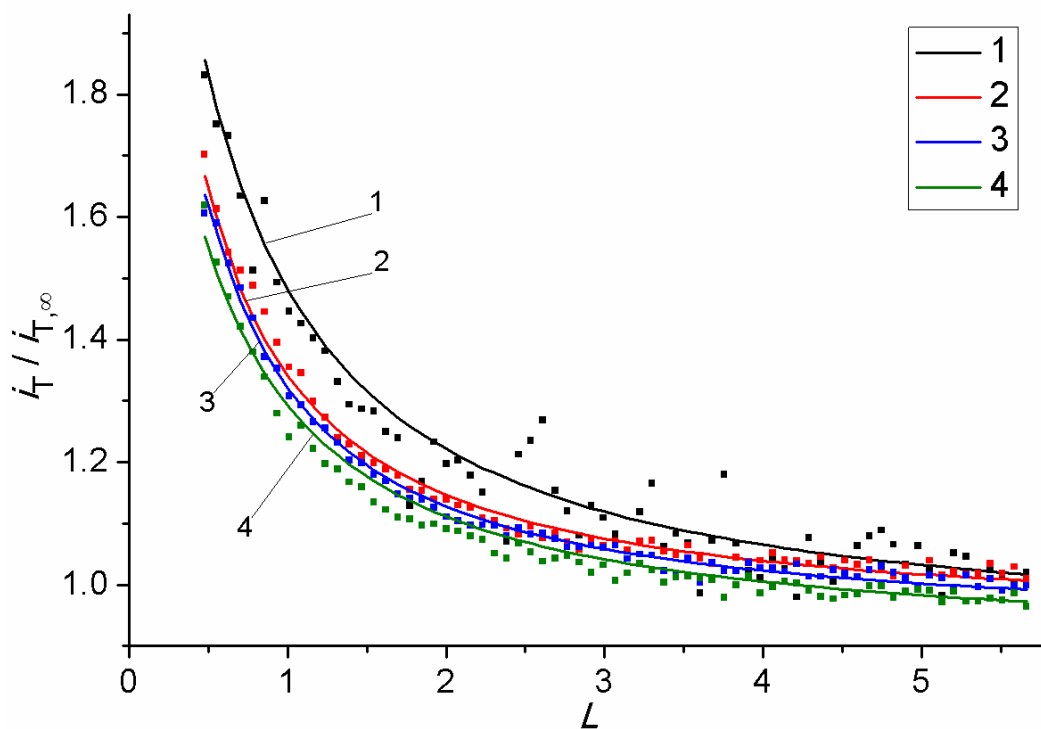


Figure 46: Approach curves and fit from NMC electrodes in 5 mM solution of DDQ in G27 electrolyte (1) uncycled; (2) cycled, SOC 0; (3) cycled, SOC 50 and (4) cycled, SOC 100. (Step size: 1 μm , $E = + 4.1$ V, $r_T = 12.5$ μm , $RG = 6.51$; fitted with the conductor model, fitted $r_T = 13.12$, $d_0 = 6.26$).²³²

For the imaging, the same procedure used for the LFP cathodes was used. The ME was approached to the electrode and the experiment was interrupted when the negative ME current is close to the double when compared to the current in the bulk solution (distance of about 10 μm to the substrate). For short term comparisons, forward and reverse images recorded in the first hours of experiment and after a time interval. These images are presented along with a normalized difference plot which consists in the variation of current measured in the corresponding data points from the forward and reverse scan within a threshold of 10% of the overall average current. The scale of the fluctuations was also normalized by the overall average current of the forward scan of the respective images, so they could be compared.

Figure 47 presents the images recorded from the uncycled electrodes. In this case, that no CEI or any passivation layer is expected, in both cases of forward and reverse scans at the beginning of the experiment (fig. 47a-b) and after several hours of operation (fig. 47d-e), not many long-term variations could be observed. In the normalized difference plots (fig. 47c and 47f), only fluctuations

under 5% of the overall current range could be seen in general with only few exceptions, showing the stability of the uncycled electrode did not change along the experiment.

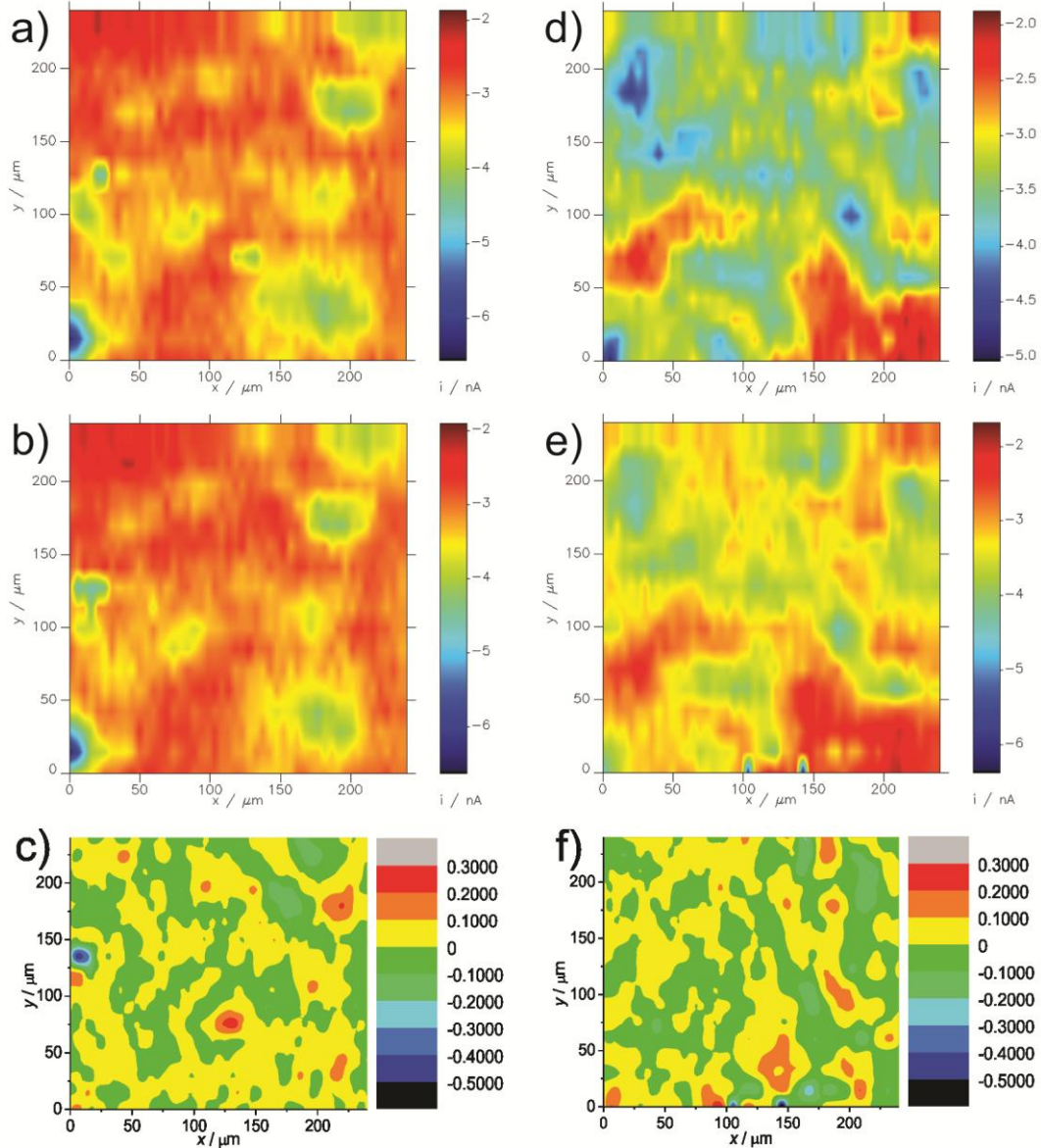


Figure 47: SECM image comparison from the NMC uncycled electrodes in 5 mM solution of DDQ in G27 electrolyte **(a)** forward scan at the first hours of experiment; **(b)** reverse scan of the same region; **(c)** difference plot of images (a) and (b); **(d)** forward scan 22 hours later; **(e)** reverse scan of the same region and **(f)** difference plot of images (d) and (e). ($E_T = -0.2$ V, $r_T \approx 12.5$ μm , difference threshold = 10%).

Figure 48 shows the image comparison for the cycled electrodes at SOC 100. For these cathodes, it is expected that the CEI was formed during the cycling. Figures 48a-b and 48d-e are from the same region and some features oscillated when comparing the images recorded with a 20 hours time gap. Regarding short-term

changes, figure 48c presents very small fluctuations that barely reach ± 0.02 in the normalized scale (0.5% of the image average current). When looking at the difference plot in figure 48f, the fluctuations observed appear to increase, but the range is still comparable to figure 48c, with even the spike ($x = 120 \mu\text{m}$; $y = 240 \mu\text{m}$) no surpassing 1% of the image average current. The overall trend possibly indicates that the layer formed has enough driving force to keep the coverage stability along the experiment.

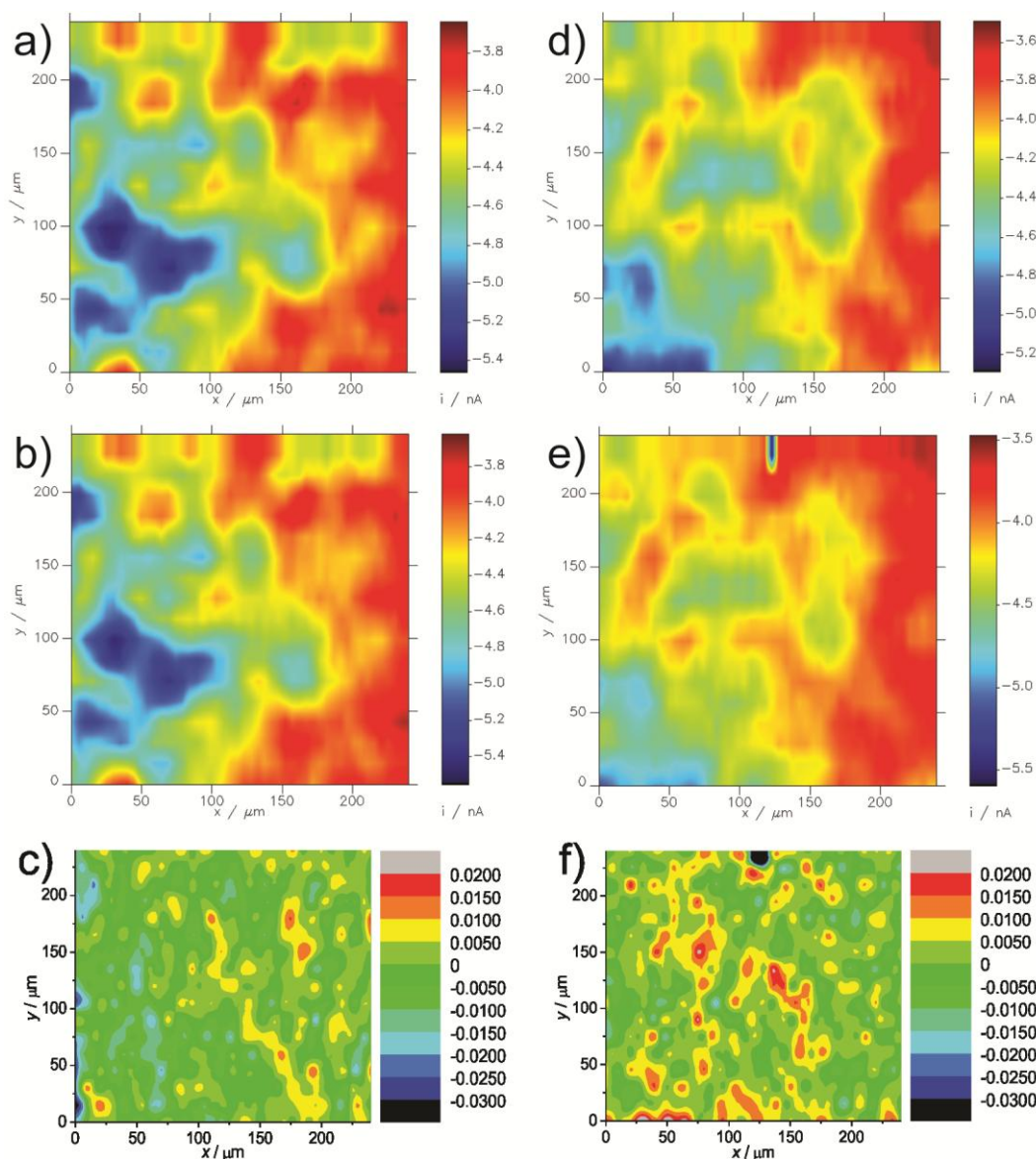


Figure 48: SECM image comparison of cycled electrodes at the SOC 100 in 5 mM solution of DDQ in G27 electrolyte (a) forward scan at the first hours of experiment; (b) reverse scan of the same region; (c) difference plot of images (a) and (b); (d) forward scan 20 hours later; (e) reverse scan of the same region and (f) difference plot of images (d) and (e). ($E_T = -0.2 \text{ V}$, $r_T \approx 12.5 \mu\text{m}$, difference threshold = 10%).

The cycled electrodes at the SOC 50 can be seen in figure 49. The images recorded at the beginning of the experiment (fig. 49a-b) and the ones recorded 22 hours later (fig. 49d-e), appear to be with some shift on the position, but still some similar features can be seen in both (feature around $x < 50 \mu\text{m}$, for example). The normalized difference plot in figure 49c has fluctuations that do not exceed 1% current overall. Figure 49f has fluctuations on a similar range, but in this case, they are proportionally higher, as the respective images presented a current decay. Also, the surface reactivity seems to be slightly more heterogeneous.

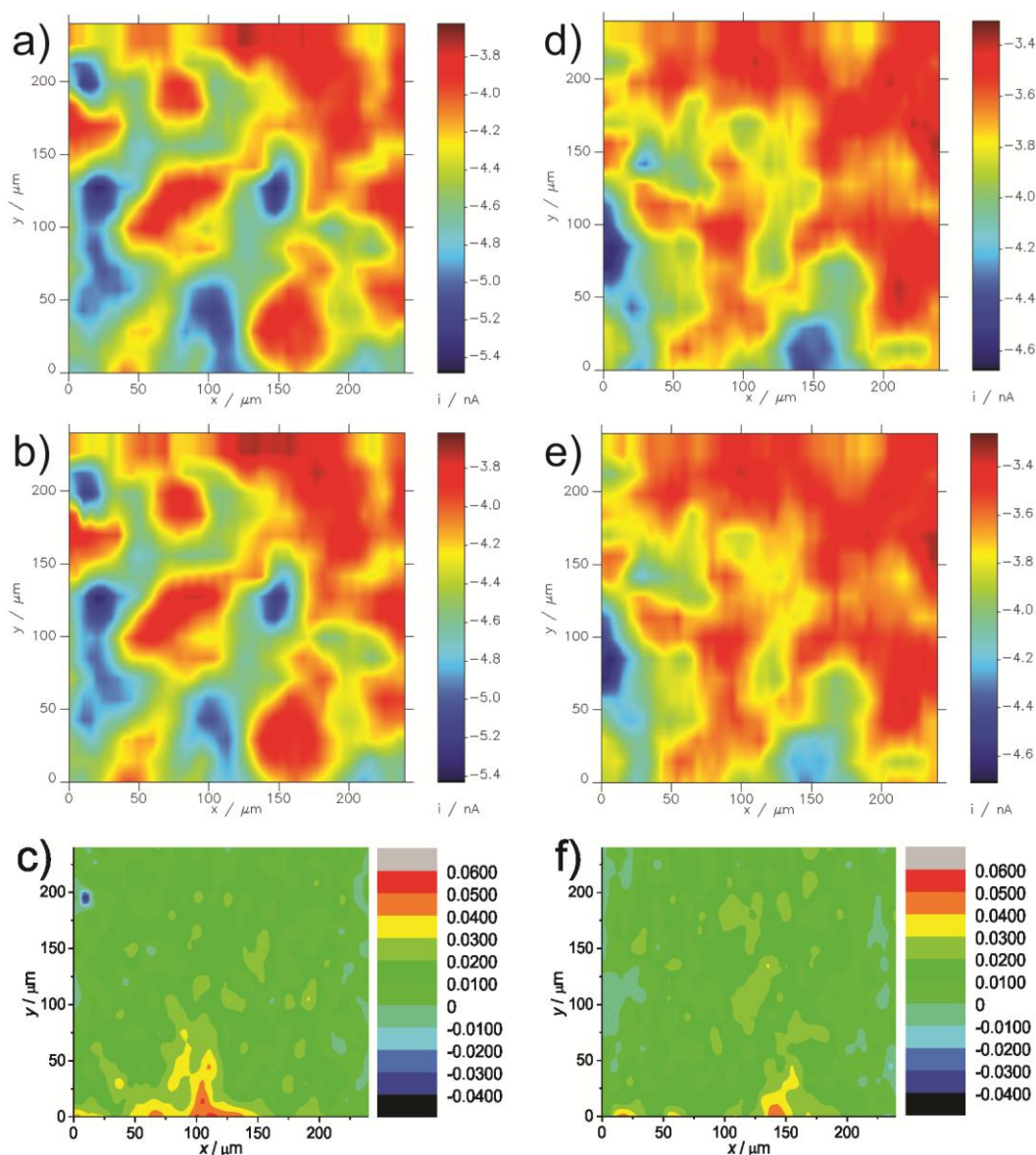


Figure 49: SECM image comparison from the NMC cycled electrodes at the SOC 50 in 5 mM solution of DDQ in G27 electrolyte (a) forward scan at the first hours of experiment; (b) reverse scan of the same region; (c) difference plot of images (a) and (b); (d) forward scan 22 hours later; (e) reverse scan of the same region and (f) difference plot of images (d) and (e). ($E_T = -0.2 \text{ V}$, $r_T \approx 12.5 \mu\text{m}$, difference threshold = 10%).

Figure 50 shows the SECM image comparison for the cycled electrodes with SOC 0. In this case, also no noticeable long-term changes could be observed when comparing the images recorded at the beginning of the experiment (fig. 50a-b) with the images recorded 9 hours later (fig. 50d-e). What could be observed similarly to the cycled electrodes at SOC 50 was a current decay could be observed again between them, this time within a shorter interval of 9 hours. In the normalized difference plot for the initial images (fig. 50c) more fluctuations appear but usually none exceed 3% of the overall current. In the case of the other difference plot (fig. 50f), the first impression is of less fluctuations, but as there was a current decay between the images, the fluctuations are proportionally a little higher (around 4%).

The pattern observed in the normalized difference plots of the cycled electrodes was in agreement with the similarities seen in the approach curves (fig. 46). On the electrodes at SOC 50 and SOC 0 the proportional increase that was observed along the experiment occurs probably due to a lower driving force which results in a less effective stabilization of the electrode after the removal of the battery setup. The electrode at SOC 100 could be more stable along the experiment duration. It is possible to observe that the insulating behavior of the apparent layer formed is much less effective than an SEI observed in a negative electrode.²³¹

In order to better understand if there was effectively a CEI formed on the electrode after cycling, SEM images were recorded from the electrodes. Figure 51 present the images for the uncycled and all the different SOC's of the NMC electrodes. At first, it was already possible to see a difference in the particle size of the material, with NMC being much larger than the LFP and the surface much rougher (figs. 51a-b). Furthermore, it is possible to see that the particles are partially covered by an insulating layer on the cycled samples (fig. 51c-h), corroborating with the SECM images. Some of the particles, especially in the case of SOC 50 (fig. 51f) and SOC 100 (fig.51h) appear to be cracked.

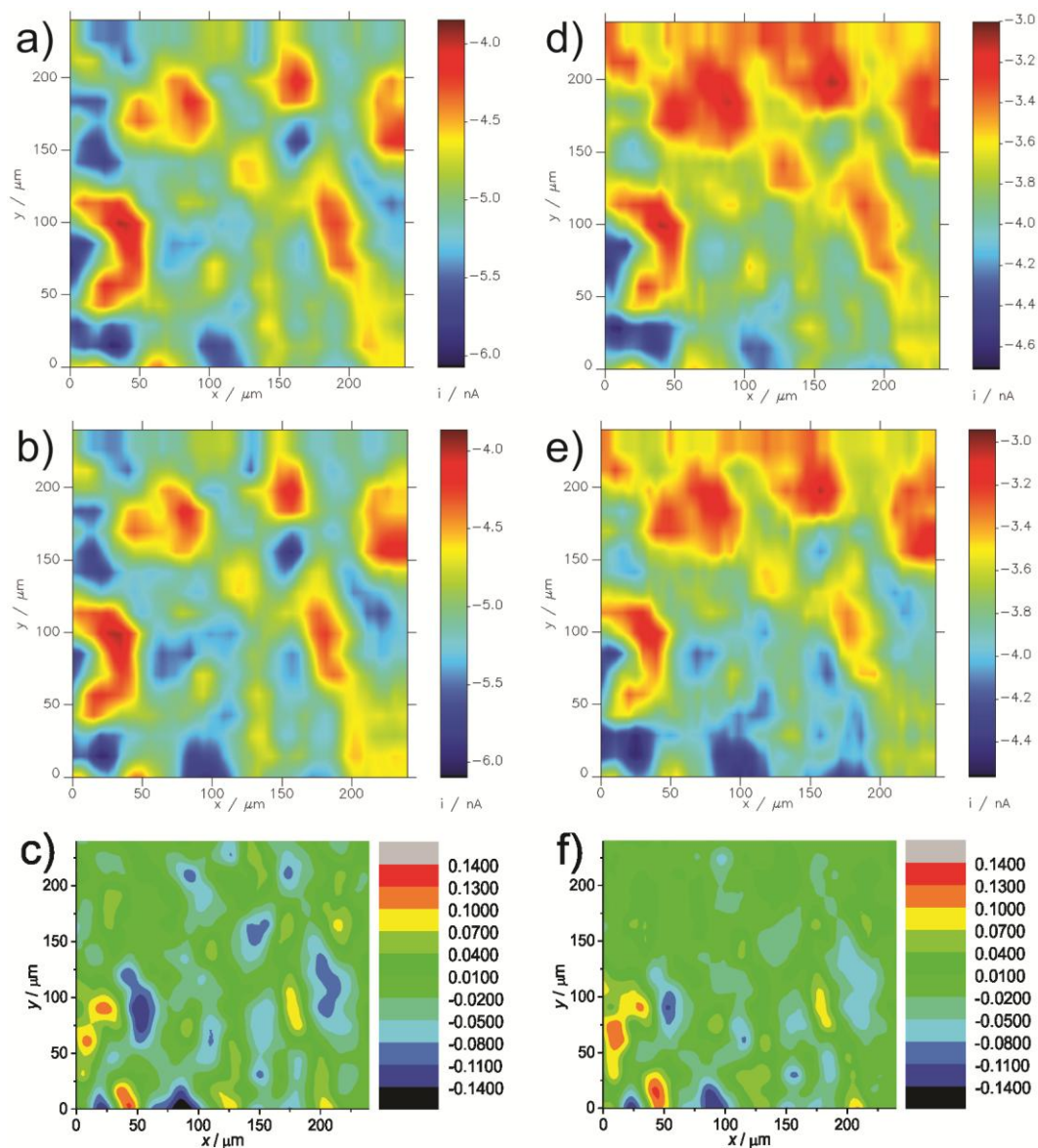


Figure 50: SECM image comparison from the NMC cycled electrodes at the SOC 0 in 5 mM solution of DDQ in G27 electrolyte **(a)** forward scan at the first hours of experiment; **(b)** reverse scan of the same region; **(c)** difference plot of images (a) and (b); **(d)** forward scan 9 hours later; **(e)** reverse scan of the same region and **(f)** difference plot of images (d) and (e). ($E_T = -0.2$ V, $r_T \approx 12.5$ μm , difference threshold = 10%).

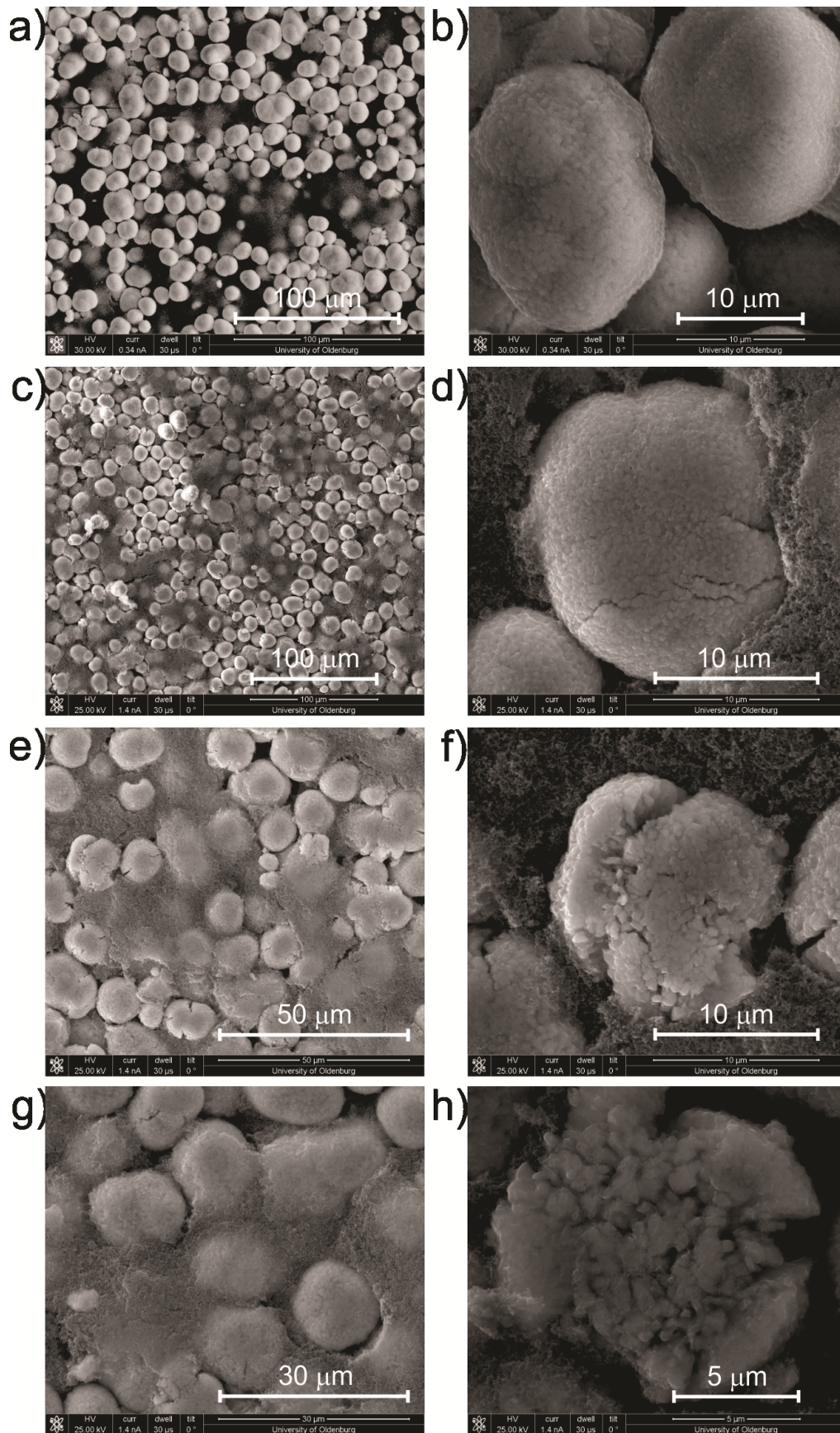


Figure 48: SEM images of the NMC (a)/(b) uncycled; (c)/(d) cycled 100 times with SOC 0 and (e)/(f) cycled 100 times with SOC 50 and (g)/(h) cycled 100 times with SOC 100.

9 Summary

In summary, the feedback mode of scanning electrochemical microscopy (SECM) was applied with 2,5-di-*tert*-butyl-1,4-dimethoxybenzene (DBDMB) as redox mediator to investigate the electron transfer at silicon electrodes in battery grade electrolytes. Initially the electrodes were investigated prior to the SEI formation regarding the influence of the native SiO₂ passivation. By a mechanical abrasion by the Pt ME and the hydrofluoric acid dip were shown to be successful for the partial removal of SiO₂ and to increase k_{eff} significantly.³⁶ After SiO₂ removal the conductivity increased considerably. Therefore, the HF etched Si electrodes with increased k_{eff} values and long-term stability were taken as suitable for the investigation of SEI formation. X-ray photoelectron microscopy (XPS) was applied to understand better the composition and thickness of the SiO₂ layer.

The SEI formation and the lithiation happening on a Si anode are processes of key importance for the performance of battery and were investigated in full charge-discharge cycles. The expected drawbacks of this material^{11,21} could be seen on SECM images. Further investigations with the interrupted charging experiment made it possible to observe the SEI formation happening *in situ* step-by-step. The passivation of the electrode was shown to happen in a similar way of a nucleation process.²³¹

The same technique and mediator was also applied to investigate metallic lithium electrodes in the bis(trifluoromethanesulfonyl)imide (Pyr14TFSI) ionic liquid. Performing SECM measurements in this ionic liquid were the first challenge, but the DBDMB has proven to be stable and soluble in this new electrolyte employed. Furthermore, the Li electrodes were prepared using a new method which made it possible to obtain fresh surfaces that had no previous contact to any compound.²⁵⁸ This also made it possible to cut the electrodes using an SEI precursor to investigate the formation process. SECM approach curves and images made it possible to investigate the SEI and dendrite formation effects by comparing electrodes directly after cutting and electrodes that were cycled galvanostatically.

Both Si and Li electrodes are suitable materials for application as anodes of Li-ion batteries. Moreover, two cathode materials were also investigated using

SECM feedback mode with the new 2,3-dichloro-5,6-dicyano-1,4-benzoquinone (DDQ) as mediator. After researching several compounds, DDQ has shown good stability and appropriate potential range for investigations of cathode materials.

One commercial cathode material (LFP) and one high voltage material (NMC) were investigated in order to understand the CEI formation process and its influence on the properties and performance of a battery. Approach curves, SECM and SEM images were used to investigate and compare these materials in different states of charge (SOC) after 100 times cycling. The LFP electrodes were substantially affected in the electrochemical response to the ME, with the cycled electrodes presenting a much hindered diffusion in the approach curves. On the other hand, the NMC presented variations that were similar independently of the SOC and did not reduce the conductivity of the electrodes so dramatically. This occurred probably due to the deposition of organic and/or inorganic compounds that passivate the LFP, while at the NMC cathodes, the layer formed presents properties of interest for a CEI. Furthermore, when looking at the SEM images, a layer could be observed in the cycled samples in all SOC, but with variations on the coverage.

In summary, significant contributions to the understanding of electron transport, the impact of the native SiO₂ layer at Si negative electrodes on the local electron transport and local electrolyte reduction and dynamics of SEI at silicon electrodes by the application of SECM and the new interrupted charging experiment. Metallic Li electrodes obtained with tunable conditions were investigated using ionic liquids in SECM feedback mode in order to investigate SEI and dendrite formation. Furthermore, in this thesis a new mediator (DDQ) was found to work with cathode materials. Thus, two different possible electrode materials were investigated in order to understand better the CEI formation process.

10 Outlook

SECM investigations with DBDMB as redox mediator has been shown to be applicable in various electrodes^{41,217} and also could be employed for investigations in an ionic liquid, which can be applied on LIBs in the near future. Besides, it is likely that it can be applied to investigations in the more recent batteries, such as sodium-ion^{280,281} and sodium-sulfur²⁸² batteries.

The DBDMB was shown to be useful for all the investigations performed in the anode materials and still maintain its stability even after many hours of operation. Its solubility in the ionic liquid employed for the investigations in metallic lithium electrodes also open the possibility of employing DBDMB with even further versatility.

The results obtained with the interrupted charging experiment could observe the SEI nucleation like formation process and step towards a better understanding of the properties and the influence of the SEI in a battery. Addressing the lithiation process in silicon electrodes would require the look for alternatives to prevent the loss of mechanical stability, e. g. microstructured electrodes⁴ instead of the flat electrodes. Another possibility is to investigate the stability of the SEI by raising the potentials in small steps as well.

The possibility to obtain tunable metallic Li surfaces, bring a good possibility of regulating the thickness and the properties of the SEI formed by using different SEI precursors and additives.²⁵⁸ Further investigations can lead to better understanding of how such compounds affect the formation and stability of the SEI. The combination with SEM allowed the comparison of features but for understanding the species present in the SEI, XPS can be employed to verify which species can affect more positively the performance of a battery.

The investigations on the positive electrode and the CEI formation can also lead to better understanding, which can improve the performance of a battery. Although similarities are expected as both the SEI and CEI are formed by electrolyte reduction,^{154,191} different thickness and impact on the battery may require adaptations on the SECM setup for a more detailed understanding of the CEI. A larger variety of materials can be investigate and might even be possible to perform a similar experiment of the interrupted charging to see if the effects are

similar to the SEI demonstrated in this thesis. Alternative mediators or even the use of a mixture involving reversible and irreversible redox mediators for the separate and subsequent determination of the ME-substrate distance d and the rate constant κ can also be helpful on investigations to cathode materials.²⁷⁹

Improvements in the electrochemical cell such as temperature control, tilt table and miniaturization (reducing the volumes of electrolyte to a proportion closer to a real battery) can be valuable for reducing errors and fluctuations in the measurements. Hence, the implementation of both positive and negative electrodes in the SECM would be a long-term goal.

11 References

- (1) Winter, M.; Brodd, R. J. What are batteries, fuel cells, and supercapacitors? *Chem. Rev. (Washington, DC, U. S.)* **2004**, *104*, 4245–4269.
- (2) Huggins, R. *Advanced Batteries: Materials Science Aspects*; Springer: New York, 2008.
- (3) Yoshino, A. Development of lithium-ion battery. *Mol. Cryst. Liq. Cryst. Sci. Technol., Sect. A* **2000**, *340*, 425–429.
- (4) Janski, R.; Fugger, M.; Forster, M.; Sorger, M.; Dunst, A.; Hanzu, I.; Sternad, M.; Wilkening, M. Lithium barrier materials for on-chip Si-based microbatteries. *J. Mater. Sci.: Mater. Electron.* **2017**, *28*, 14605–14614.
- (5) Wang, Y.; Liu, B.; Li, Q.; Cartmell, S.; Ferrara, S.; Deng, Z. D.; Xiao, J. Lithium and lithium ion batteries for applications in microelectronic devices: A review. *J. Power Sources* **2015**, *286*, 330–345.
- (6) Scrosati, B.; Hassoun, J.; Sun, Y.-K. Lithium-ion batteries. A look into the future. *Energy Environ. Sci.* **2011**, *4*, 3287–3295.
- (7) Tarascon, J. M.; Armand, M. Issues and challenges facing rechargeable lithium batteries. *Nature* **2001**, *414*, 359–367.
- (8) Manthiram, A. Materials Challenges and Opportunities of Lithium Ion Batteries. *J. Phys. Chem. Lett.* **2011**, *2*, 176–184.
- (9) Thackeray, M. M.; Wolverton, C.; Isaacs, E. D. Electrical energy storage for transportation—approaching the limits of, and going beyond, lithium-ion batteries. *Energy Environ. Sci.* **2012**, *5*, 7854–7863.
- (10) Goodenough, J. B. Electrochemical energy storage in a sustainable modern society. *Energy Environ. Sci.* **2014**, *7*, 14–18.
- (11) Bresser, D.; Hosoi, K.; Howell, D.; Li, H.; Zeisel, H.; Amine, K.; Passerini, S. Perspectives of automotive battery R&D in China, Germany, Japan, and the USA. *J. Power Sources* **2018**, *382*, 176–178.
- (12) Etacheri, V.; Marom, R.; Elazari, R.; Salitra, G.; Aurbach, D. Challenges in the development of advanced Li-ion batteries: a review. *Energy Environ. Sci.* **2011**, *4*, 3243–3262.
- (13) Leuthner, S. Übersicht zu Lithium-Ionen-Batterien. In *Handbuch Lithium-Ionen-Batterien*; Korthauer, R., Ed.; Springer Vieweg: Berlin, Heidelberg, 2013; p 13.

-
- (14) Xu, K. Nonaqueous Liquid Electrolytes for Lithium-Based Rechargeable Batteries. *Chem. Rev. (Washington, DC, U. S.)* **2004**, *104*, 4303–4417.
- (15) Yamaki, J. Secondary Batteries - Lithium Rechargeable Systems: Lithium-Ion: Overview. In *Encyclopedia of Electrochemical Power Sources Volume 5*; Garche, J., Dyer, C. K., Moseley, P. T., Ogumi, Z., Rand, D.A.J., Scrosati, B., Eds.; Elsevier Science: Amsterdam, 2009; p 183.
- (16) Kim, H.; Oh, S.-M.; Scrosati, B.; Sun, Y.-K. High-performance electrode materials for lithium-ion batteries for electric vehicles. In *Advances in Battery Technologies for Electric Vehicles*; Scrosati, B., Garche, J., Tillmetz, W., Eds.; Woodhead Publishing: Cambridge, 2015; p 191.
- (17) Bagotsky, V. S.; Skundin, A. M.; Volkovich, Y. M. *Electrochemical Power Sources: Batteries, Fuel Cells, and Supercapacitors*; John Wiley & Sons: Hoboken, 2015.
- (18) Wakihara, M. Recent developments in lithium ion batteries. *Mater. Sci. Eng., R* **2001**, *33*, 109–134.
- (19) Atkins, P. W.; Overton, T. L.; Rourke, J. P.; Weller, M. T.; Armstrong, F. A. *Shriver and Atkins' Inorganic Chemistry*, 5th; Oxford University Press: Oxford, 2010.
- (20) Graf, C. Kathodenmaterialien für Lithium-Ionen-Batterien. In *Handbuch Lithium-Ionen-Batterien*; Korthauer, R., Ed.; Springer Vieweg: Berlin, Heidelberg, 2013; p 31.
- (21) Skaarup, S.; West, K.; Zachau-Christiansen, B.; Popall, M.; Kappel, J.; Kron, J.; Eichinger, G.; Semrau, G. Towards solid state lithium batteries based on ORMOCER electrolytes. *Electrochim. Acta* **1998**, *43*, 1589–1592.
- (22) Vetter, J.; Novák, P.; Wagner, M. R.; Veit, C.; Möller, K. C.; Besenhard, J. O.; Winter, M.; Wohlfahrt-Mehrens, M.; Vogler, C.; Hammouche, A. Ageing mechanisms in lithium-ion batteries. *J. Power Sources* **2005**, *147*, 269–281.
- (23) Aurbach, D.; Gamolsky, K.; Markovsky, B.; Gofer, Y.; Schmidt, M.; Heider, U. On the use of vinylene carbonate (VC) as an additive to electrolyte solutions for Li-ion batteries. *Electrochim. Acta* **2002**, *47*, 1423–1439.
- (24) Sternad, M.; Forster, M.; Wilkening, M. The microstructure matters: Breaking down the barriers with single crystalline silicon as negative electrode in Li-ion batteries. *Sci. Rep.* **2016**, *6*, 31712.

-
- (25) Peled, E.; Menachem, C.; Bar-Tow, D.; Melman, A. Improved Graphite Anode for Lithium-Ion Batteries Chemically: Bonded Solid Electrolyte Interface and Nanochannel Formation. *J. Electrochem. Soc.* **1996**, *143*, L4-L7.
- (26) Peled, E.; Golodnitsky, D.; Penciner, J. The Anode/Electrolyte Interface. In *Handbook of Battery Materials, Second Edition, Vol. 1*; Daniel, C., Besenhard, J. O., Eds.; Wiley: Weinheim, 2012; pp 479–524.
- (27) Xu, K.; Cresce, A. von. Interfacing electrolytes with electrodes in Li ion batteries. *J. Mater. Chem.* **2011**, *21*, 9849–9864.
- (28) Winter, M.; Besenhard, J. O. Lithiated Carbons. In *Handbook of Battery Materials, Second Edition, Vol. 1*; Daniel, C., Besenhard, J. O., Eds.; Wiley: Weinheim, 2012; pp 433–478.
- (29) Verma, P.; Maire, P.; Novák, P. A review of the features and analyses of the solid electrolyte interphase in Li-ion batteries. *Electrochim. Acta* **2010**, *55*, 6332–6341.
- (30) Winter, M. The solid electrolyte interphase - the most important and the least understood solid electrolyte in rechargeable Li batteries. *Z. Phys. Chem. (Muenchen, Ger.)* **2009**, *223*, 1395–1406.
- (31) Agubra, V. A.; Fergus, J. W. The formation and stability of the solid electrolyte interface on the graphite anode. *J. Power Sources* **2014**, *268*, 153–162.
- (32) Nitta, N.; Wu, F.; Lee, J. T.; Yushin, G. Li-ion battery materials: present and future. *Mater. Today* **2014**, *18*, 252.
- (33) Bruce, P. G.; Freunberger, S. A.; Hardwick, L. J.; Tarascon, J.-M. Li-O₂ and Li-S batteries with high energy storage. *Nat. Mater.* **2012**, *11*, 19–29.
- (34) Edström, K.; Gustafsson, T.; Thomas, J. O. The cathode–electrolyte interface in the Li-ion battery. *Electrochim. Acta* **2004**, *50*, 397–403.
- (35) Wittstock, G.; Burchardt, M.; Pust, S. E.; Shen, Y.; Zhao, C. Scanning Electrochemical Microscopy for Direct Imaging of Reaction Rates. *Angew. Chem., Int. Ed.* **2007**, *46*, 1584–1617.
- (36) Bültner, H.; Sternad, M.; dos Santos Sardinha, E.; Witt, J.; Dosche, C.; Wilkening, M.; Wittstock, G. Investigation of the Electron Transfer at Si Electrodes: Impact and Removal of the Native SiO₂ Layer. *J. Electrochem. Soc.* **2016**, *163*, A504-A512.
- (37) Zhang, L.; Zhang, Z.; Amine, K. Redox shuttles for overcharge protection of lithium-ion batteries. *ECS Trans.* **2013**, *45*, 57-66, 10 pp.

-
- (38) Zhang, L.; Zhang, Z.; Amine, K. Redox shuttle additives for lithium-ion battery. In *Lithium Ion Batteries: New Developments*; Belharouak, I., Ed.; InTech: Rijeka, 2012; pp 173–188.
- (39) Chen, Z.; Qin, Y.; Amine, K. Redox shuttles for safer lithium-ion batteries. *Electrochim. Acta* **2009**, *54*, 5605–5613.
- (40) Chen, Z.; Qin, Y.; Amine, K. Chemical Overcharge Protection of Lithium-Ion Cells. In *Lithium Batteries: Research, Technology, and Applications*; Dahlin, G. R., Strom, K. E., Eds.; Nova Science Pub Incorporated: New York, 2010; p 119.
- (41) Bültner, H.; Peters, F.; Schwenzel, J.; Wittstock, G. Spatiotemporal Changes of the Solid Electrolyte Interphase in Lithium-Ion Batteries Detected by Scanning Electrochemical Microscopy. *Angew. Chem., Int. Ed.* **2014**, *53*, 10531–10535.
- (42) Hu, M.; Pang, X.; Zhou, Z. Recent progress in high-voltage lithium ion batteries. *J. Power Sources* **2013**, *237*, 229–242.
- (43) Harks, P. P. R. M. L.; Mulder, F. M.; Notten, P. H. L. In situ methods for Li-ion battery research: review of recent developments. *J. Power Sources* **2015**, *288*, 92–105.
- (44) Novák, P.; Panitz, J. C.; Joho, F.; Lanz, M.; Imhof, R.; Coluccia, M. Advanced in situ methods for the characterization of practical electrodes in lithium-ion batteries. *J. Power Sources* **2000**, *90*, 52–58.
- (45) Winter, M.; Besenhard, J. O.; Spahr, M. E.; Novák, P. Insertion electrode materials for rechargeable lithium batteries. *Adv. Mater.* **1998**, *10*, 725–763.
- (46) Armand, M.; Tarascon, J. M. Building better batteries. *Nature* **2008**, *451*, 652–657.
- (47) Wang, K.-X.; Li, X.-H.; Chen, J.-S. Surface and Interface Engineering of Electrode Materials for Lithium-Ion Batteries. *Adv. Mater.* **2015**, *27*, 527–545.
- (48) Roy, P.; Srivastava, S. K. Nanostructured anode materials for lithium ion batteries. *J. Mater. Chem. A* **2015**, *3*, 2454.
- (49) Osiak, M.; Geaney, H.; Armstrong, E.; O'Dwyer, C. Structuring materials for lithium-ion batteries: advancements in nanomaterial structure, composition, and defined assembly on cell performance. *J. Mater. Chem. A* **2014**, *2*, 9433–9460.
- (50) Mauger, A.; Julien, C. Surface modifications of electrode materials for lithium-ion batteries: status and trends. *Ionics* **2014**, *20*, 751–787.

-
- (51) Erickson, E. M.; Ghanty, C.; Aurbach, D. New Horizons for Conventional Lithium Ion Battery Technology. *J. Phys. Chem. Lett.* **2014**, *5*, 3313–3324.
- (52) Wang, Y.; Zhong, W.-H. Development of Electrolytes towards Achieving Safe and High-Performance Energy-Storage Devices: A Review. *ChemElectroChem* **2015**, *2*, 22–36.
- (53) Nowak, S.; Winter, M. Review—Chemical Analysis for a Better Understanding of Aging and Degradation Mechanisms of Non-Aqueous Electrolytes for Lithium Ion Batteries: Method Development, Application and Lessons Learned. *J. Electrochem. Soc.* **2015**, *162*, A2500-A2508.
- (54) Hassoun, J.; Scrosati, B. Review—Advances in Anode and Electrolyte Materials for the Progress of Lithium-Ion and beyond Lithium-Ion Batteries. *J. Electrochem. Soc.* **2015**, *162*, A2582-A2588.
- (55) Deimede, V.; Elmasides, C. Separators for Lithium-Ion Batteries: A Review on the Production Processes and Recent Developments. *Energy Technol. (Weinheim, Ger.)* **2015**, *3*, 453–468.
- (56) Lee, H.; Yanilmaz, M.; Toprakci, O.; Fu, K.; Zhang, X. A review of recent developments in membrane separators for rechargeable lithium-ion batteries. *Energy Environ. Sci.* **2014**, *7*, 3857–3886.
- (57) Bresser, D.; Paillard, E.; Passerini, S. Chapter 6 - Lithium-ion batteries (LIBs) for medium- and large-scale energy storage: current cell materials and components. In *Advances in Batteries for Medium and Large-Scale Energy Storage*; Menictas, C., Skyllas-Kazacos, M., Mariana, L., Eds.; Woodhead Publishing: Cambridge, 2015; pp 125–211.
- (58) Kim, S. W.; Cho, K. Y. Current collectors for flexible lithium ion batteries: a review of materials. *J. Electrochem. Sci. Technol.* **2015**, *6*, 10–15.
- (59) Ferg, E.; Gummow, R. J.; Kock, A. de; Thackeray, M. M. Spinel Anodes for Lithium-Ion Batteries. *J. Electrochem. Soc.* **1994**, *141*, L147-L150.
- (60) Aldon, L.; Kubiak, P.; Womes, M.; Jumas, J. C.; Olivier-Fourcade, J.; Tirado, J. L.; Corredor, J. I.; Pérez Vicente, C. Chemical and Electrochemical Li-Insertion into the $\text{Li}_4\text{Ti}_5\text{O}_{12}$ Spinel. *Chem. Mater.* **2004**, *16*, 5721–5725.
- (61) Hahn, R.; Möller, K. C. Electrical Buffer Storage for Energy Harvesting. In *Handbook of Energy Harvesting Power Supplies and Applications*; Spies, P., Pollak, M., Mateu, L., Eds.; CRC Press: Boca Raton, 2013; p 463.

-
- (62) Pistoia, G. *Lithium-Ion Batteries: Advances and Applications*; Elsevier Science: Amsterdam, 2014.
- (63) Obrovac, M. N.; Christensen, L. Structural Changes in Silicon Anodes during Lithium Insertion/Extraction. *Electrochem. Solid-State Lett.* **2004**, *7*, A93-A96.
- (64) Bourderau, S.; Brousse, T.; Schleich, D. M. Amorphous silicon as a possible anode material for Li-ion batteries. *J. Power Sources* **1999**, *81–82*, 233–236.
- (65) Kang, K.; Lee, H.-S.; Han, D.-W.; Kim, G.-S.; Lee, D.; Lee, G.; Kang, Y.-M.; Jo, M.-H. Maximum Li storage in Si nanowires for the high capacity three-dimensional Li-ion battery. *Appl. Phys. Lett.* **2010**, *96*, 53110.
- (66) Beattie, S. D.; Larcher, D.; Morcrette, M.; Simon, B.; Tarascon, J.-M. Si Electrodes for Li-Ion Batteries—A New Way to Look at an Old Problem. *J. Electrochem. Soc.* **2008**, *155*, A158-A163.
- (67) Pereira-Nabais, C.; Swiatowska, J.; Chagnes, A.; Gohier, A.; Zanna, S.; Seyeux, A.; Tran-Van, P.; Cojocar, C.-S.; Cassir, M.; Marcus, P. Insight on the Solid Electrolyte Interphase (SEI) onto Si Nanowires in Lithium-Ion Battery: Chemical and Morphological Modifications upon Cycling. *J. Phys. Chem. C* **2014**, *118*, 2919.
- (68) Arreaga-Salas, D. E.; Sra, A. K.; Roodenko, K.; Chabal, Y. J.; Hinkle, C. L. Progression of Solid Electrolyte Interphase Formation on Hydrogenated Amorphous Silicon Anodes for Lithium-Ion Batteries. *J. Phys. Chem. C* **2012**, *116*, 9072–9077.
- (69) Wen, C. J.; Huggins, R. A. Chemical diffusion in intermediate phases in the lithium-silicon system. *J. Solid State Chem.* **1981**, *37*, 271–278.
- (70) Liu, X. H.; Wang, J. W.; Huang, S.; Fan, F.; Huang, X.; Liu, Y.; Krylyuk, S.; Yoo, J.; Dayeh, S. A.; Davydov, A. V. *et al.* In situ atomic-scale imaging of electrochemical lithiation in silicon. *Nat. Nanotechnol.* **2012**, *7*, 749–756.
- (71) Stearns, L. A.; Gryko, J.; Diefenbacher, J.; Ramachandran, G. K.; McMillan, P. F. Lithium monosilicide (LiSi), a low-dimensional silicon-based material prepared by high pressure synthesis: NMR and vibrational spectroscopy and electrical properties characterization. *J. Solid State Chem.* **2003**, *173*, 251–258.
- (72) Kubota, Y.; Escaño, M. C. S.; Nakanishi, H.; Kasai, H. Crystal and electronic structure of Li₁₅Si₄. *J. Appl. Phys.* **2007**, *102*, 53704.

-
- (73) Kubota, Y.; Escaño, M. C. S.; Nakanishi, H.; Kasai, H. Electronic structure of LiSi. *J. Alloys Compd.* **2008**, *458*, 151–157.
- (74) Leuken; Wijs, G. A. de; van der Lugt, W.; Groot, R. A. d. Electronic structure of Li₁₂Si₇. *Phys. Rev. B Condens. Matter (Physical Review B: Condensed Matter)* **1996**, *53*, 10599–10604.
- (75) Limthongkul, P.; Jang, Y.-I.; Dudney, N. J.; Chiang, Y.-M. Electrochemically-driven solid-state amorphization in lithium-silicon alloys and implications for lithium storage. *Acta Mater.* **2003**, *51*, 1103–1113.
- (76) Baggetto, L.; Niessen, R. A. H.; Roozeboom, F.; Notten, P. H. L. High Energy Density All-Solid-State Batteries: A Challenging Concept Towards 3D Integration. *Adv. Funct. Mater.* **2008**, *18*, 1057–1066.
- (77) Kim, H.; Chou, C.-Y.; Ekerdt, J. G.; Hwang, G. S. Structure and Properties of Li–Si Alloys: A First-Principles Study. *J. Phys. Chem. C* **2010**, *115*, 2514–2521.
- (78) Xu, W.; Wang, J.; Ding, F.; Chen, X.; Nasybulin, E.; Zhang, Y.; Zhang, J.-G. Lithium metal anodes for rechargeable batteries. *Energy Environ. Sci.* **2014**, *7*, 513–537.
- (79) Bieker, G.; Winter, M.; Bieker, P. Electrochemical in situ investigations of SEI and dendrite formation on the lithium metal anode. *Phys. Chem. Chem. Phys.* **2015**, *17*, 8670–8679.
- (80) Thomas, M. G. S. R.; Bruce, P. G.; Goodenough, J. B. AC Impedance Analysis of Polycrystalline Insertion Electrodes: Application to Li_{1-x}CoO₂. *J. Electrochem. Soc.* **1985**, *132*, 1521.
- (81) Aurbach, D.; Gamolsky, K.; Markovsky, B.; Salitra, G.; Gofer, Y.; Heider, U.; Oesten, R.; Schmidt, M. The Study of Surface Phenomena Related to Electrochemical Lithium Intercalation into Li_xMO_y Host Materials (M = Ni, Mn). *J. Electrochem. Soc.* **2000**, *147*, 1322.
- (82) Chen, C.H.; Liu, J.; Amine, K. Symmetric cell approach and impedance spectroscopy of high power lithium-ion batteries. *J. Power Sources* **2001**, *96*, 321–328.
- (83) Lu, W.; Zhang, J.; Xu, J.; Wu, X.; Chen, L. In Situ Visualized Cathode Electrolyte Interphase on LiCoO₂ in High Voltage Cycling. *ACS Appl. Mater. Interfaces* **2017**, *9*, 19313–19318.

-
- (84) Tan, H.; Takeuchi, S.; Bharathi, K. K.; Takeuchi, I.; Bendersky, L. A. Microscopy Study of Structural Evolution in Epitaxial LiCoO₂ Positive Electrode Films during Electrochemical Cycling. *ACS Appl. Mater. Interfaces* **2016**, *8*, 6727–6735.
- (85) Amatucci, G.; Tarascon, J. M.; Klein, L. C. Cobalt dissolution in LiCoO₂-based non-aqueous rechargeable batteries. *Solid State Ionics* **1996**, *83*, 167–173.
- (86) Tebbe, J. L.; Holder, A. M.; Musgrave, C. B. Mechanisms of LiCoO₂ Cathode Degradation by Reaction with HF and Protection by Thin Oxide Coatings. *ACS Appl. Mater. Interfaces* **2015**, *7*, 24265–24278.
- (87) Zuo, X.; Fan, C.; Xiao, X.; Liu, J.; Nan, J. High-voltage performance of LiCoO₂/graphite batteries with methylene methanedisulfonate as electrolyte additive. *J. Power Sources* **2012**, *219*, 94–99.
- (88) Takeuchi, T.; Kyuna, T.; Morimoto, H.; Tobishima, S.-i. Influence of surface modification of LiCoO₂ by organic compounds on electrochemical and thermal properties of Li/LiCoO₂ rechargeable cells. *J. Power Sources* **2011**, *196*, 2790–2801.
- (89) Abraham, K. M.; Jiang, Z. A Polymer Electrolyte-Based Rechargeable Lithium/Oxygen Battery. *J. Electrochem. Soc.* **1996**, *143*, 1–5.
- (90) Peled, E. The Electrochemical Behavior of Alkali and Alkaline Earth Metals in Nonaqueous Battery Systems - The Solid Electrolyte Interphase Model. *J. Electrochem. Soc.* **1979**, *126*, 2047–2051.
- (91) Dell, R. M.; Rand, D. A. J. *Understanding Batteries*; Royal Society of Chemistry: Cambridge, 2001.
- (92) Girishkumar, G.; McCloskey, B.; Luntz, A. C.; Swanson, S.; Wilcke, W. Lithium–Air Battery: Promise and Challenges. *J. Phys. Chem. Lett.* **2010**, *1*, 2193–2203.
- (93) Yoo, H. D.; Markevich, E.; Salitra, G.; Sharon, D.; Aurbach, D. On the challenge of developing advanced technologies for electrochemical energy storage and conversion. *Mater. Today* **2014**, *17*, 110–121.
- (94) Dey, A. N.; Sullivan, B. P. The Electrochemical Decomposition of Propylene Carbonate on Graphite. *J. Electrochem. Soc.* **1970**, *117*, 222–224.
- (95) Edström, K.; Herstedt, M.; Abraham, D. P. A new look at the solid electrolyte interphase on graphite anodes in Li-ion batteries. *J. Power Sources* **2006**, *153*, 380–384.

-
- (96) Goodenough, J. B.; Park, K.-S. The Li-Ion Rechargeable Battery: A Perspective. *J. Am. Chem. Soc.* **2013**, *135*, 1167–1176.
- (97) White, W. M. *Geochemistry*; Wiley-Blackwell: New York, 2013.
- (98) Bülter, H. Electron Transport Through the Solid Electrolyte Interphase in Lithium-Ion Batteries. PhD, Carl von Ossietzky University, Oldenburg, 2016.
- (99) *Nonaqueous electrochemistry*; Aurbach, D., Ed.; Marcel Dekker, Inc.: New York, 1999.
- (100) Bernhard, R.; Metzger, M.; Gasteiger, H. A. Gas Evolution at Graphite Anodes Depending on Electrolyte Water Content and SEI Quality Studied by On-Line Electrochemical Mass Spectrometry. *J. Electrochem. Soc.* **2015**, *162*, A1984-A1989.
- (101) Smith, A. J.; Burns, J. C.; Zhao, X.; Xiong, D.; Dahn, J. R. A High Precision Coulometry Study of the SEI Growth in Li/Graphite Cells. *J. Electrochem. Soc.* **2011**, *158*, A447-A452.
- (102) Ahn, D.; Xiao, X. Enhanced Rate Capability of Oxide Coated Lithium Titanate within Extended Voltage Ranges. *Front. Energy Res.* **2015**, *3*, DOI: 10.3389/fenrg.2015.00021.
- (103) Xu, M.; Dalavi, S.; Lucht, B. L. Electrolytes for Lithium-Ion Batteries with High-Voltage Cathodes. In *Lithium Batteries: Advanced Technologies and Applications*; Scrosati, B., Abraham, K. M., van Schalkwijk, W. A., Hassoun, J., Eds.; Wiley: New Jersey, 2013.
- (104) Winter, M.; Moeller, K. C.; Besenhard, J. O. Carbonaceous and Graphitic Anodes. In *Lithium-Ion Batteries: Science and Technologies*; Yoshio, M., Brodd, R. J., Kozawa, A., Eds.; Springer, 2010; p 144.
- (105) Besenhard, J. O.; Winter, M.; Yang, J.; Biberacher, W. Filming mechanism of lithium-carbon anodes in organic and inorganic electrolytes. *J. Power Sources* **1995**, *54*, 228–231.
- (106) Besenhard, J. O. The electrochemical preparation and properties of ionic alkali metal- and NR_4 -graphite intercalation compounds in organic electrolytes. *Carbon* **1976**, *14*, 111–115.
- (107) Besenhard, J. O.; Fritz, H. P. Cathodic reduction of graphite in organic solutions of alkali and NR_4^+ salts. *J. Electroanal. Chem. Interfacial Electrochem.* **1974**, *53*, 329–333.

-
- (108) Abe, T.; Kawabata, N.; Mizutani, Y.; Inaba, M.; Ogumi, Z. Correlation Between Cointercalation of Solvents and Electrochemical Intercalation of Lithium into Graphite in Propylene Carbonate Solution. *J. Electrochem. Soc.* **2003**, *150*, A257-A261.
- (109) Wagner, M. R.; Albering, J. H.; Moeller, K. C.; Besenhard, J. O.; Winter, M. XRD evidence for the electrochemical formation of in PC-based electrolytes. *Electrochem. Commun.* **2005**, *7*, 947–952.
- (110) Aurbach, D.; Markovsky, B.; Weissman, I.; Levi, E.; Ein-Eli, Y. On the correlation between surface chemistry and performance of graphite negative electrodes for Li ion batteries. *Electrochim. Acta* **1999**, *45*, 67–86.
- (111) Nakai, H.; Kubota, T.; Kita, A.; Kawashima, A. Investigation of the Solid Electrolyte Interphase Formed by Fluoroethylene Carbonate on Si Electrodes. *J. Electrochem. Soc.* **2011**, *158*, A798.
- (112) Choi, N.-S.; Yew, K. H.; Lee, K. Y.; Sung, M.; Kim, H.; Kim, S.-S. Effect of fluoroethylene carbonate additive on interfacial properties of silicon thin-film electrode. *J. Power Sources* **2006**, *161*, 1254–1259.
- (113) Chen, L.; Wang, K.; Xie, X.; Xie, J. Effect of vinylene carbonate (VC) as electrolyte additive on electrochemical performance of Si film anode for lithium ion batteries. *J. Power Sources* **2007**, *174*, 538–543.
- (114) Aurbach, D. Review of selected electrode solution interactions which determine the performance of Li and Li ion batteries. *J. Power Sources* **2000**, *89*, 206–218.
- (115) Kawamura, T.; Kimura, A.; Egashira, M.; Okada, S.; Yamaki, J.-I. Thermal stability of alkyl carbonate mixed-solvent electrolytes for lithium ion cells. *J. Power Sources* **2002**, *104*, 260–264.
- (116) Snook, G. A.; Huynh, T. D.; Hollenkamp, A. F.; Best, A. S. Rapid SECM probing of dissolution of LiCoO₂ battery materials in an ionic liquid. *J. Electroanal. Chem.* **2012**, *687*, 30–34.
- (117) Arora, P.; Doyle, M.; White, R. E. Mathematical Modeling of the Lithium Deposition Overcharge Reaction in Lithium-Ion Batteries Using Carbon-Based Negative Electrodes. *J. Electrochem. Soc.* **1999**, *146*, 3543–3553.
- (118) Vogl, U. S.; Lux, S. F.; Crumlin, E. J.; Liu, Z.; Terborg, L.; Winter, M.; Kostecki, R. The Mechanism of SEI Formation on a Single Crystal Si(100) Electrode. *J. Electrochem. Soc.* **2015**, *162*, A603-A607.

-
- (119) Nagao, Y.; Sakaguchi, H.; Honda, H.; Fukunaga, T.; Esaka, T. Structural Analysis of Pure and Electrochemically Lithiated SiO Using Neutron Elastic Scattering. *J. Electrochem. Soc.* **2004**, *151*, A1572.
- (120) Miyachi, M.; Yamamoto, H.; Kawai, H.; Ohta, T.; Shirakata, M. Analysis of SiO Anodes for Lithium-Ion Batteries. *J. Electrochem. Soc.* **2005**, *152*, A2089.
- (121) McDowell, M. T.; Lee, S. W.; Ryu, I.; Wu, H.; Nix, W. D.; Choi, J. W.; Cui, Y. Novel size and surface oxide effects in silicon nanowires as lithium battery anodes. *Nano letters* **2011**, *11*, 4018–4025.
- (122) Sun, Q.; Zhang, B.; Fu, Z.-W. Lithium electrochemistry of SiO₂ thin film electrode for lithium-ion batteries. *Appl. Surf. Sci.* **2008**, *254*, 3774–3779.
- (123) Lindgren, F.; Xu, C.; Niedzicki, L.; Marcinek, M.; Gustafsson, T.; Björefors, F.; Edström, K.; Younesi, R. SEI Formation and Interfacial Stability of a Si Electrode in a LiTDI-Salt Based Electrolyte with FEC and VC Additives for Li-Ion Batteries. *ACS Appl. Mater. Interfaces* **2016**, *8*, 15758–15766.
- (124) Niedzicki, L.; Kasprzyk, M.; Kuziak, K.; Żukowska, G. Z.; Armand, M.; Bukowska, M.; Marcinek, M.; Szczeciński, P.; Wieczorek, W. Modern generation of polymer electrolytes based on lithium conductive imidazole salts. *J. Power Sources* **2009**, *192*, 612–617.
- (125) Niedzicki, L.; Kasprzyk, M.; Kuziak, K.; Żukowska, G. Z.; Marcinek, M.; Wieczorek, W.; Armand, M. Liquid electrolytes based on new lithium conductive imidazole salts. *J. Power Sources* **2011**, *196*, 1386–1391.
- (126) Scheers, J.; Johansson, P.; Szczeciński, P.; Wieczorek, W.; Armand, M.; Jacobsson, P. Benzimidazole and imidazole lithium salts for battery electrolytes. *J. Power Sources* **2010**, *195*, 6081–6087.
- (127) Mazouzi, D.; Delpuech, N.; Oumellal, Y.; Gauthier, M.; Cerbelaud, M.; Gaubicher, J.; Dupré, N.; Moreau, P.; Guyomard, D.; Roué, L. *et al.* New insights into the silicon-based electrode's irreversibility along cycle life through simple gravimetric method. *J. Power Sources* **2012**, *220*, 180–184.
- (128) Xu, C.; Lindgren, F.; Philippe, B.; Gorgoi, M.; Björefors, F.; Edström, K.; Gustafsson, T. Improved Performance of the Silicon Anode for Li-Ion Batteries: Understanding the Surface Modification Mechanism of Fluoroethylene Carbonate as an Effective Electrolyte Additive. *Chem. Mater.* **2015**, *27*, 2591–2599.
- (129) Etacheri, V.; Haik, O.; Goffer, Y.; Roberts, G. A.; Stefan, I. C.; Fasching, R.; Aurbach, D. Effect of fluoroethylene carbonate (FEC) on the performance and
-

surface chemistry of Si-nanowire Li-ion battery anodes. *Langmuir* **2012**, *28*, 965–976.

(130) El Ouatani, L.; Dedryvère, R.; Siret, C.; Biensan, P.; Reynaud, S.; Iratçabal, P.; Gonbeau, D. The Effect of Vinylene Carbonate Additive on Surface Film Formation on Both Electrodes in Li-Ion Batteries. *J. Electrochem. Soc.* **2009**, *156*, A103.

(131) Leung, K.; Rempe, S. B.; Foster, M. E.; Ma, Y.; La Martinez del Hoz, J. M.; Sai, N.; Balbuena, P. B. Modeling Electrochemical Decomposition of Fluoroethylene Carbonate on Silicon Anode Surfaces in Lithium Ion Batteries. *J. Electrochem. Soc.* **2013**, *161*, A213-A221.

(132) Tasaki, K.; Goldberg, A.; Lian, J.-J.; Walker, M.; Timmons, A.; Harris, S. J. Solubility of Lithium Salts Formed on the Lithium-Ion Battery Negative Electrode Surface in Organic Solvents. *J. Electrochem. Soc.* **2009**, *156*, A1019.

(133) Jones, J.; Anouti, M.; Caillon-Caravanier, M.; Willmann, P.; Sizaret, P.-Y.; Lemordant, D. Solubilization of SEI lithium salts in alkylcarbonate solvents. *Fluid Phase Equilib.* **2011**, *305*, 121–126.

(134) Xu, K.; Lam, Y.; Zhang, S. S.; Jow, T. R.; Curtis, T. B. Solvation Sheath of Li⁺ in Nonaqueous Electrolytes and Its Implication of Graphite/Electrolyte Interface Chemistry. *J. Phys. Chem. C* **2007**, *111*, 7411–7421.

(135) Yamada, A.; Chung, S. C.; Hinokuma, K. Optimized LiFePO₄ for Lithium Battery Cathodes. *J. Electrochem. Soc.* **2001**, *148*, A224.

(136) Padhi, A. K.; Nanjundaswamy, K.; Goodenough, J. B. Phospho-olivines as Positive-Electrode Materials for Rechargeable Lithium Batteries. *J. Electrochem. Soc.* **1997**, *144*, 1188.

(137) Manthiram, A.; Goodenough, J. B. Lithium insertion into Fe₂(MO₄)₃ frameworks: Comparison of M = W with M = Mo. *J. Solid State Chem.* **1987**, *71*, 349–360.

(138) Manthiram, A.; Goodenough, J. B. Lithium insertion into Fe₂(SO₄)₃ frameworks. *J. Power Sources* **1989**, *26*, 403–408.

(139) Padhi, A. K.; Nanjunclawamy, K.; Masquelier, C.; Okada, S.; Goodenough, J. B. Effect of Structure on the Fe³⁺/Fe²⁺ Redox Couple in Iron Phosphates. *J. Electrochem. Soc.* **1997**, *144*, 1609.

(140) Goodenough, J. B. Mapping of Redox Energies. *Mol. Cryst. Liq. Cryst.* **2006**, *311*, 1–14.

-
- (141) E. Peled, S. M. Review—SEI: Past, Present and Future. *J. Electrochem. Soc.* **2017**, *164*.
- (142) Wang, A.; Kadam, S.; Li, H.; Shi, S.; Qi, Y. Review on modeling of the anode solid electrolyte interphase (SEI) for lithium-ion batteries. *npj Comput Mater* **2018**, *4*, 359.
- (143) Geronov, Y.; Schwager, F.; Muller, R. H. Electrochemical Studies of the Film Formation on Lithium in Propylene Carbonate Solutions under Open-Circuit Conditions. *J. Electrochem. Soc.* **1982**, *129*, 1422–1429.
- (144) Aurbach, D.; Weissman, I.; Zaban, A.; Chusid, O. Correlation between surface chemistry, morphology, cycling efficiency and interfacial properties of Li electrodes in solutions containing different Li salts. *Electrochim. Acta* **1994**, *39*, 51–71.
- (145) Aurbach, D.; Ein-Eli, Y.; Chusid, O.; Carmeli, Y.; Babai, M.; Yamin, H. The Correlation Between the Surface Chemistry and the Performance of Li-Carbon Intercalation Anodes for Rechargeable ‘Rocking-Chair’ Type Batteries. *J. Electrochem. Soc.* **1994**, *141*, 603–611.
- (146) Aurbach, D.; Zaban, A.; Gofer, Y.; Ely, Y. E.; Weissman, I.; Chusid, O.; Abramson, O. Recent studies of the lithium-liquid electrolyte interface Electrochemical, morphological and spectral studies of a few important systems. *J. Power Sources* **1995**, *54*, 76–84.
- (147) Kanamura, K.; Shiraishi, S.; Takehara, Z.-I. Electrochemical Deposition of Very Smooth Lithium Using Nonaqueous Electrolytes Containing HF. *J. Electrochem. Soc.* **1996**, *143*, 2187–2197.
- (148) Kanamura, K.; Tamura, H.; Shiraishi, S.; Takehara, Z.-I. XPS Analysis of Lithium Surfaces Following Immersion in Various Solvents Containing LiBF₄. *J. Electrochem. Soc.* **1995**, *142*, 340–347.
- (149) Aurbach, D.; Zaban, A.; Ein-Eli, Y.; Weissman, I.; Chusid, O.; Markovsky, B.; Levi, M.; Levi, E.; Schechter, A.; Granot, E. Recent studies on the correlation between surface chemistry, morphology, three-dimensional structures and performance of Li and Li-C intercalation anodes in several important electrolyte systems. *J. Power Sources* **1997**, *68*, 91–98.
- (150) Mori, S.; Asahina, H.; Suzuki, H.; Yonei, A.; Yokoto, K. Chemical properties of various organic electrolytes for lithium rechargeable batteries: 1.

-
- Characterization of passivating layer formed on graphite in alkyl carbonate solutions. *J. Power Sources* **1997**, *68*, 59–64.
- (151) Andersson, A. M.; Edström, K. Chemical Composition and Morphology of the Elevated Temperature SEI on Graphite. *J. Electrochem. Soc.* **2001**, *148*, A1100-A1109.
- (152) Andersson, A. M.; Henningson, A.; Siegbahn, H.; Jansson, U.; Edström, K. Electrochemically lithiated graphite characterised by photoelectron spectroscopy. *J. Power Sources* **2003**, *119-121*, 522–527.
- (153) Niehoff, P.; Passerini, S.; Winter, M. Interface Investigations of a Commercial Lithium Ion Battery Graphite Anode Material by Sputter Depth Profile X-ray Photoelectron Spectroscopy. *Langmuir* **2013**, *29*, 5806–5816.
- (154) Peled, E.; Golodnitsky, D.; Ardel, G. Advanced Model for Solid Electrolyte Interphase Electrodes in Liquid and Polymer Electrolytes. *J. Electrochem. Soc.* **1997**, *144*, L208-L210.
- (155) Augustsson, A.; Herstedt, M.; Guo, J. H.; Edström, K.; Zhuang, G. V.; Ross, P. N., JR; Rubensson, J. E.; Nordgren, J. Solid electrolyte interphase on graphite Li-ion battery anodes studied by soft X-ray spectroscopy. *Phys. Chem. Chem. Phys.* **2004**, *6*, 4185–4189.
- (156) Zhuang, G. V.; Ross, P. N. Analysis of the Chemical Composition of the Passive Film on Li-Ion Battery Anodes Using Attenuated Total Reflection Infrared Spectroscopy. *Electrochem. Solid-State Lett.* **2003**, *6*, A136-A139.
- (157) Aurbach, D.; Levi, M. D.; Levi, E.; Schechter, A. Failure and Stabilization Mechanisms of Graphite Electrodes. *J. Phys. Chem. A* **1997**, *101*, 2195–2206.
- (158) Aurbach, D.; Markovsky, B.; Shechter, A.; Ein-Eli, Y.; Cohen, H. A Comparative Study of Synthetic Graphite and Li Electrodes in Electrolyte Solutions Based on Ethylene Carbonate-Dimethyl Carbonate Mixtures. *J. Electrochem. Soc.* **1996**, *143*, 3809–3820.
- (159) Ein-Eli, Y.; Markovsky, B.; Aurbach, D.; Carmeli, Y.; Yamin, H.; Luski, S. The dependence of the performance of Li-C intercalation anodes for Li-ion secondary batteries on the electrolyte solution composition. *Electrochim. Acta* **1994**, *39*, 2559–2569.
- (160) Peled, E.; Golodnitsky, D.; Menachem, C.; Bar-Tow, D. An Advanced Tool for the Selection of Electrolyte Components for Rechargeable Lithium Batteries. *J. Electrochem. Soc.* **1998**, *145*, 3482–3486.

-
- (161) Peled, E.; Bar Tow, D.; Merson, A.; Gladkikh, A.; Burstein, L.; Golodnitsky, D. Composition, depth profiles and lateral distribution of materials in the SEI built on HOPG-TOF SIMS and XPS studies. *J. Power Sources* **2001**, 97-98, 52–57.
- (162) Aurbach, D.; Gofer, Y.; Ben-Zion, M.; Aped, P. An International Journal Devoted to all Aspects of Electrode Kinetics, Interfacial Structure, Properties of Electrolytes, Colloid and Biological Electrochemistry The behaviour of lithium electrodes in propylene and ethylene carbonate: The major factors that influence Li cycling efficiency. *J. Electroanal. Chem.* **1992**, 339, 451–471.
- (163) Aurbach, D.; Zaban, A. An International Journal Devoted to all Aspects of Electrode Kinetics, Interfacial Structure, Properties of Electrolytes, Colloid and Biological Electrochemistry Impedance spectroscopy of lithium electrodes. *J. Electroanal. Chem.* **1993**, 348, 155–179.
- (164) Aurbach, D.; Cohen, Y. The Application of Atomic Force Microscopy for the Study of Li Deposition Processes. *J. Electrochem. Soc.* **1996**, 143, 3525–3532.
- (165) Aurbach, D.; Moshkovich, M. A Study of Lithium Deposition-Dissolution Processes in a Few Selected Electrolyte Solutions by Electrochemical Quartz Crystal Microbalance. *J. Electrochem. Soc.* **1998**, 145, 2629–2639.
- (166) Morigaki, K.-i.; Ohta, A. Analysis of the surface of lithium in organic electrolyte by atomic force microscopy, Fourier transform infrared spectroscopy and scanning auger electron microscopy. *J. Power Sources* **1998**, 76, 159–166.
- (167) Schmitz, R.; Ansgar Müller, R.; Wilhelm Schmitz, R.; Schreiner, C.; Kunze, M.; Lex-Balducci, A.; Passerini, S.; Winter, M. SEI investigations on copper electrodes after lithium plating with Raman spectroscopy and mass spectrometry. *J. Power Sources* **2013**, 233, 110–114.
- (168) Zhang, H.-L.; Li, F.; Liu, C.; Tan, J.; Cheng, H.-M. New Insight into the Solid Electrolyte Interphase with Use of a Focused Ion Beam. *J. Phys. Chem. A* **2005**, 109, 22205–22211.
- (169) Kang, S. H.; Abraham, D. P.; Xiao, A.; Lucht, B. L. Investigating the solid electrolyte interphase using binder-free graphite electrodes. *J. Power Sources* **2008**, 175, 526–532.
- (170) Kominato, A.; Yasukawa, E.; Sato, N.; Ijuuin, T.; Asahina, H.; Mori, S. Analysis of surface films on lithium in various organic electrolytes. *J. Power Sources* **1997**, 68, 471–475.

-
- (171) Aurbach, D.; Daroux, M. L.; Faguy, P. W.; Yeager, E. Identification of Surface Films Formed on Lithium in Propylene Carbonate Solutions. *J. Electrochem. Soc.* **1987**, *134*, 1611–1620.
- (172) Bar-Tow, D.; Peled, E.; Burstein, L. A study of highly oriented pyrolytic graphite as a model for the graphite anode in Li-ion batteries. *J. Electrochem. Soc.* **1999**, *146*, 824–832.
- (173) Heine, J.; Hilbig, P.; Qi, X.; Niehoff, P.; Winter, M.; Bieker, P. Fluoroethylene Carbonate as Electrolyte Additive in Tetraethylene Glycol Dimethyl Ether Based Electrolytes for Application in Lithium Ion and Lithium Metal Batteries. *J. Electrochem. Soc.* **2015**, *162*, A1094-A1101.
- (174) Xu, K. Electrolytes and Interphases in Li-Ion Batteries and Beyond. *Chem. Rev. (Washington, DC, U. S.)* **2014**, *114*, 11503–11618.
- (175) Dunst, A.; Sternad, M.; Epp, V.; Wilkening, M. Fast Li⁺ Self-Diffusion in Amorphous Li–Si Electrochemically Prepared from Semiconductor Grade, Monocrystalline Silicon: Insights from Spin-Locking Nuclear Magnetic Relaxometry. *J. Phys. Chem. C* **2015**, *119*, 12183–12192.
- (176) Philippe, B.; Dedryvère, R.; Allouche, J.; Lindgren, F.; Gorgoi, M.; Rensmo, H.; Gonbeau, D.; Edström, K. Nanosilicon Electrodes for Lithium-Ion Batteries: Interfacial Mechanisms Studied by Hard and Soft X-ray Photoelectron Spectroscopy. *Chem. Mater.* **2012**, *24*, 1107–1115.
- (177) Gao, B.; Sinha, S.; Fleming, L.; Zhou, O. Alloy Formation in Nanostructured Silicon. *Adv. Mater.* **2001**, *13*, 816–819.
- (178) Li, H.; Huang, X.; Chen, L.; Zhou, G.; Zhang, Z.; Yu, D. Mo, Y.J.; Pei, N. The crystal structural evolution of nano-Si anode caused by lithium insertion and extraction at room temperature. *Solid State Ionics* **2000**, *135*, 181–191.
- (179) Netz, A.; Huggins, R. A.; Weppner, W. The formation and properties of amorphous silicon as negative electrode reactant in lithium systems. *J. Power Sources* **2003**, *119-121*, 95–100.
- (180) Hatchard, T. D.; Dahn, J. R. In Situ XRD and Electrochemical Study of the Reaction of Lithium with Amorphous Silicon. *J. Electrochem. Soc.* **2004**, *151*, A838.
- (181) Li, J.; Dahn, J. R. An In Situ X-Ray Diffraction Study of the Reaction of Li with Crystalline Si. *J. Electrochem. Soc.* **2007**, *154*, A156.

-
- (182) Ryu, J. H.; Kim, J. W.; Sung, Y.-E.; Oh, S. M. Failure Modes of Silicon Powder Negative Electrode in Lithium Secondary Batteries. *Electrochem. Solid-State Lett.* **2004**, *7*, A306.
- (183) Ma, D.; Cao, Z.; Hu, A. Si-Based Anode Materials for Li-Ion Batteries: A Mini Review. *Nano-Micro Lett.* **2014**, *6*, 347–358.
- (184) Chan, C. K.; Peng, H.; Liu, G.; McIlwrath, K.; Zhang, X. F.; Huggins, R. A.; Cui, Y. High-performance lithium battery anodes using silicon nanowires. *Nat. Nanotechnol.* **2008**, *3*, 31–35.
- (185) Wu, H.; Chan, G.; Choi, J. W.; Ryu, I.; Yao, Y.; McDowell, M. T.; Lee, S. W.; Jackson, A.; Yang, Y.; Hu, L. *et al.* Stable cycling of double-walled silicon nanotube battery anodes through solid-electrolyte interphase control. *Nat. Nanotechnol.* **2012**, *7*, 310–315.
- (186) Kikkawa, J.; Terada, S.; Gunji, A.; Nagai, T.; Kurashima, K.; Kimoto, K. Chemical States of Overcharged LiCoO₂ Particle Surfaces and Interiors Observed Using Electron Energy-Loss Spectroscopy. *J. Phys. Chem. C* **2015**, *119*, 15823–15830.
- (187) Park, Y.; Shin, S. H.; Lee, S. M.; Kim, S. P.; Choi, H. C.; Jung, Y. M. 2D Raman correlation analysis of formation mechanism of passivating film on overcharged LiCoO₂ electrode with additive system. *J. Mol. Struct.* **2014**, *1069*, 183–187.
- (188) Liu, Y.-M.; Nicolau, B.; Esbenschade, J. L.; Gewirth, A. A. Characterization of the Cathode Electrolyte Interface in Lithium Ion Batteries by Desorption Electrospray Ionization Mass Spectrometry. *Anal. Chem.* **2016**, *88*, 7171–7177.
- (189) Hoffmann, M.; Zier, M.; Oswald, S.; Eckert, J. Challenges for lithium species identification in complementary Auger and X-ray photoelectron spectroscopy. *J. Power Sources* **2015**, *288*, 434–440.
- (190) Gauthier, M.; Carney, T. J.; Grimaud, A.; Giordano, L.; Pour, N.; Chang, H.-H.; Fenning, D. P.; Lux, S. F.; Paschos, O.; Bauer, C. *et al.* Electrode-electrolyte interface in Li-ion batteries: Current understanding and new insights. *J. Phys. Chem. Lett.* **2015**, *6*, 4653–4672.
- (191) Niehoff, P.; Winter, M. Composition and Growth Behavior of the Surface and Electrolyte Decomposition Layer of/on a Commercial Lithium Ion Battery

-
- $\text{Li}_x\text{Ni}_{1/3}\text{Mn}_{1/3}\text{Co}_{1/3}\text{O}_2$ Cathode Determined by Sputter Depth Profile X-ray Photoelectron Spectroscopy. *Langmuir* **2013**, *29*, 15813–15821.
- (192) Verdier, S.; El Ouatani, L.; Dedryvère, R.; Bonhomme, F.; Biensan, P.; Gonbeau, D. XPS Study on Al_2O_3 - and AlPO_4 -Coated LiCoO_2 Cathode Material for High-Capacity Li Ion Batteries. *J. Electrochem. Soc.* **2007**, *154*, A1088.
- (193) Christensen, J.; Newman, J. A Mathematical Model for the Lithium-Ion Negative Electrode Solid Electrolyte Interphase. *J. Electrochem. Soc.* **2004**, *151*, A1977-A1988.
- (194) Aurbach, D.; Zinigrad, E.; Cohen, Y.; Teller, H. A short review of failure mechanisms of lithium metal and lithiated graphite anodes in liquid electrolyte solutions. *Solid State Ionics* **2002**, *148*, 405–416.
- (195) Xu, K.; Wald Cresce, A. von. Li^+ -solvation/desolvation dictates interphasial processes on graphitic anode in Li ion cells. *J. Mater. Res.* **2012**, *27*, 2327–2341.
- (196) Tang, M.; Newman, J. Electrochemical Characterization of SEI-Type Passivating Films Using Redox Shuttles. *J. Electrochem. Soc.* **2011**, *158*, A530-A536.
- (197) Patterson, M. L. Molecular Imprinting: Does It Play a Role in the Reduction of Oxidized Redox Shuttle Molecules. *ECS Trans.* **2011**, *35*, 203–212.
- (198) Burns, J. C.; Jain, G.; Smith, A. J.; Eberman, K. W.; Scott, E.; Gardner, J. P.; Dahn, J. R. Evaluation of Effects of Additives in Wound Li-Ion Cells Through High Precision Coulometry. *J. Electrochem. Soc.* **2011**, *158*, A255-A261.
- (199) Smith, A. J.; Burns, J. C.; Dahn, J. R. A High Precision Study of the Coulombic Efficiency of Li-Ion Batteries. *Electrochem. Solid-State Lett.* **2010**, *13*, A177-A179.
- (200) Smith, A. J.; Burns, J. C.; Trussler, S.; Dahn, J. R. Precision Measurements of the Coulombic Efficiency of Lithium-Ion Batteries and of Electrode Materials for Lithium-Ion Batteries. *J. Electrochem. Soc.* **2010**, *157*, A196-A202.
- (201) Zampardi, G.; La Mantia, F.; Schuhmann, W. In-operando evaluation of the effect of vinylene carbonate on the insulating character of the solid electrolyte interphase. *Electrochem. Commun.* **2015**, *58*, 1.
- (202) Aurbach, D.; Ein-Eli, Y.; Zaban, A. The Surface Chemistry of Lithium Electrodes in Alkyl Carbonate Solutions. *J. Electrochem. Soc.* **1994**, *141*, L1-L3.

-
- (203) Park, G.; Nakamura, H.; Lee, Y.; Yoshio, M. The important role of additives for improved lithium ion battery safety. *J. Power Sources* **2009**, *189*, 602–606.
- (204) MacNeil, D. D.; Larcher, D.; Dahn, J. R. Comparison of the Reactivity of Various Carbon Electrode Materials with Electrolyte at Elevated Temperature. *J. Electrochem. Soc.* **1999**, *146*, 3596–3602.
- (205) Zhang, S. S.; Xu, K.; Jow, T. R. Electrochemical impedance study on the low temperature of Li-ion batteries. *Electrochim. Acta* **2004**, *49*, 1057–1061.
- (206) Churikov, A. V. Transfer mechanism in solid-electrolyte layers on lithium: influence of temperature and polarization. *Electrochim. Acta* **2001**, *46*, 2415–2426.
- (207) Krueger, S.; Kloepsch, R.; Li, J.; Nowak, S.; Passerini, S.; Winter, M. How do reactions at the anode/electrolyte interface determine the cathode performance in lithium-ion batteries? *J. Electrochem. Soc.* **2013**, *160*, A542-A548.
- (208) Chen, C. H.; Liu, J.; Amine, K. Symmetric cell approach towards simplified study of cathode and anode behavior in lithium ion batteries. *Electrochem. Commun.* **2001**, *3*, 44–47.
- (209) Amine, K.; Chen, C. H.; Liu, J.; Hammond, M.; Jansen, A.; Dees, D.; Bloom, I.; Vissers, D.; Henriksen, G. Factors responsible for impedance rise in high power lithium ion batteries. *J. Power Sources* **2001**, *97-98*, 684–687.
- (210) Li, J.; Murphy, E.; Winnick, J.; Kohl, P. A. The effects of pulse charging on cycling characteristics of commercial lithium-ion batteries. *J. Power Sources* **2001**, *102*, 302–309.
- (211) Wang, H. TEM Study of Electrochemical Cycling-Induced Damage and Disorder in LiCoO₂ Cathodes for Rechargeable Lithium Batteries. *J. Electrochem. Soc.* **1999**, *146*, 473.
- (212) Engstrom, R. C.; Weber, M.; Wunder, D. J.; Burgess, R.; Winquist, S. Measurements within the Diffusion Layer Using a Microelectrode Probe. *Anal. Chem.* **1986**, *58*, 844–848.
- (213) Bard, A. J.; Fan, F.-R. F.; Kwak, J.; Lev, O. Scanning Electrochemical Microscopy. Introduction and Principles. *Anal. Chem.* **1989**, *61*, 132–138.
- (214) Wittstock, G.; Burchardt, M.; Pust, S. E. Applications of Scanning Electrochemical Microscopy (SECM). In *Applied Scanning Probe Methods VII*; Bhushan, B., Fuchs, H., Eds.; Springer: Berlin, 2007; pp 259–299.
-

-
- (215) Zampardi, G.; Klink, S.; Kuznetsov, V.; Erichsen, T.; Maljusch, A.; La Mantia, F.; Schuhmann, W.; Ventosa, E. Combined AFM/SECM Investigation of the Solid Electrolyte Interphase in Li-Ion Batteries. *ChemElectroChem* **2015**, 1607.
- (216) Zampardi, G.; La Mantia, F.; Schuhmann, W. Determination of the formation and range of stability of the SEI on glassy carbon by local electrochemistry. *RSC Adv.* **2015**, 5, 31166–31171.
- (217) Bülter, H.; Peters, F.; Schwenzel, J.; Wittstock, G. Comparison of Electron Transfer Properties of the SEI on Graphite Composite and Metallic Lithium Electrodes by SECM at OCP. *J. Electrochem. Soc.* **2015**, 162, A7024-A7036.
- (218) Bülter, H.; Peters, F.; Schwenzel, J.; Wittstock, G. In Situ Quantification of the Swelling of Graphite Composite Electrodes by Scanning Electrochemical Microscopy. *J. Electrochem. Soc.* **2016**, 163, A27.
- (219) Bülter, H.; Peters, F.; Wittstock, G. Scanning Electrochemical Microscopy for the In Situ Characterization of Solid-Electrolyte Interphases: Highly Oriented Pyrolytic Graphite versus Graphite Composite. *Energy Technol.* **2016**, 4, 1486–1494.
- (220) Ventosa, E.; Schuhmann, W. Scanning electrochemical microscopy of Li-ion batteries. *Phys. Chem. Chem. Phys.* **2015**, 28441.
- (221) Snook, G. A.; Huynh, T. D.; Best, A. S. SECM Dissolution Studies of Pasted Battery Cathodes in Ionic Liquid Electrolytes. *ECS Trans.* **2014**, 58, 1–8.
- (222) Baek, B.; Xu, F.; Jung, C. Indirect oxidation of LiCoO₂ electrodes: more severe conditions to analyze the interface performance. *Int. J. Electrochem. Sci.* **2011**, 6, 6599–6606.
- (223) Xu, F.; Jung, C. Electrolyte research near graphite particles by the feedback current using a Li metal probe. *Int. J. Electrochem. Sci.* **2014**, 9, 380-389, 10 pp.
- (224) Xu, F.; Baek, B.; Jung, C. In situ electrochemical studies for Li⁺ ions dissociation from the LiCoO₂ electrode by the substrate-generation/tip-collection mode in SECM. *J. Solid State Electrochem.* **2012**, 16, 305–311.
- (225) Takahashi, Y.; Kumatani, A.; Munakata, H.; Inomata, H.; Ito, K.; Ino, K.; Shiku, H.; Unwin, P. R.; Korchev, Y. E.; Kanamura, K. *et al.* Nanoscale visualization of redox activity at lithium-ion battery cathodes. *Nat. Commun.* **2014**, 5, 5450-1 - 5450-7.

-
- (226) Zampardi, G.; Ventosa, E.; La Mantia, F.; Schuhmann, W. Scanning Electrochemical Microscopy Applied to the Investigation of Lithium (De-)Insertion in TiO₂. *Electroanalysis* **2015**, *27*, 1017–1025.
- (227) Zampardi, G.; Ventosa, E.; La Mantia, F.; Schuhmann, W. In situ visualization of Li-ion intercalation and formation of the solid electrolyte interphase on TiO₂ based paste electrodes using scanning electrochemical microscopy. *Chem. Commun. (Cambridge, U. K.)* **2013**, *49*, 9347–9349.
- (228) Katayama, Y.; Onodera, H.; Yamagata, M.; Miura, T. Electrochemical Reduction of Oxygen in Some Hydrophobic Room-Temperature Molten Salt Systems. *J. Electrochem. Soc.* **2004**, *151*, A59-A63.
- (229) Katayama, Y.; Sekiguchi, K.; Yamagata, M.; Miura, T. Electrochemical Behavior of Oxygen/Superoxide Ion Couple in 1-Butyl-1-methylpyrrolidinium Bis(trifluoromethylsulfonyl)imide Room-Temperature Molten Salt. *J. Electrochem. Soc.* **2005**, *152*, E247-E250.
- (230) Levi, M. D.; Aurbach, D. Diffusion Coefficients of Lithium Ions during Intercalation into Graphite Derived from the Simultaneous Measurements and Modeling of Electrochemical Impedance and Potentiostatic Intermittent Titration Characteristics of Thin Graphite Electrodes. *J. Phys. Chem. A* **1997**, *101*, 4641–4647.
- (231) dos Santos Sardinha, E.; Sternad, M.; Wilkening, H. M.; Wittstock, G. Nascent SEI-Surface Films on Single Crystalline Silicon Investigated by Scanning Electrochemical Microscopy. *ACS Appl. Energy Mater.* **2019**, DOI: 10.1021/acsaem.8b01967.
- (232) Cornut, R.; Lefrou, C. New analytical approximation of feedback approach curves with a microdisk SECM tip and irreversible kinetic reaction at the substrate. *J. Electroanal. Chem.* **2008**, *621*, 178–184.
- (233) Tang, M.; Newman, J. Transient Characterization of Solid-Electrolyte-Interphase Using Ferrocene. *J. Electrochem. Soc.* **2012**, *159*, A281-A289.
- (234) Tang, M.; Newman, J. Why is the solid-electrolyte-interphase selective?: Through-film ferrocenium reduction on highly oriented pyrolytic graphite. *J. Electrochem. Soc.* **2012**, *159*, A1922-A1927.
- (235) Kaymaksiz, S.; Wachtler, M.; Wohlfahrt-Mehrens, M. Influence of the solid electrolyte interphase on the performance of redox shuttle additives in Li-ion

batteries - A rotating ring-disc electrode study. *J. Power Sources* **2015**, *273*, 123–127.

(236) Moshurchak, L. M.; Bulinski, M.; Lamanna, W. M.; Wang, R. L.; Dahn, J. R. Direct comparison of 2,5-di-tert-butyl-1,4-dimethoxybenzene and 4-tert-butyl-1,2-dimethoxybenzene as redox shuttles in LiFePO₄-based Li-ion cells. *Electrochem. Commun.* **2007**, *9*, 1497–1501.

(237) Moshurchak, L. M.; Buhrmester, C.; Wang, R. L.; Dahn, J. R. Comparative studies of three redox shuttle molecule classes for overcharge protection of LiFePO₄-based Li-ion cells. *Electrochim. Acta* **2007**, *52*, 3779–3784.

(238) Liu, X.-R.; Deng, X.; Liu, R.-R.; Yan, H.-J.; Guo, Y.-G.; Wang, D.; Wan, L.-J. Single nanowire electrode electrochemistry of silicon anode by in situ atomic force microscopy: solid electrolyte interphase growth and mechanical properties. *ACS Appl. Mater. Interfaces* **2014**, *6*, 20317–20323.

(239) Bhushan, B.; Koinkar, V. N. Tribological studies of silicon for magnetic recording applications (invited). *J. Appl. Phys.* **1994**, *75*, 5741–5746.

(240) Santinacci, L.; Djenizian, T.; Schmuki, P. Nanoscale patterning of Si(100) surfaces by scratching through the native oxide layer using atomic force microscope. *Appl. Phys. Lett.* **2001**, *79*, 1882–1884.

(241) Santinacci, L.; Djenizian, T.; Hildebrand, H.; Ecoffey, S.; Mokdad, H.; Campanella, T.; Schmuki, P. Selective palladium electrochemical deposition onto AFM-scratched silicon surfaces. *Electrochim. Acta* **2003**, *48*, 3123–3130.

(242) Becker, C. R.; Strawhecker, K. E.; McAllister, Q. P.; Lundgren, C. A. In Situ Atomic Force Microscopy of Lithiation and Delithiation of Silicon Nanostructures for Lithium Ion Batteries. *ACS Nano* **2013**, *7*, 9173–9182.

(243) Barton Zachary, J.; Rodriguez-Lopez, J. Lithium ion quantification using mercury amalgams as in situ electrochemical probes in nonaqueous media. *Anal. Chem.* **2014**, *86*, 10660–10667.

(244) Lipson, A. L.; Ginder, R. S.; Hersam, M. C. Nanoscale In Situ Characterization of Li-ion Battery Electrochemistry Via Scanning Ion Conductance Microscopy. *Adv. Mater.* **2011**, *23*, 5613–5617.

(245) Buhrmester, C.; Moshurchak, L.; Wang, R. L.; Dahn, J. R. Phenothiazine Molecules- Possible Redox Shuttle Additives for Chemical Overcharge and Overdischarge Protection for Lithium-Ion Batteries. *J. Electrochem. Soc.* **2006**, *153*, A288-A294.

-
- (246) Zhang, Z.; Zhang, L.; Schlueter, J. A.; Redfern, P. C.; Curtiss, L.; Amine, K. Understanding the redox shuttle stability of 3,5-di-tert-butyl-1,2-dimethoxybenzene for overcharge protection of lithium-ion batteries. *J. Power Sources* **2010**, *195*, 4957–4962.
- (247) Feng, J. K.; Ai, X. P.; Cao, Y. L.; Yang, H. X. A highly soluble dimethoxybenzene derivative as a redox shuttle for overcharge protection of secondary lithium batteries. *Electrochem. Commun.* **2007**, *9*, 25–30.
- (248) Buhrmester, C.; Chen, J.; Moshurchak, L.; Jiang, J.; Wang, R. L.; Dahn, J. R. Studies of Aromatic Redox Shuttle Additives for LiFePO₄-Based Li-Ion Cells. *J. Electrochem. Soc.* **2005**, *152*, A2390-A2399.
- (249) Chen, J. H.; He, L. M.; Wang, R. L. Correlation between the stability of redox shuttles in Li ion cells and the reactivity defined by the binding energy of redox shuttle cations with ethyl radical. *J. Electrochem. Soc.* **2012**, *159*, A1636-A1645.
- (250) Wang, R. L.; Dahn, J. R. Computational Estimates of Stability of Redox Shuttle Additives for Li-Ion Cells. *J. Electrochem. Soc.* **2006**, *153*, A1922-A1928.
- (251) Huang, J.; Azimi, N.; Cheng, L.; Shkrob, I.; Xue, Z.; Zhang, J.; Dietz, N.; Curtiss, L. A.; Amine, K.; Zhang, Z. *et al.* The Organophosphine Oxide Redox Shuttle Additive That Delivers Long-term Overcharge Protection in 4 V Lithium-ion Batteries. *J. Mater. Chem. A* **2015**, *3*, 10710.
- (252) Huang, J.; Shkrob, I. A.; Wang, P.; Cheng, L.; Pan, B.; He, M.; Liao, C.; Zhang, Z.; Curtiss, L. A.; Zhang, L. 1,4-Bis(trimethylsilyl)-2,5-dimethoxybenzene: a novel redox shuttle additive for overcharge protection in lithium-ion batteries that doubles as a mechanistic chemical probe. *J. Mater. Chem. A* **2015**, *3*, 7332.
- (253) Golovin, M. N.; Wilkinson, D. P.; Dudley, J. T.; Holonko, D.; Woo, S. Applications of Metallocenes in Rechargeable Lithium Batteries for Overcharge Protection. *J. Electrochem. Soc.* **1992**, *139*, 5–10.
- (254) Abraham, K. M.; Pasquariello, D. M.; Willstaedt, E. B. n-Butylferrocene for Overcharge Protection of Secondary Lithium Batteries. *J. Electrochem. Soc.* **1990**, *137*, 1856–1857.
- (255) Ates, M. N.; Allen, C. J.; Mukerjee, S.; Abraham, K. M. Electronic effects of substituents on redox shuttles for overcharge protection of Li-ion batteries. *J. Electrochem. Soc.* **2012**, *159*, A1057-A1064.
-

-
- (256) Barrio, R.; Maffiotte, C.; Gandía, J. J.; Cárabe, J. Surface characterisation of wafers for silicon-heterojunction solar cells. *J. Non-Cryst. Solids* **2006**, *352*, 945–949.
- (257) Appetecchi, G. B.; Scaccia, S.; Tizzani, C.; Alessandrini, F.; Passerini, S. Synthesis of Hydrophobic Ionic Liquids for Electrochemical Applications. *J. Electrochem. Soc.* **2006**, *153*, A1685.
- (258) Ding, M. S.; Koch, S. L.; Passerini, S. The Effect of 1-Pentylamine as Solid Electrolyte Interphase Precursor on Lithium Metal Anodes. *Electrochim. Acta* **2017**, *240*, 408–414.
- (259) Nunes Kirchner, C.; Szunerits, S.; Wittstock, G. Scanning Electrochemical Microscopy (SECM) Based Detection of Oligonucleotide Hybridization and Simultaneous Determination of the Surface Concentration of Immobilized Oligonucleotides on Gold. *Electroanalysis* **2007**, *19*, 1258–1267.
- (260) Nogala, W.; Szot, K.; Burchardt, M.; Roelfs, F.; Rogalski, J.; Opallo, M.; Wittstock, G. Feedback mode SECM study of laccase and bilirubin oxidase immobilised in a sol-gel processed silicate film. *Analyst* **2010**, *135*, 2051–2058.
- (261) Bard, A. J. Effect of Electrode Configuration and Transition Time in Solid Electrode Chronopotentiometry. *Anal. Chem.* **1961**, *33*, 11–15.
- (262) Heinze, J. Diffusion Processes at Finite (Micro) Disk Electrodes Solved by Digital Simulation. *J. Electroanal. Chem.* **1981**, *124*, 73–86.
- (263) Bond, A. M.; Oldham, K. B.; Zoski, C. G. Steady-State Voltammetry. *Anal. Chim. Acta* **1989**, *216*, 177–230.
- (264) Kim, H.; Lee, E.-J.; Sun, Y.-K. Recent advances in the Si-based nanocomposite materials as high capacity anode materials for lithium ion batteries. *Mater. Today* **2014**, *17*, 285–297.
- (265) Ma, D. D. D.; Lee, C. S.; Au, F. C. K.; Tong, S. Y.; Lee, S. T. Small-Diameter Silicon Nanowire Surfaces. *Science* **2003**, *299*, 1874–1877.
- (266) Chan, C. K.; Ruffo, R.; Hong, S. S.; Cui, Y. Surface chemistry and morphology of the solid electrolyte interphase on silicon nanowire lithium-ion battery anodes. *J. Power Sources* **2009**, *189*, 1132–1140.
- (267) He, Y.; Piper, D. M.; Gu, M.; Travis, J. J.; George, S. M.; Lee, S.-H.; Genc, A.; Pullan, L.; Liu, J.; Mao, S. X. *et al.* In Situ Transmission Electron Microscopy Probing of Native Oxide and Artificial Layers on Silicon Nanoparticles for Lithium Ion Batteries. *ACS Nano* **2014**, *8*, 11816–11823.

-
- (268) Naumkin, A. V.; Kraut-Vass, A.; Gaarenstroom, S. W.; Powell, C. J. *X-ray Photoelectron Spectroscopy Database XPS, Version 4.1, NIST Standard Reference Database 20*, 2012.
- (269) Thermo Fisher Scientific. *Angle Resolved XPS*. Application Note, 2008 (31014).
- (270) Buqa, H.; Golob, P.; Winter, M.; Besenhard, J. O. Modified carbons for improved anodes in lithium ion cells. *J. Power Sources* **2001**, 97-98, 122–125.
- (271) Santner, H. J.; Korepp, C.; Winter, M.; Besenhard, J. O.; Möller, K.-C. In-situ FTIR investigations on the reduction of vinylene electrolyte additives suitable for use in lithium-ion batteries. *Anal. Bioanal. Chem.* **2004**, 379, 266–271.
- (272) Santner, H. J.; Möller, K.-C.; Ivančo, J.; Ramsey, M. G.; Netzer, F. P.; Yamaguchi, S.; Besenhard, J. O.; Winter, M. Acrylic acid nitrile, a film-forming electrolyte component for lithium-ion batteries, which belongs to the family of additives containing vinyl groups. *J. Power Sources* **2003**, 119-121, 368–372.
- (273) Bard, A. J.; Faulkner, L. R. *Electrochemical Methods: Fundamentals and Applications*, 2nd; John Wiley & Sons: New York, 2001.
- (274) Ma, G.; Wen, Z.; Wu, M.; Shen, C.; Wang, Q.; Jin, J.; Wu, X. A lithium anode protection guided highly-stable lithium-sulfur battery. *Chem. Commun. (Cambridge, U. K.)* **2014**, 50, 14209–14212.
- (275) Grande, L.; Paillard, E.; Kim, G.-T.; Monaco, S.; Passerini, S. Ionic liquid electrolytes for Li-air batteries: Lithium metal cycling. *Int. J. Mol. Sci.* **2014**, 15, 8122–8137.
- (276) Arning, M. D.; Minter, S. D. Electrode Potentials. In *Handbook of Electrochemistry: Chapter 18 - Electrode Potentials*; Arning, D., Minter, S., Zoski, C., Eds.; Elsevier, 2007; pp 813–827.
- (277) Shen, Z.; Dai, J.; Xiong, J.; He, X.; Mo, W.; Hu, B.; Sun, N.; Hu, X. 2,3-Dichloro-5,6-dicyano-1,4-benzoquinone (DDQ)/tert-Butyl Nitrite/Oxygen: A Versatile Catalytic Oxidation System. *Adv. Synth. Catal.* **2011**, 353, 3031–3038.
- (278) Hong, Y.; Fang, T.; Li, M.; Shen, Z.; Hu, X.; Mo, W.; Hu, B.; Sun, N.; Jin, L. 2,3-Dichloro-5,6-dicyano-1,4-benzoquinone-catalyzed aerobic oxidation reactions via multistep electron transfers with iron(ii) phthalocyanine as an electron-transfer mediator. *RSC Adv.* **2016**, 6, 51908–51913.

-
- (279) Lhenry, S.; Leroux Yann, R.; Hapiot, P. Chemically irreversible redox mediator for SECM kinetics investigations. Determination of the absolute tip-sample distance. *Anal. Chem.* **2013**, *85*, 1840–1845.
- (280) Palomares, V.; Serras, P.; Villaluenga, I.; Hueso, K. B.; Carretero-González, J.; Rojo, T. Na-ion batteries, recent advances and present challenges to become low cost energy storage systems. *Energy Environ. Sci.* **2012**, *5*, 5884–5901.
- (281) Slater, M. D.; Kim, D.; Lee, E.; Johnson, C. S. Sodium-Ion Batteries. *Adv. Funct. Mater.* **2013**, *23*, 947–958.
- (282) Adelhelm, P.; Hartmann, P.; Bender, C. L.; Busche, M.; Eufinger, C.; Janek, J. From lithium to sodium: cell chemistry of room temperature sodium–air and sodium–sulfur batteries. *Beilstein J. Nanotechnol.* **2015**, *6*, 1016–1055.

12 Appendix

12.1 List of Symbols and Abbreviations

Table 4: List of symbols.

Symbol	Description
$\langle i_T \rangle$	Average microelectrode current of the image
A	Area
c	Bulk concentration
d	Distance between microelectrode and sample
D	Diffusion coefficient
F	Faraday constant (96485 C mol^{-1})
i_T	Current of the microelectrode
I_T	Normalized current of the microelectrode ($i_T / i_{T,\infty}$)
$i_{T,\infty}$	Current of the microelectrode at quasi-infinite distance to the sample
k_{eff}	Apparent heterogeneous rate constant
L	Normalized distance (d / r_T)
n	Number of transferred electrons
r	Total radius of a microelectrode including the insulating glass sheath
RG	Ratio between the total radius r and electrode radius of electrochemically active area r_T
r_T	Radius of electrochemically active area of a microelectrode
U	Cell voltage
κ	Dimensionless first-order rate constant
χ	Swell rate ($\delta_{\text{film}} / z_0$)

Table 5: List of abbreviations.

Abbreviation	Description
AFM	Atomic force microscopy
CE	Counter electrode
CEI	Cathode electrolyte interphase
CLSM	Confocal laser scanning microscopy
CV	Cyclic voltammetry, cyclic voltammogram
DBDMB	2,5-di- <i>tert</i> -butyl-1,4-dimethoxy benzene
DEC	Diethyl carbonate
DMC	Dimethyl carbonate
EC	Ethylene carbonate
EIS	Electrochemical impedance spectroscopy
Fc	Ferrocene
FIB	Focused ion beam
FTIR	Fourier transform infrared
GC	Glassy carbon
LIB	Lithium ion battery
Li-O ₂	Lithium air (oxygen) battery
Li-S	Lithium sulfur battery
ME	Microelectrode
NMR	Nuclear magnetic resonance
O	Oxidized species of the redox mediator
OCP	Open circuit potential
PC	Propylene carbonate
PTFE	Polytetrafluoroethylene
PVDF	Polyvinylidene fluoride
R	Reduced species of the redox mediator
RC	Redox competition
RDE	Rotating disc electrode
RE	Reference electrode
RRDE	Rotating ring-disc electrode
SC	Sample collection
SECCM	Scanning electrochemical cell microscopy

SECM	Scanning electrochemical microscopy
SEI	Solid electrolyte interphase
SEM	Scanning electron microscopy
SICM	Scanning electrochemical ion conductance microscopy
XPS	X-ray photoelectron spectroscopy

12.2 Curriculum Vitae

Personal information

Full Name: Eduardo dos Santos Sardinha
Date of birth: 17th September 1991
Place of birth: São Caetano do Sul (Brazil)
Nationality: Brazilian

Education

Since 07/2015 Doctoral candidate at the University of Oldenburg
Since 02/2017 Graduate study „Interface Science“ of the graduate school „Science and Technology“
02/2013 – 03/2015 Master Degree in Science and Technology/Chemistry at the Federal University of ABC (Brazil)
02/2009 – 12/2012 Bachelor and Licentiate in Chemistry at the Mackenzie University (São Paulo - Brazil)

Professional experience

Since 07/2015 PhD Student at the University of Oldenburg in the research group of Prof. Dr. Wittstock
02/2013 – 03/2015 Master Student at the Federal University of ABC (Brazil)
01/2011 – 12/2012 Intern in Analytical Laboratory and Research and Development of Solid Catalysts at Oxiteno S/A Indústria e Comércio (Brazil)
08/2009 – 12/2010 Chemistry Tutor at Colégio Petrópolis – Etapa (Brazil)

Grants

09/2018 Partial travel grants of GDCh and Oltech graduate school “Science and Technology” of the University of Oldenburg

	for “Electrochemistry 2018” (Ulm, Germany)
03/2018	Partial travel grant of the Arbeitsgemeinschaft Elektrochemischer Forschungsinstitutionen e.V. (AGEF) for the conference “23 th Topical Meeting of the International Society of Electrochemistry” (Tokyo, Japan)
08/2017	Travel grant of the CNPq (Brazil) for the conference “9 th SECM Workshop” (Serock, Poland)
09/2016	Travel grant of the CNPq (Brazil) for the conference “Electrochemistry 2016” (Goslar, Germany)
08/2016	Travel grant of the CNPq (Brazil) for the conference “67 th Annual Meeting of the International Society of Electrochemistry” (The Hague, Netherlands)
05/2016	Travel grant of the CNPq (Brazil) for the conference “Bunsentagung” (Rostock, Germany)
07/2015 – 12/2018	PhD grant of the CNPq (Brazil)
08/2014	Partial travel grant of the CNPq (Brazil) for the conference “65 th Annual Meeting of the International Society of Electrochemistry” (Lausanne, Switzerland)
05/2014	Travel grant of the CNPq (Brazil) for the conference “37 th Annual Meeting of the Brazilian Society of Chemistry” (Natal, Brazil)
02/2013 – 03/2015	Master grant of the CAPES (Brazil). Thesis: "Antioxidant Potentials of Vitamins Determined by an Interfacial Electrochemical Technique"

Membership in scientific societies

Since 08/2014	International Society of Electrochemistry (ISE) – Division 3 (Electrochemical Energy Conversion and Storage)
---------------	--

13 Own Publications and Scientific Presentations

13.1 Own Publications

- E. d. S. Sardinha; M. Sternad; M. Wilkening; G. Wittstock. Nascent SEI-Surface Films on Single Crystalline Silicon Investigated by Scanning Electrochemical Microscopy. *ACS Applied Energy Materials*, Accepted, 2019. DOI: 10.1021/acsaem.8b01967.
- H. Bülter, M. Sternad, E. d. S. Sardinha, J. Witt, C. Dosche, M. Wilkening, G. Wittstock, Investigation of the Electron Transfer at Si Electrodes: Impact and Removal of the Native SiO₂ Layer, *J. Electrochem. Soc.*, **163** (3) A504-A512 (2016).

13.2 Oral Presentations

Table 6: List of oral presentations.

Time	Presentation description
04/2018	<u>E. dos Santos Sardinha</u> , M. Sternad, M. Wilkening, G. Wittstock – <i>Scanning Electrochemical Microscopy Study of the Formation of Solid Electrolyte Interfaces and Lithiation on Silicon Electrodes</i> , 22 nd Topical Meeting of the International Society of Electrochemistry, Tokyo, Japan
08/2017	<u>E. dos Santos Sardinha</u> , M. Sternad, M. Wilkening, G. Wittstock – <i>Scanning Electrochemical Microscopy Study of the Formation of the Solid Electrolyte Interphase and Lithiation on Silicon Electrodes</i> , 9 th Workshop on Scanning Electrochemical Microscopy and Related Techniques, Serock, Poland
05/2016	<u>E. dos Santos Sardinha</u> , H. Bülter, M. Sternad, M. Wilkening, G. Wittstock – <i>Removal of the SiO₂ Native Layer from Silicon Electrodes - Scanning Electrochemical Microscopy and X-ray Photoelectron Spectroscopy</i> , 115 th General Assembly of the German Bunsen Society for Physical Chemistry, Rostock, Germany

13.3 Poster Presentations

Table 7: List of presented posters.

Time	Poster description
09/2018	<u>E. dos Santos Sardinha</u> , A. Gräfenstein, G. Wittstock – <i>2,3-dichloro-5,6-dicyano-1,4-benzoquinone as a Mediator for Scanning Electrochemical Microscopy Investigations in Cathode Materials</i> , Electrochemistry 2018, Ulm, Germany
09/2016	<u>E. dos Santos Sardinha</u> , M. Ding, S. Passerini, G. Wittstock – <i>SECM Investigation on Freshly Prepared Li Surfaces for Application as a Negative Electrode in Li-ion Batteries</i> , Electrochemistry 2016, Goslar, Germany
08/2016	<u>E. dos Santos Sardinha</u> , H. Bülter, M. Sternad, M. Wilkening, G. Wittstock – <i>Passive Layers on Si Negative Electrodes Investigated by Scanning Electrochemical Microscopy and X-ray Photoelectron Spectroscopy</i> , 67 th Annual Meeting of the International Society of Electrochemistry, The Hague, Netherlands

14 Acknowledgement

First of all I would like to thank Prof. Gunther Wittstock for the possibility to work on an attractive topic within a versatile and interesting graduate program. I owe thanks to Gerd Gertjegerdes from the working group from Prof. Wittstock for the functionality and very fast repair of cables and electric devices. Many thanks go to all former and present coworkers of the Wittstock group for the introduction into experimental techniques, helpful advice, the enjoyable atmosphere and friendship during the PhD time.

It was a pleasure to work together with several people during the project. I am very grateful for their interest and their efforts. I am especially thankful to Dr. Carsten Dosche, Dr. Heinz Bülter and Dr. Julia Witt for the contribution to the own work. I would also like to thank Dr. Michael Sternad and Prof. Dr. Martin Wilkening from Graz University of Technology in Graz for the discussions and contributions and the silicon electrodes provided. I would also like to thank Dr. Markus Ding, Prof. Stefano Passerini from the Helmholtz Institute in Ulm and the Institute of Technology in Karlsruhe for the lithium anodes and MSc. Alexander Gräfenstein for the discussion and providing the positive electrode materials.

I am very thankful for the Conselho Nacional de Pesquisa e desenvolvimento (Brazil), which supported financially this PhD project. Besides, one of the most important parts of the PhD is the presentations at conferences and the interesting scientific discussions these occasions proportionate. I am thankful for the financial support from the CNPq, AGEF, GDCh and Oltech graduate school that made it possible the attendance to various conferences.

15 Eidesstattliche Erklärung

Hiermit versichere ich, dass ich diese Arbeit selbständig verfasst und nur die angegebenen Quellen und Hilfsmittel benutzt habe. Aus der Dissertation sind die zuvor genannten Veröffentlichungen hervorgegangen. Die Dissertation hat weder zu Teilen noch in Gänze einer anderen wissenschaftlichen Hochschule zur Begutachtung in einem Promotionsverfahren vorgelegen.

A handwritten signature in blue ink, reading "Eddy Sawlich". The signature is written in a cursive style with a large, sweeping flourish at the end.

Oldenburg, den 02.07.19